

15138

APPLICATION OF THE WEDGE TECHNIQUE  
TO THE MEASUREMENT OF STARK  
SHIFTS OF PLASMA LINES

by

ROBERT NORTON MORRIS

B.Sc., UNIVERSITY OF BRITISH COLUMBIA, 1966

M.Sc., UNIVERSITY OF BRITISH COLUMBIA, 1968

A THESIS SUBMITTED IN PARTIAL FULFILLMENT OF  
THE REQUIREMENTS FOR THE DEGREE OF  
DOCTOR OF PHILOSOPHY  
in the Department  
of  
Physics

We accept this theses as conforming to the  
required standard.

THE UNIVERSITY OF BRITISH COLUMBIA  
NOVEMBER, 1972

In presenting this thesis in partial fulfilment of the requirements for an advanced degree at the University of British Columbia, I agree that the Library shall make it freely available for reference and study.

I further agree that permission for extensive copying of this thesis for scholarly purposes may be granted by the Head of my Department or by his representatives. It is understood that copying or publication of this thesis for financial gain shall not be allowed without my written permission.

Department of Physics

The University of British Columbia  
Vancouver 8, Canada

Date November 30, 1972

ABSTRACT

The ability of the GBKO Stark broadening theory to predict the position of the mean of a plasma spectral line is experimentally investigated for three isolated neutral helium lines at electron temperatures of about 1.5 eV and electron densities in the region of  $(0.5 \text{ to } 2.0) \times 10^{16} \text{ cm}^{-3}$ . General agreement was found between experimental and theoretical shifts of the mean of the lines HeI 5016, HeI 4713 and HeI 3889 from their unperturbed wavelengths.

A semi-empirical relationship is derived which gives the shift of the mean in terms of the electron impact width,  $w$ , and shift,  $d$ , as well as in terms of the ion-broadening parameter,  $\alpha$ , and the Debye-shielding parameter,  $r$ :

$$\Delta\bar{\lambda} \approx \left[ \frac{d}{w} \pm 4.1\alpha(1 - 0.5r) \right] w .$$

This relationship estimates the shift of the mean within 5% of the width,  $w$ , over the ranges  $0 \leq \alpha \leq 0.4$  and  $0 \leq r \leq 0.8$ .

The shifts in the means of the observed lines were measured by a new technique employing a linearly varying neutral density filter mounted in the exit plane of a monochromator. This "wedge technique" has a wide range of possible application from steady state to pulsed conditions for observation of Doppler shifts, van der Waals shifts, Stark shifts or Zeemann shifts. It requires that the line is reasonably isolated and it is useful when the shift to width ratio is either large or small. A complete discussion of the technique is presented along with the important design criteria for linearity, resolution and sensitivity.

## TABLE OF CONTENTS

	Page
ABSTRACT. . . . .	i
TABLE OF CONTENTS . . . . .	ii
LIST OF FIGURES . . . . .	iv
ACKNOWLEDGEMENTS. . . . .	vi
INTRODUCTION TO THE THESIS. . . . .	1
PART I - MEASUREMENT OF STARK SHIFTS. . . . .	4
CHAPTER I-1 INTRODUCTION . . . . .	4
CHAPTER I-2 OBTAINING LOCAL EMISSION PROFILES. . . . .	6
A. General Approach - Abel Inversion . . . . .	6
B. Data Recording - Equipment and Experimental Techniques. . . . .	12
C. Data Handling - Software Techniques and Calculations. . . . .	18
D. Testing the Systems . . . . .	20
CHAPTER I-3 PLASMA CONDITIONS. . . . .	24
A. Experimental Operating Conditions of the Plasma Jet . . . . .	24
B. Electron Density Measurements. . . . .	27
C. Measurement of Electron Temperature. . . . .	34
CHAPTER I-4 STARK SHIFT MEASUREMENTS AND COMPARISONS .	45
A. Shift Measurements . . . . .	45
B. Comparison of Measured and Calculated Shifts . . . .	51
PART II - DESIGN CRITERIA FOR APPLICATION OF THE WEDGE TECHNIQUE TO THE MEASUREMENT OF LINE SHIFTS . . .	56
CHAPTER II-1 INTRODUCTION. . . . .	56
CHAPTER II-2 THE WEDGE TECHNIQUE (DESCRIPTION) . . . . .	58
CHAPTER II-3 LINEARITY . . . . .	65
A. Edge Effects . . . . .	65
B. Wedge Non-Linearities. . . . .	78
CHAPTER II-4 ACCURACY AND RESOLUTION . . . . .	83
CHAPTER II-5 EXPERIMENTAL EXAMPLE USING A REAL WEDGE .	87

CHAPTER II-6 APPLICATION OF THE WEDGE TECHNIQUE TO SHIFT MEASUREMENTS IN AN INHOMOGENEOUS (CYLINDRICALLY SYMMETRIC) PLASMA. . . . .	94
A. Abel Unfolding of Shifts . . . . .	95
B. Relating the Wedge Technique to Unfolding Shifts .	98
PART III - CONCLUSIONS. . . . .	102
APPENDIX I - RADIAL DISTRIBUTION OF LINE WIDTHS . . . . .	108
APPENDIX II - THEORETICAL WIDTHS AND SHIFTS . . . . .	113
APPENDIX III - AREA CORRECTION FOR INTEGRATION OF A LORENTZ PROFILE TO FINITE LIMITS . . . . .	119
APPENDIX IV - EXCITED STATE POPULATION DENSITIES. . . . .	124
APPENDIX V - WEDGE TECHNIQUE DESIGN PROCEDURE . . . . .	127
BIBLIOGRAPHY. . . . .	131

## LIST OF FIGURES

Figure		Page
I-2.1	EXPERIMENTAL COORDINATE SYSTEM . . . . .	7
I-2.2	OBSERVED INTENSITY PROFILE . . . . .	11
I-2.3	LOCAL EMISSION PROFILES. . . . .	11
I-2.4	SCHEMATIC OF MONOCHROMATOR SHOWING SCANNING PLATE AND LEVER. . . . .	13
I-2.5	SCHEMATIC OF RECORDING APPARATUS . . . . .	16
I-2.6	PROGRAM TEST . . . . .	23
I-3.1	OPERATING CONDITIONS OF THE PLASMA JET . . . . .	24
I-3.2	THE PLASMA JET . . . . .	26
I-3.3	RADIAL DISTRIBUTION OF ELECTRON DENSITY. . . . .	28
I-3.4	OPTICAL SYSTEM FOR EXAMINATION OF SELF ABSORPTION . . . . .	33
I-3.5	RADIAL DISTRIBUTION OF ELECTRON TEMPERATURE. . . . .	37
I-4.1	RADIAL DISTRIBUTION OF SHIFT FOR HeI 5016. . . . .	47
I-4.2	RADIAL DISTRIBUTION OF SHIFT FOR HeI 4713. . . . .	48
I-4.3	RADIAL DISTRIBUTION OF SHIFT FOR HeI 3889. . . . .	49
I-4.4	COMPARISON OF MEASURED AND CALCULATED SHIFTS . . . . .	54
II-2.1	SCHEMATIC ELEVATION OF MONOCHROMATOR . . . . .	59
II-2.2	WEDGE TRANSMISSION . . . . .	62
II-3.1	A RECTANGULAR INTENSITY PROFILE. . . . .	66
II-3.2	LINEARITY FOR A RECTANGULAR INTENSITY PROFILE. . . . .	70
II-3.3	LINEARITY FOR A PURE GAUSSIAN LINE PROFILE . . . . .	73
II-3.4	LINEARITY FOR A LORENTZ LINE PROFILE . . . . .	74
II-3.5	WEDGE NON-LINEARITIES. . . . .	80
II-5.1	WEDGE OUTPUT SIGNALS FOR A NARROW GEISSLER LINE . . . . .	88
II-5.2	WEDGE OUTPUT FOR A WIDENED GEISSLER LINE . . . . .	89
II-5.3	WEDGE OUTPUT FOR A BROADENED LINE. . . . .	90
II-5.4	EXPERIMENTAL INVESTIGATION OF A REAL WEDGE . . . . .	91
AI-1	RADIAL DISTRIBUTION OF (FULL) HALF WIDTHS OF $H_{\beta}$ . . . . .	109

AI-2	RADIAL DISTRIBUTION OF (FULL) HALF WIDTHS OF HeI 5016. . . . .	.110
AI-3	RADIAL DISTRIBUTION OF (FULL) HALF WIDTHS OF HeI 4713. . . . .	.111
AI-4	RADIAL DISTRIBUTION OF (FULL) HALF WIDTHS OF HeI 3889. . . . .	.112
AII-1	(FULL) HALF WIDTHS OF $H_{\beta}$ AS A FUNCTION OF $n_e$ FOR $5,000^{\circ}\text{K} \leq T_e \leq 40,000^{\circ}\text{K}$ . . . . .	.114
AII-2	ELECTRON DENSITY vs. (HALF) HALF WIDTH OF HeI 5016 . . . . .	.115
AII-3	(HALF) HALF WIDTHS OF HeI 3889 . . . . .	.116
AII-4	(HALF) HALF WIDTHS OF HeI 4713 . . . . .	.117
AII-5	DEBYE-SHIELDING PARAMETER, $r_G$ . . . . .	.118
AIII-1	AREA CORRECTION FOR INTEGRATION OF A LORENTZ PROFILE TO FINITE LIMITS . . . . .	.123
AIV-1	EXCITED STATE POPULATION DENSITIES FOR $n=3$ .	.125
AIV-2	EXCITED STATE POPULATION DENSITIES FOR $n=4$ .	.126

## ACKNOWLEDGEMENTS

I wish to express my most sincere appreciation to my supervisor, Dr. B. Ahlborn, whose advice and encouragement was paramount in all facets of the work. Important contributions were also made by Dr. A.J. Barnard and Dr. J. Cooper through their expertise in the theory of Stark broadening. The technique for measuring the radial distribution of electron temperature came from a suggestion by Dr. J. Meyer and greatly extended the completeness of the measurements.

The electronic equipment used in the experiment was largely created and maintained by Messrs. D.G. Sieberg and J.A. Zanganeh. Their help was well appreciated. The mechanical aspects of the experiment were handled for the most part by two very able machinists: Mr. J. Bosma, who developed the optical systems required, and Mr. T. Knopf, who built and helped to design the plasma jet.

My association with the Plasma Physics Group at U.B.C. has been very important to me. The discussions that I have had with both graduate students and faculty members contributed not only to the work presented here but to many other activities that I have or will pursue.

This work has been supported by a grant from the Atomic Energy Control Board of Canada.

## INTRODUCTION TO THE THESIS

Considerable effort has been expended by physicists studying the effects of Stark broadening on the profiles of plasma spectral lines. This has been justified through expanded insight in the realm of atomic interactions as well as through the creation of valuable diagnostic tools for the study of laboratory plasmas and stellar structures.

For the latter of these two uses, a significant portion of the total effort has focused on extraction of the half-intensity widths of the spectral intensity distributions. The reason is that the extracted width provides a single parameter which probes the condition of the plasma, avoiding the complicated need to fit a full experimental profile at many points to establish the same results.

By comparison, however, extraction of the accompanying Stark shifts of the distributions for the same diagnostic purpose has been almost ignored. This, of course, is no simple oversight. Two significant problems have coupled to discourage more vigorous pursuit of this facet of the general topic. They are:

- a) Most Stark shifts are difficult to measure accurately since the shift is comparable to or smaller than the Stark width for many plasma lines;
- b) The calculated shifts (extracted from theoretical profiles) are less accurate than the correspondingly calculated widths.

As a result, experimental plasma physicists have preferred line width measurements as a means of determining electron density and temperature in plasmas. Theoreticians, in turn, have sought more vigorously to improve the accuracy of the width calculations since these have been received with the most wide-spread interest.

On the other hand, several features make shift measurements more appealing to the experimentalist than line width measurements. They are:

- a) Shift measurements are not as severely affected as width measurements by the instrument function of the monochromator used to examine the line;
- b) Fewer plasma processes contribute to the shift of a spectral line than contribute to its width. Among these are: self-absorption, thermal (Doppler) broadening and resonance broadening.

Yet, as appealing as these features make them, the practicality of using Stark shifts measurements as a diagnostic technique is still diminished by the two problems mentioned earlier -- difficulty of shift measurement, and unreliable calibration data. This work is a response to both of these objections.

To offset the first of the objections, a technique is developed and presented in this thesis which can very accurately measure a shift in the mean of a spectral line even when the shift to width ratio is much less than unity. In addition, the technique -- called the "wedge" technique -- is experimentally simple and practical to use. Its applicability extends beyond the detection of Stark shifts to any mechanism which will cause a shift in the mean of the spectral distribution.

The second objection to the use of Stark shifts as a plasma diagnostic tool provides the motivation for the other part of the work presented in this thesis. If accurate shift measurements can be made under conditions of known electron temperature and density, the true accuracy of shift calculations can be determined. The result will be that these will either be trusted to a greater degree or that any revealed discrepancies between calculated and measured shifts will inspire theoreticians to hone their considerations and offer more reliable figures.

These two parts of the work are presented in two distinct parts of the thesis. The investigation of Stark shifts of neutral helium lines is presented in Part I, while because of its general applicability, the wedge technique is presented separately in Part II. It is hoped that this format will more adequately accommodate the range of interest that readers may have.

## PART I - MEASUREMENT OF STARK SHIFTS

### CHAPTER I-1 INTRODUCTION

This part of the thesis is devoted to the measurement of the Stark shifts of three isolated neutral helium lines under known plasma conditions. The intent of the experiment, as expressed in the Introduction To The Thesis, was to test the accuracy with which Stark broadening theory -- in this case the \*GBKO theory -- will predict the shift in the mean of a plasma line. Thus, the experiment consists of measuring the shifts of the spectral lines produced by these conditions and comparing these with the shifts predicted by the GBKO theory.

As a source, an atmospheric plasma jet was used. This provided a steady, reproducible plasma whose regular spatial inhomogeneity covered a convenient range of plasma conditions. Helium was chosen as the working gas because of its heavy theoretical attention, its interest to astrophysicists (helium is a main constituent in stellar atmospheres), and its tractability in the jet.

Several spectral lines of the helium jet were studied spectroscopically to obtain the spatial distributions of electron density and electron temperature. Then, using the wedge technique (described in Part II of this thesis), the spatial distributions of the Stark shifts of these same lines were measured, correlated with the coincident plasma conditions, and compared with calculated shifts over the same conditions.

\*Griem, Baranger, Kolb and Oertel (1962)

The first chapter in this Part describes the obtaining of local spectral line profiles. This is the most important procedural aspect of the experiment since all later measurements derive from these results. Consequently, this is a very detailed chapter and probably will prove tedious for a casual reader. However, in order to obtain a reasonable understanding of the experiment it is advisable to read the first part of Chapter I-1. It will then be possible to skip immediately to the last chapter of Part I and still retain an overall understanding of the experiment.

The interim chapters of Part I (as the steps in the experimental sequence) follow logically and document the complete experiment. Their contents and the justifications for their presence are obvious from their titles.

## CHAPTER I-2 OBTAINING LOCAL EMISSION PROFILES

### A. GENERAL APPROACH - ABEL INVERSION

All of the spectroscopic measurements used in this experiment to obtain the spatial distributions of electron density, electron temperature and Stark shifts, required a knowledge of the emission profile\* for each chosen spectral line at various local points in the plasma. However, all actual observations of these spectral lines do not directly yield local emission profiles. Instead, one observes intensity profiles which are composites of the local emission profiles due to the unavoidable integration along the line of observation through the plasma. Obviously, this complicates the manner in which emission profiles are obtained. Fortunately, it does not prevent their acquisition.

Under most operating conditions (except very low currents), the flame produced by a plasma jet is cylindrically symmetric. Thus, all the properties of the flame -- including electron, ion and neutral densities and temperatures -- which in general would be specified by functions of the form  $f(r,z,\theta)$ , (where  $r, z$  and  $\theta$  form a cylindrical coordinate system as shown in Figure I-2.1) can be written as functions without the  $\theta$  dependence:  $f(r,z)$ . In this experiment, since all measurements were taken at a fixed  $z$  position (just at the surface of the anode), the  $z$  dependence will not be shown explicitly. Instead, it will be taken as understood that the functional form  $f(r)$  specifies plasma conditions at the anode ( $z = 0$ ).

\* The word "profile" is used to indicate the intensity distribution of a spectral line as a function of wavelength.

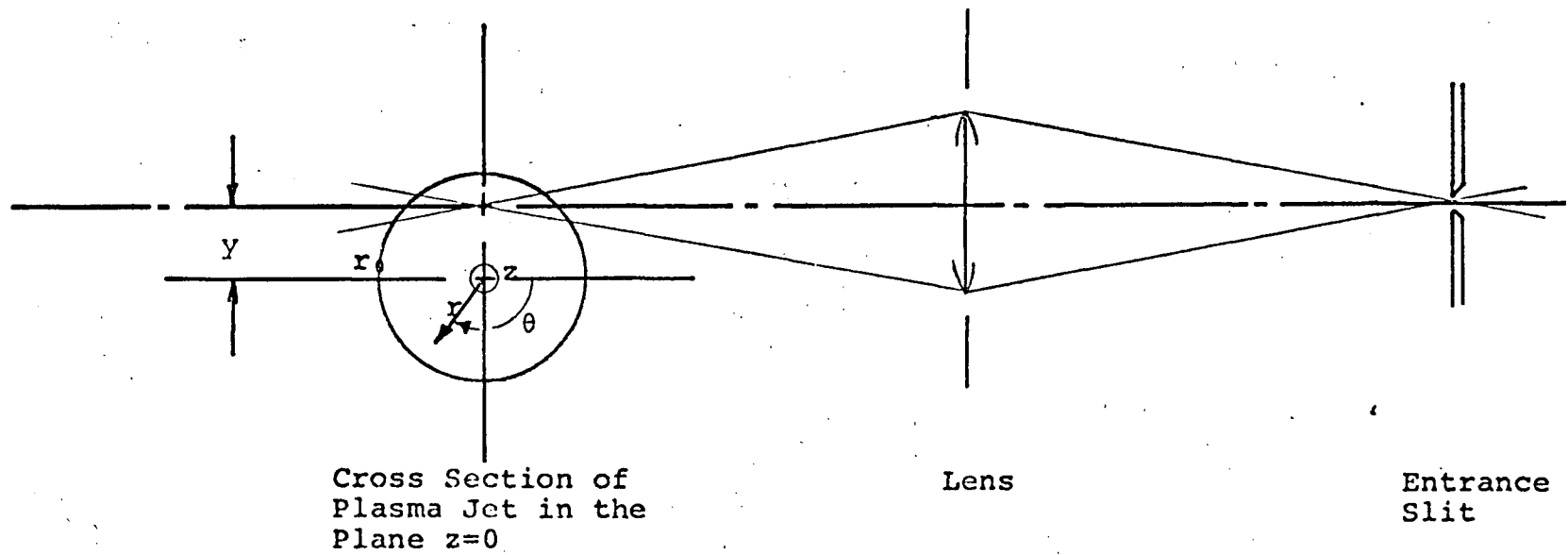


Figure I-2.1  
EXPERIMENTAL COORDINATE SYSTEM

With this condition of cylindrical symmetry (and fixed  $z$ ), it is possible to relate the observed intensity profile  $i_{\lambda_0}(y, \lambda)$  of a spectral line (power per unit area per unit wavelength per unit solid angle for the line with nominal wavelength  $\lambda_0$  when the acceptance cone of the optical system looking through the jet is a distance  $y$  from the cylindrical axis of symmetry) to the local emission profiles for the same line,  $\epsilon_{\lambda_0}(r, \lambda)$  (power per unit volume per unit wavelength per unit solid angle), through the integral:

$$i_{\lambda_0}(y, \lambda) = 2 \int_y^{r_0} \frac{\epsilon_{\lambda_0}(r, \lambda) r dr}{(r^2 - y^2)^{\frac{1}{2}}} \quad \text{I-2.1}$$

where  $r_0$  is a radius that specifies the outer limit of the flame where the emission has fallen to zero.

Obtainment of emission profiles from the observed intensity profiles means inverting Equation I-2.1. This is accomplished by the well known Abel transform (Griem, 1964):

$$\epsilon_{\lambda_0}(r, \lambda) = - \frac{1}{\pi} \int_r^{r_0} \frac{i'_{\lambda_0}(y, \lambda) dy}{(y^2 - r^2)^{\frac{1}{2}}} \quad \text{I-2.2}$$

where the prime (') indicates the derivative with respect to  $y$ .

It is obvious from the limits of the integral in this last equation that to retrieve the emission profile at one radial position,  $r$ , intensity profiles must be observed from  $y=r$  out to  $y=r_0$ . A complete "set" of intensity profiles for  $0 \leq y \leq r_0$  must be observed to obtain the on-axis emission profile  $\epsilon_{\lambda_0}(0, \lambda)$ . This complete set then suffices for recovery of all emission profiles  $0 < r < r_0$ .

Thus, the experimental procedure for taking a complete set of spectroscopic data would consist of the following steps:

1. Position the jet so the acceptance cone of the optical system just grazes the outer limits of the flame ( $y=r_0$ );
2. Scan the observed intensity profile by recording the photomultiplier output voltage at various wavelengths;
3. Reposition the jet so the acceptance cone passes some distance in toward the axis from the outer edge of the flame ( $y<r_0$ );
4. Scan the observed profile;
5. Repeat steps 3 and 4 until  $y\leq 0$ .

The number of observed profiles, the number of points per profile, the types of profiles and their spatial dependence will determine the accuracy with which the emission profiles can be obtained.

The complete set of data consists of a field of voltage readings,  $v_{\lambda_0}(y, \lambda)$ , which are linearly related to the intensity profiles by the absolute response of the apparatus,  $k_{\lambda_0}$ . This response is assumed to be independent of  $y$  and  $\lambda$  over the region of the line:

$$i_{\lambda_0}(y, \lambda) = k_{\lambda_0} v_{\lambda_0}(y, \lambda)$$

I-2.3

This field of voltage readings forms a surface over the  $y$ - $\lambda$  plane as illustrated in Figure I-2.2, which, if unfolded along lines of constant wavelength using Equations I-2.2 and I-2.3, produces a new field of voltages,  $u_{\lambda_0}(r, \lambda)$ , which forms a surface above the  $r$ - $\lambda$  plane as indicated in Figure I-2.3. The local emission profiles are obtained from this new field by the relation:

$$\varepsilon_{\lambda_0}(r, \lambda) = k_{\lambda_0} u_{\lambda_0}(r, \lambda) \quad \text{I-2.4}$$

by considering the curves as a function of wavelength at constant radius.

It can be seen now that the experimental procedure is broken into two fairly distinct operations. The first involves the experimental procedure and apparatus used to record the observed intensity profile voltages; the second involves the software techniques for handling the resulting data and applying the Abel transform to obtain local emission profiles.

These two operations will now be described in detail for interested readers. Those who are willing to accept the fact that local emission profiles are reliably obtained and who are not particularly concerned with their precise method of obtainment can ignore these sections and proceed immediately to either Chapter I-3, or to the last Chapter without interruption of essential scientific continuity.

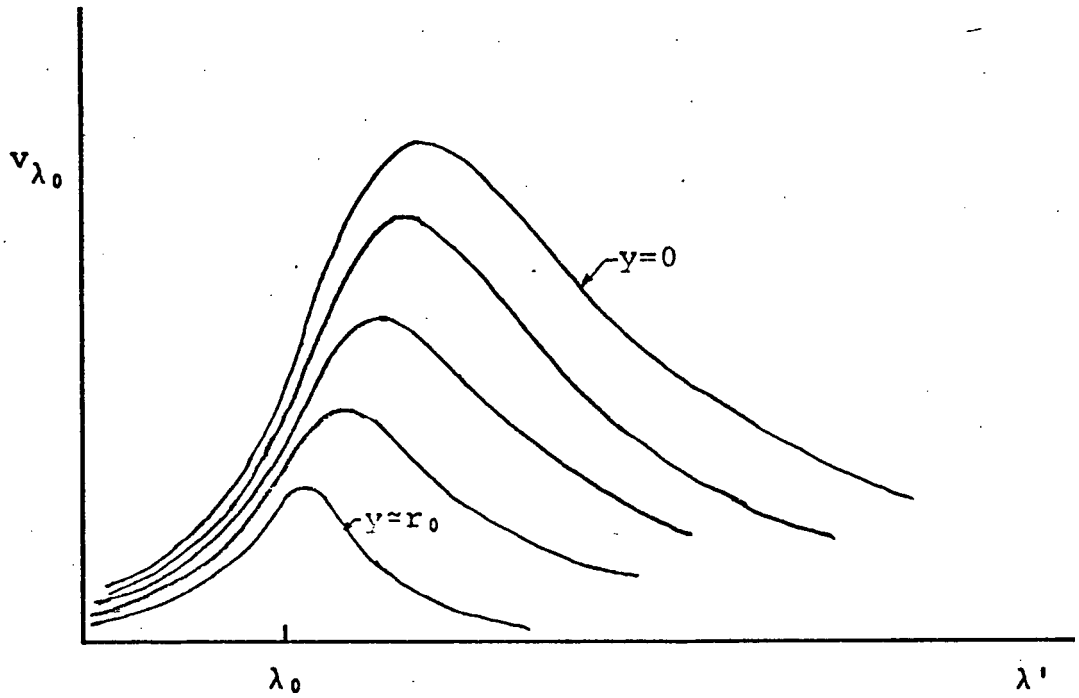


Figure I-2.2 - OBSERVED INTENSITY PROFILES

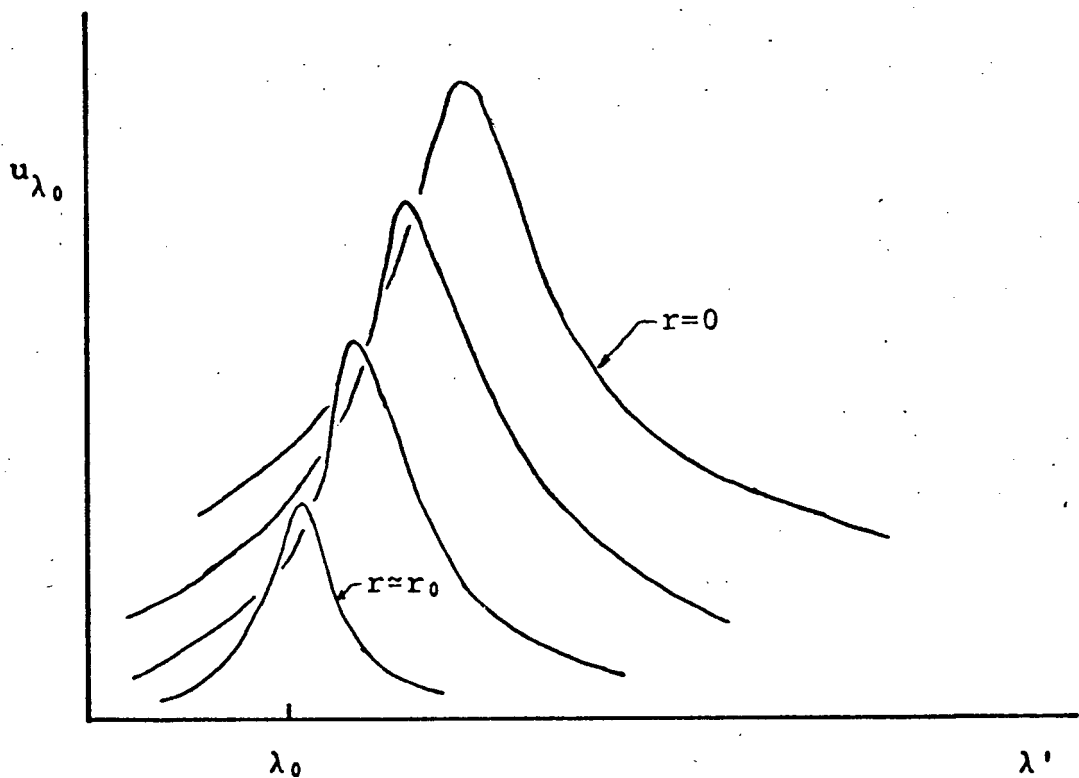


Figure I-2.3 - LOCAL EMISSION PROFILES

## B. DATA RECORDING

The spectral lines were observed using a Spex 3/4 meter monochromator with a nominal (universe) dispersion of  $10 \text{ \AA/mm}$  in first order. The monochromator had an additional "scanning plate" mounted between the camera mirror and the exit slit which, when rotated, displaced the image of the spectral line in the wavelength direction. (See Figure I-2.4) A lever of length  $L$ , ( $\approx 1 \text{ m.}$ ) connected at one end to the axis of rotation allowed very accurate rotation of the plate. For small angles,  $\theta \approx \ell/L$  the distance moved by the end of the scanning lever,  $\ell$ , was linearly proportional to the amount of sideways displacement,  $d$ , of the line image and therefore, linearly proportional to the wavelength setting of the monochromator.

$$d \approx t \frac{\ell}{L} \left\{ 1 - \frac{1}{n} \right\}$$

where:  $t$  is the thickness of the scan plate and  
 $n$  is the index of refraction.

At the end of the scanning lever was a slide which made contact with a Nichrome potentiometer wire (resistance  $0.75 \text{ ohms/in.}$ ) with enough current running through it to allow the voltage of the slide to vary from zero to 1 volt over its full motion. This voltage provided a means of monitoring the wavelength setting of the monochromator.

One of two Pyrex windows of thickness  $0.130 \text{ in.}$  or  $0.242 \text{ in.}$  were selected as scanning plates depending on the wavelength sensitivity and range required. The thinner of the two plates gave a wavelength sensitivity of  $0.31 \text{ \AA}$  per inch of scan lever displacement at the potentiometer wire, allowing a total observable range of  $3.7 \text{ \AA}$ . (A total range of 12

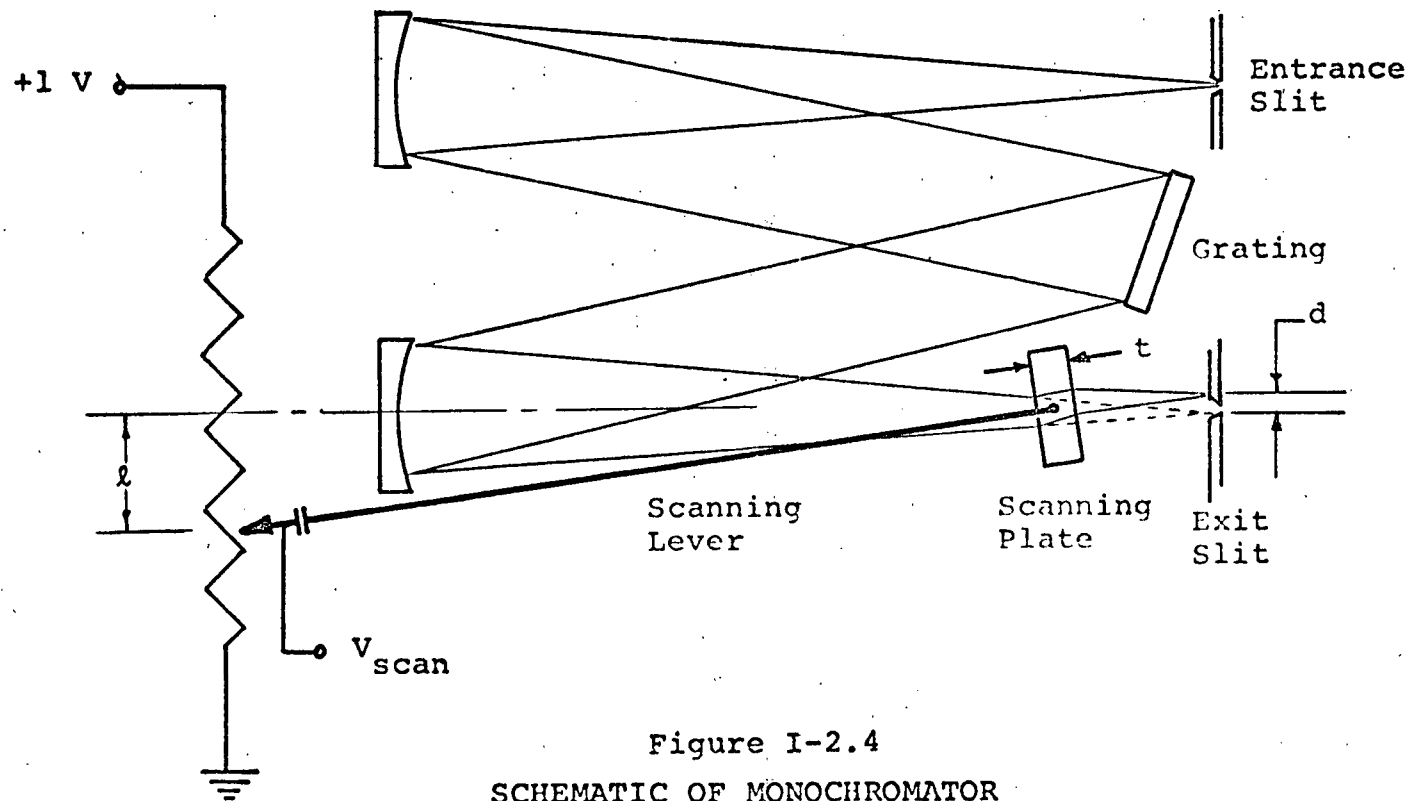


Figure I-2.4  
 SCHEMATIC OF MONOCHROMATOR  
 SHOWING SCANNING PLATE AND LEVER

inches of lever motion kept the angles small, assuring linear voltage response to the wavelength scale within 1% at the extreme excursions of the lever.) The thicker scan plate gave a sensitivity of  $0.58 \text{ \AA}$  per inch for a total range of  $7.0 \text{ \AA}$ .

The scan plates were selected to give adequate range out into the wings of the spectral line under examination. The thin plate was used to scan HeI 3889 while the thick plate was used for HeI 5016 and HeI 4713. When wider lines were encountered (such as  $H_{\beta}$  and HeI 4921) it was necessary to scan using the grating screw because of the much wider ranges required ( $\approx 30 \text{ \AA}$ ). In this case, a rotary potentiometer was mounted colinear with the grating screw and served the same purpose as the slide-wire potentiometer on the scanning lever.

Because the addition of a scan plate extended the focal point of the monochromator, it was necessary to refocus the instrument each time the scan plate was changed. This was easily and very accurately accomplished using an exit slit and photomultiplier assembly mounted on a slide mechanism which allowed screw adjustment of its position. When in good focus with equally wide entrance and exit slits, the instrument had a transmission function which was (roughly) triangular with a (full) half-width of  $.23 \text{ \AA}$ .

For immediate, in-progress viewing of a particular scan, the wavelength monitoring voltage from the slide wire (or grating screw) potentiometer was connected to one input of an XY plotter while the voltage across the load resistor of the photomultiplier was connected to the other input. This resulted in direct plots of the line profile being scanned.

The main apparatus for recording line profiles was a digital magnetic tape recording system. This consisted of a custom designed interface controlling a MOS-FET six channel scanner, a Fluke 3200A sampling digital voltmeter (DVM), and a Kennedy 1600 seven track incremental digital magnetic tape recorder. The system functioned in the following manner (see Figure I-2.5):

A thumbwheel switch on the interface front panel selected the number of channels (one to six) to be scanned. The equivalent number of voltage sources to be monitored were connected to the inputs of the scanner. The single output of the scanner was connected to the input of the scanning DVM whose binary coded decimal (BCD) outputs were connected through the interface to the digital magnetic tape recorder.

Upon command to scan (via a front panel switch), the interface opened the first transmission gate of the scanner, thereby connecting that voltage input to the input of the DVM. A signal from the interface then triggered the DVM to sample its analog input (with a sample aperture of 500 usec.), convert it to digital form and store it in a buffer memory as eight BCD characters. The interface then serially recalled each character from memory, recorded it as one byte on the magnetic tape and then advanced the tape one increment. When all 8 bytes were recorded, the interface closed the first transmission gate, opened the second and repeated the entire process. Each input was thus sampled

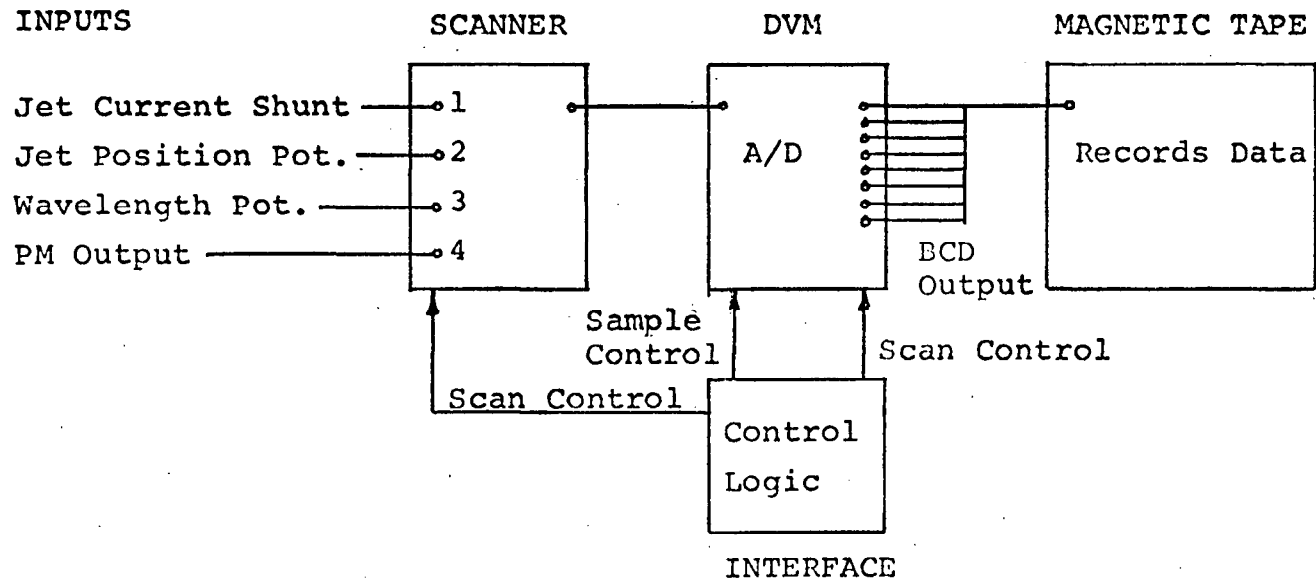


Figure I-2.5  
SCHEMATIC OF RECORDING APPARATUS

and recorded. When the selected number of channels were recorded, the procedure was repeated beginning with channel 1 again. This continued until the command to stop was received by the interface.

The maximum recording rate, set by the maximum incremental rate of the magnetic tape (750 bytes/sec.), was approximately 94 readings (channels) per second. Hence, if only 4 of the 6 possible channels were used, each would get sampled at a rate of about  $23 \text{ sec}^{-1}$ . (Since scans of the selected number of channels could be initiated individually, the minimum record rate was arbitrary.) With a tape density of 556 bytes/inch. the longest tape (1200 ft.) that would fit onto the recorder allowed  $10^7$  readings to be recorded. This capacity was never needed for this experiment.

For recording the line profiles in this experiment, 4 channels were used. The information monitored on each was:

- Channel 1 - Jet Current (voltage across the arc current shunt)
- Channel 2 - Jet Position (voltage on a potentiometer monitoring the y-position of the jet.)
- Channel 3 - Wavelength (scanning lever slide voltage)
- Channel 4 - Spectral Line Intensity (output voltage of the photomultiplier tube)

A profile was obtained by setting the position of the jet (y), starting the recording apparatus and slowly moving the scanning lever from one extreme position to the other.

Scans were obtained from the edge of the flame first, then, successively, (in increments of about .010 in.) from points toward (and beyond) the axis of the flame. Usually about 12 scans were taken of each line with approximately 300 points per profile. In addition, a scan of the Geissler line was made. A file gap (triggered by a switch) on the recorder front panel) was inserted between each profile. Two or more successive file gaps marked the end of data on the tape.

### C. DATA HANDLING

The 7-track magnetic tape containing the experimental profiles was delivered to the computing centre where its data was decoded, sorted and translated into binary numbers suitable for numerical operations. This resulting data was labelled and collected from each experimental run on a 9-track tape which remained at the center. The 7-track tape was returned for reuse in the experiment.

Each experimental profile consisted of a number of intensity (photomultiplier output voltages) points which were unequally spaced in wavelength. In order to apply the Abel inversion along  $y$  at constant wavelength it was first necessary to transform each of the profiles into an ensemble of intensity points which were equally spaced in wavelength. This was done using a linear interpolation procedure between the closely spaced, recorded points and resulted in profiles each with 300 equally spaced points.

The intensity was then plotted as a function of  $y$  at several wavelengths to obtain the  $y$  position of the jet axis. Once obtained, a value of  $r_0$  (the radius where the intensity fell to zero) was chosen and at constant wavelength twenty intensity points equally spaced in  $y$  were obtained by piece-wise quadratic interpolation of 12 to 16 points. To these points, Barr's (1961) method of Abel inversion was applied to give an equivalent number of radial emission points at constant wavelength.

Radial emission curves (not profiles) were unfolded successively at every second wavelength point of the equally spaced observed profiles. This meant 150 applications of the interpolation and Abel inversion program per line examined.

Once all of the inversions were complete, the emission profiles were obtained by plotting out the unfolded emission points along wavelength at constant radius. These points were held in disc storage, available for immediate computation and were also stored on another 9-track magnetic tape as a back-up precaution against accidental destruction of the disc storage.

The Geissler line profile, as well as the jet current, were obtained by the appropriate print-out from the initial decoded data.

#### D. TESTING THE SYSTEMS

The equipment was thoroughly examined using known voltages to assure that the signals were being reliably recorded. Also, the maximum wavelength scan rate was determined to assure the lines were not being scanned faster than the system would follow. This was limited, not by the recording system itself, but by the integrating capacitors used on the photomultiplier to reduce noise. Occasionally, if the scan lever was inadvertently jerked in the region of high gradient in intensity, a capacitive "jag" would appear in the unfolding program. However, these could be kept to a tolerable level with good technique, a smooth-running scan lever and minimum capacitance.

The most important source of uncertainty in the unfolded emission profiles arose through the data handling and inversion programs. To make some estimate of this effect several checks were made.

Firstly, the linear interpolation technique for "spacing out" the observed profiles was examined by plotting an unequally-spaced profile over its equally-spaced descendent. No difference in the profile could be observed at an accuracy of 1%.

Secondly, the Abel program (Barr's technique) was used to unfold several "observed" distributions which had analytic unfolded distributions. (See Bracewell, 1956 for a convenient list of these.) As Barr states in this paper, the technique works well except where sharp breaks occur in the folded intensity distribution. This is done

purposely to aid in smoothing noisy data and considerably improves the on-axis results over other techniques. However, since a sharp break usually comes where the observed intensity falls to zero, this technique tends to overestimate the emission at outer radii. This property of the technique, usually negligible in its importance, has an important effect on the measurements of this experiment which will be discussed shortly.

To get an overall idea of the ability of the software system to accurately unfold emission profiles, a third and more complete test was made. It began with the "manufacture" of a set of twenty unfolded, Lorentian emission profiles with widths, shifts and intensities that varied with radius in a manner similar to the most severe conditions encountered in the experiment.

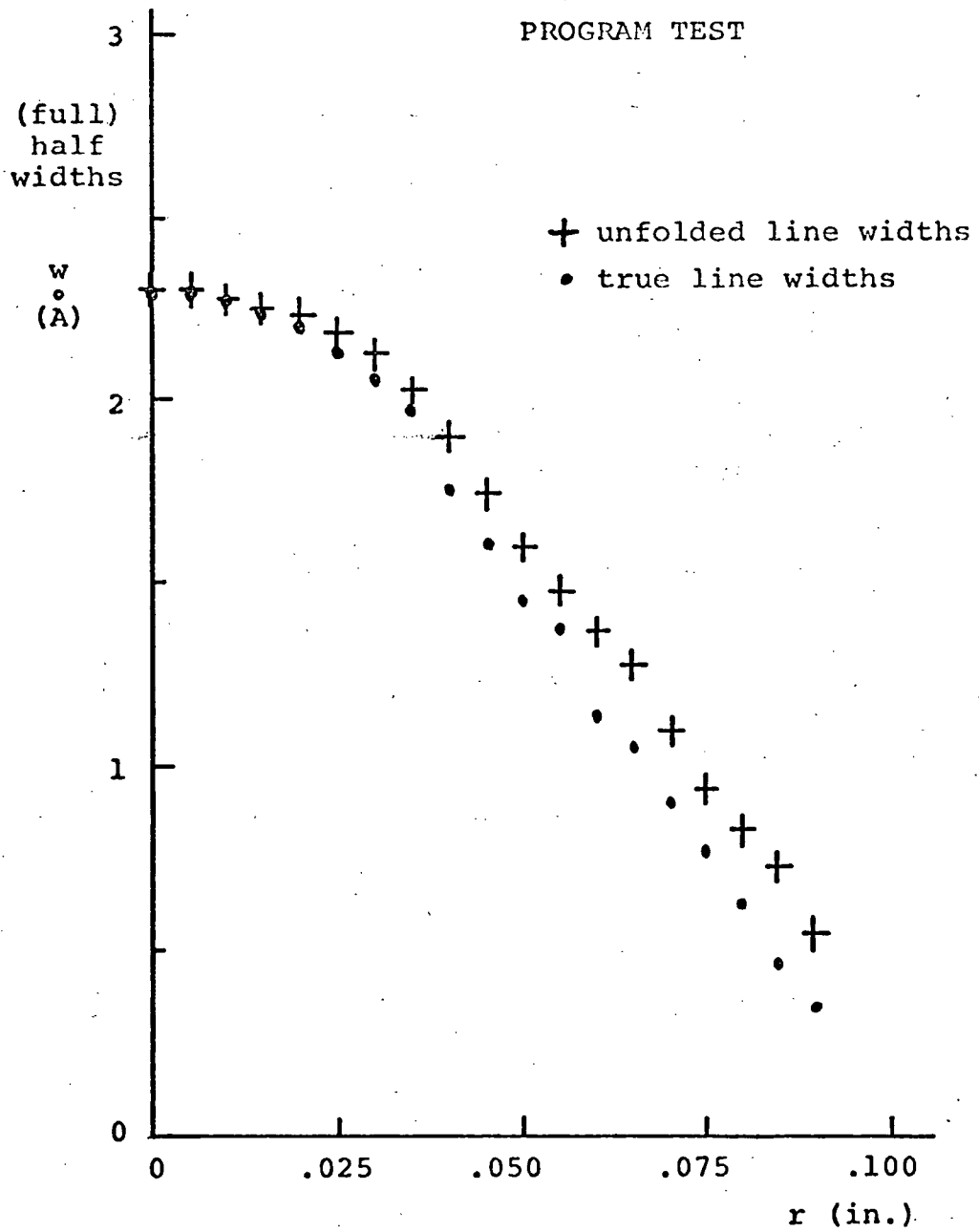
These profiles were integrated numerically along the "line of sight" at constant wavelength as given by Equation I-2.1 to obtain a set of twenty folded intensity profiles. Half of these (every other one) were then used as a set of "observed" profiles to which the entire interpolation and Abel inversion program was applied following experimental procedure. The resulting unfolded emission profiles were then compared with the original ones.

The results of this test showed very satisfactory reproduction of the original data on-axis, but a deterioration in reproduction with increasing radius. At larger radii, the emission profiles obtained by the unfolding program showed a definite spurious broadening. This is displayed in Figure I-2.6. The source of this error is the overestimation of the emission in the region where the intensity falls to zero as described above. Since the wings

of the outer lines lie in the region where the intensity is changing rapidly to zero, they are over-estimated and, consequently, the emission profile is broadened. This effect will later be referred to as "program" broadening where it causes width measurements at outer radii to be unreliable.

The unfolded shifts and total intensities were both found to compare with the original values within 5% out to a radius of  $r = 0.065$  in. with accuracies of about 2% on-axis. At larger radius, the effect of program broadening tended to over-estimate the total intensity as well as introduce an asymmetry into the line profile.

Figure I-2.6  
PROGRAM TEST



## CHAPTER 3 - PLASMA CONDITIONS

The atmospheric helium plasma jet (see Figure I-3.2) has become a very common plasma source for experiments at the University of B. C. Consequently, its construction, design and general performance are well documented (Morris, 1968; van der Kamp, 1968; Baldis, 1971; Stansfield, 1971; Morris, 1972) and would be unnecessarily repeated here. The precise conditions under which the jet is run will, however, vary from experiment to experiment and therefore do need documentation.

Hence, during experimental operation, the jet was monitored closely to assure stable and reproducible conditions. Then the electron density and the electron temperature were determined to provide the known plasma conditions under which the Stark shifts of several spectral lines were also determined.

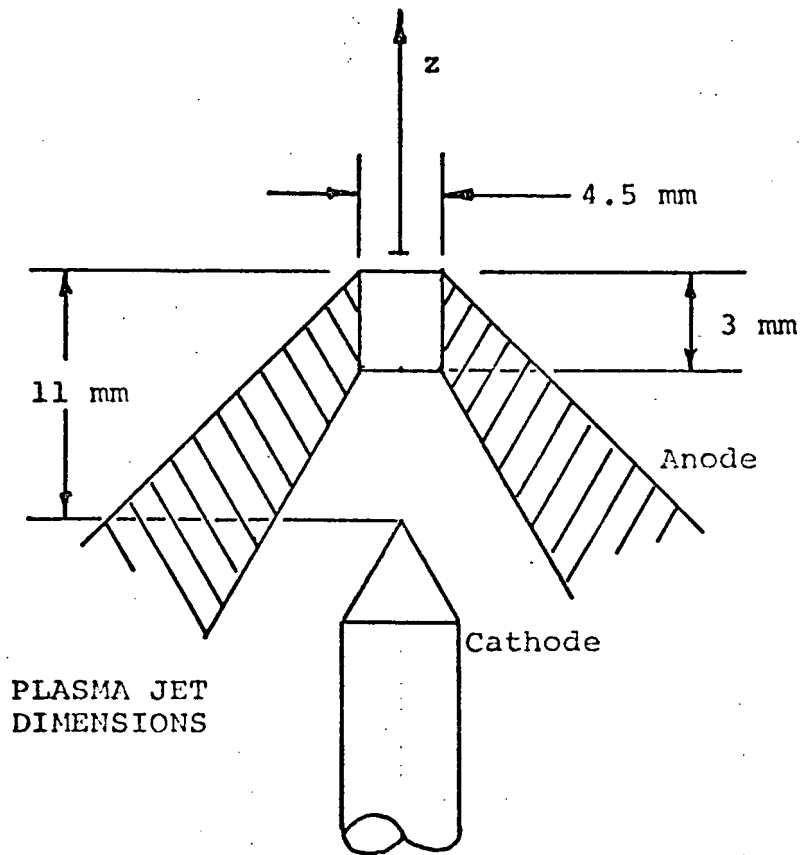
### A. EXPERIMENTAL OPERATING CONDITIONS OF THE PLASMA JET

The operating conditions presented in Figure I-3.1 apply within the stated accuracies to all subsequent measurements reported in this thesis.

Anode Dimensions	(see Figure I-3.2)
Cathode Position	(see Figure I-3.2)
Cold Gas Flow Rate	12.0 ± 0.6 liters/min.
Current	200 ± 20 amps.

Figure I-3.1  
OPERATING CONDITIONS OF THE HELIUM PLASMA JET

The arc current was supplied entirely by a bank of 12 lead-acid batteries. Four batteries were connected in series (forming a group) and three of these groups then connected in parallel. The resulting bank had a nominal voltage of 48 volts, (depending on the state of charge) and the capability of producing a flat, direct current with a fall rate of about 2 amps/min. at a discharge current of 200 amps. Because of the time required to take one set of data, this fall rate produced the only source of uncertainty in the current as quoted in Figure I-3.1. Following each experimental run, the batteries were recharged using a rectifier type d.c. welding supply.



### EXPERIMENTAL APPARATUS

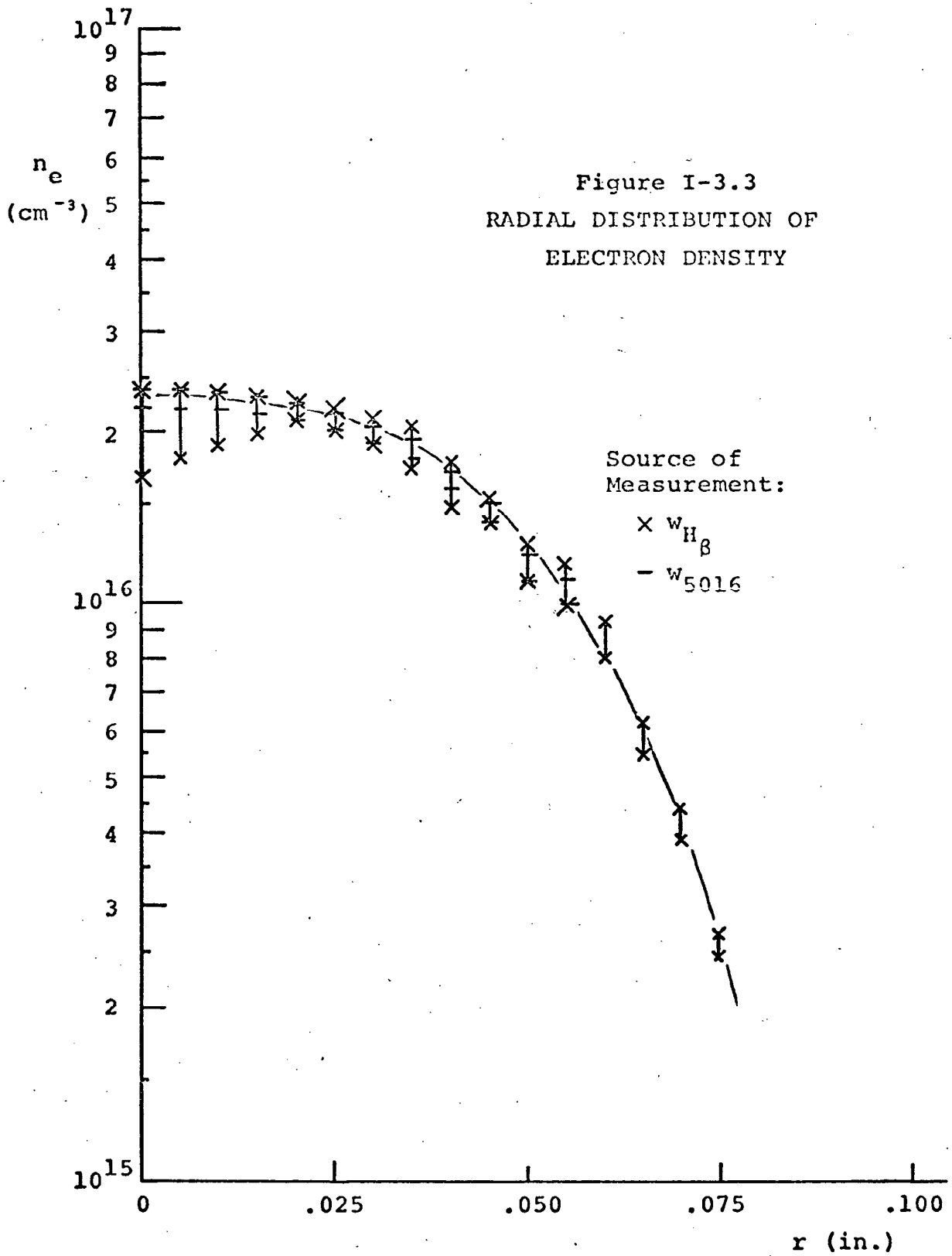
Figure I-3.2  
THE PLASMA JET

## B. ELECTRON DENSITY MEASUREMENTS

Since the general spectroscopic procedure of the experiment yielded local emission profiles for the observed spectral lines, and because of the well trusted calibration data, line broadening was chosen as the means of determining the spatial distribution of electron density in the plasma jet.

In order to use the  $H_{\beta}$  (4861A) line width as a direct and independent measure of electron density, a small amount of hydrogen (0.1% of He flow) was mixed with the cold helium flow. The line was easily detected and broad enough that the instrument width of the monochromator was negligible except at the very extremities of the flame. The observed intensity profiles were recorded and unfolded to obtain the local emission profiles according to the procedure detailed in Chapter I-2. The widths of the unfolded emission profiles (see Appendix I, Figure AI-1) were then used to calculate the radial distribution of electron density,  $n_e(r)$ , using Figure II-1 in Appendix II. These results are presented in Figure I-3.3.

Although the emission profiles were determined to a much greater accuracy than is apparent from the width measurements, uncertainty in determining the half intensity value was caused by an equivalent uncertainty in estimating the background level. This background -- due to the wing of the nearby strong line HeI 4921 -- changed significantly over the observed region of  $H_{\beta}$ . Near the center of the jet where HeI4921 was strongest and  $H_{\beta}$  widest, this uncertainty was largest. Toward the edge of the flame, the uncertainty became much less important. This situation is expressed by the large on-axis error bars for the  $H_{\beta}$  points on Figure I-3.3 which (for  $H_{\beta}$ ) represent absolute limits of uncertainty.



Future measurements using this technique can avoid the background difficulty by scanning the same wavelength region with and then without the added hydrogen. This will allow very accurate determination of the background level and will significantly reduce the uncertainties in  $n_e$  near the axis.

To assure that the addition of hydrogen had no significant effect on the electron density of the plasma, both of the lines HeI 5016 and HeI 4921 were examined with and without the added gas. Since the widths of both of these lines are quite sensitive to electron density, changes in their widths with and without hydrogen would reveal any changes in electron density due to the addition of hydrogen. It was found that the amount of hydrogen added for scanning  $H_\beta$ , the width changes of these lines indicated a reduction in electron density of less than 3%. With a large increase in the amount of hydrogen added, significant reduction in  $n_e$  was observed.

However, no quantitative data for this observation were taken.

A very nice feature of the  $H_\beta$  line is the fact that its width is (very nearly) independent of electron temperature making its width alone a direct measure of electron density (see Appendix II, Figure AII-1). Since this feature is also displayed by HeI 5016 (as can be seen in Appendix II, Figure AII-2), it too was used as a direct measure of  $n_e(r)$ . The line was scanned, unfolded, the half-widths measured at various radii (see Appendix I, Figure AI-2) and the resulting widths translated into the radial distribution of electron density using the values of width as calculated by Griem (Figure AII-2). These points are also plotted on Figure I-3.3 along with the values determined from  $H_\beta$ .

The major contribution to the error bars for the HeI 5016 points come from the uncertainty in the electron temperature. The size of the error bars reflects the limitation on the assumed temperature range (2,500 °K to 20,000°K). This allows a generous margin for error as will be seen in the section following.

For radii greater than about .055 in., the width of HeI 5016 estimates a much higher electron density than  $H_{\beta}$ . This is to be expected since both instrument broadening and "program" broadening become a problem as the width of HeI 5016 is reduced in the cooler regions of the flame. (Both of these broadening mechanisms have been considered in the last section of Chapter I-2.) In these cooler, outer regions of the flame,  $H_{\beta}$  is a much more reliable measure of electron density and therefore, the values obtained from HeI 5016 were rejected. On axis, however, the determinations of  $n_e$  by both methods agree as expected with HeI 5016 giving the least uncertain results.

With these considerations in mind, the most reasonable distribution of electron density was chosen and is indicated by the solid line in Figure I-3.3.

To have complete faith in these measurements of  $n_e(r)$  (and in some of the following temperature measurements), it was necessary to dispel the possibility that another mechanism was broadening these lines to a significant degree. Beside the instrument and "program" broadening mentioned earlier, the only real possible culprits could have been self-absorption and van der Waals broadening. Resonance broadening was ruled out because none of the states of the lines examined is connected to the ground state by an allowed transition thus disallowing any resonant interaction of the excited neutrals with ground state neutrals. Both Doppler and natural

broadening can be dismissed with a hand-wave because of the overwhelming effect of Stark broadening under the conditions encountered in the jet ( $w_{\text{Doppler}} < 0.1\text{\AA}$ ;  $w_{\text{natural}} < 0.001\text{\AA}$ ;  $w_{\text{Stark}} \approx 1\text{\AA}$ ).

The magnitude of the contribution to the line widths due to van der Waals broadening was estimated according to Griem's approximation using a neutral temperature of  $5,000^\circ\text{K}$  and a neutral density of  $10^{18}\text{ cm}^{-3}$ . The resulting (full) half-width was of the order  $10^{-2}\text{\AA}$  and thus was considered negligible in comparison with the Stark contribution to the line width for all of the lines examined.

The degree of self-absorption was examined for each line by two methods. Firstly, using approximate plasma conditions, the optical depth at the center of each line was calculated (using Griem's formula) and compared with the scale length (1 mm) of the plasma jet. For all of the lines examined in this work, the ratio of optical thickness to plasma scale length was less than 0.1 indicating that observed line widths were within 3% of the true widths of the unabsorbed lines (see Cooper, 1966).

Since Griem's formulation for the calculation of optical thickness involves an LTE assumption which was probably not upheld in the helium jet, it was desirable to establish by another, independent method that the plasma was truly optically thin to these lines. Thus, the second technique for examining the extent of self-absorption was experimental.

For this purpose, an additional lens was placed on the optical axis of the system in such a way as to collect light emitted by the plasma into the acceptance cone of the monochromator but in the opposite direction. A mirror then directed this light back through the same lens and plasma into the collecting lens and monochromator (see Figure I-3.4). Each spectral line was scanned with and without the rear optics and the ratio of the two signals calculated over a number of points along the profile.

Appreciable self-absorption would have been detected as an increase in this ratio in the region of the line center as compared with the same ratio for the wings of the line. With a measurement accuracy of 2%, no change in this ratio was observable for all of the lines used in the experiment.

In both of the above tests, the strong line HeI 5876 showed measurable self-absorption. Consequently, it was not chosen as an experimental line. In retrospect, this was an oversight since the shift of this line could nevertheless have been measured. The results of this measurement would have been interesting because of the exceptionally strong temperature dependence that the shift of this line exhibits.

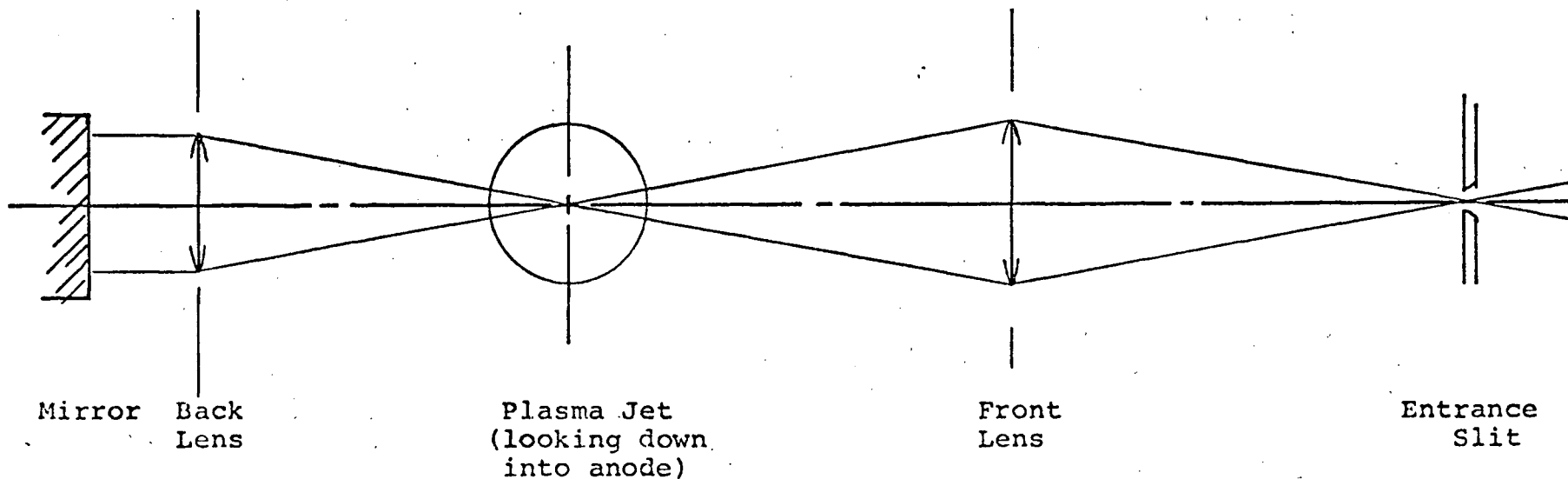


Figure I-3.4

OPTICAL SYSTEM FOR EXAMINATION OF SELF-ABSORPTION

### C. MEASUREMENT OF ELECTRON TEMPERATURE

One of the attractive features of using Stark shifts (as opposed to widths) as a diagnostic technique derives from the rather strong temperature dependence displayed by the shifts of some spectral lines.

The feature is, of course, the possibility of using the shifts as a measure of electron temperature, especially in the lower temperature range ( $T_e < 30,000^\circ\text{K}$ ) where other techniques become limited.

This feature has two ramifications for the present experiment. Firstly, it means that some estimate of electron temperature is required before any reasonable conclusions can be made about the accuracies of calculated shifts. Secondly, it means that the number of techniques available for measuring  $T_e$  will be fairly restricted since this is most certainly in the low range mentioned earlier.

In fact, to be very pessimistic, the list of spectroscopic techniques which cannot be used is quite long:

1. Since no continuum radiation is observable in the helium plasma, absolute continuum, relative continuum or line to continuum measurements are ruled out;
2. Since no HeII lines are observable, measurements of relative intensities of HeI and HeII lines are impossible;

3. With maximum upper level energy separations of only about 0.5 electron Volts for the observable HeI lines, relative intensity measurements using these lines result in temperatures with intolerably large uncertainties;
4. Since Stark broadening is the overwhelming mechanism determining the shapes of the spectral lines, there is no hope of extracting the Doppler component as a means of measuring the neutral atom kinetic temperature. Even if this were possible, one would still be left with the difficult task of relating this temperature to the kinetic temperature of the electrons.

Before considering the techniques that are still available for measuring  $T_e$  in this plasma, it will be useful to extract one piece of information from the absence of observable HeII radiation.

Assume the line HeII 4686 could not have been observed had its peak intensity given a system response of 1 millivolt. Assume also, that its (half) half-width was about  $0.5 \text{ \AA}$ . (Both of these assumptions over-estimate the presence of the line.) The peak on-axis response of the line HeI 5876 was about 2 volts and its (half) half-width was about the same ( $0.5 \text{ \AA}$ ). Since the relative response of the system for the two regions of the spectrum (4686 to 5876) was about 2, the maximum total intensity ratio of the two lines ( $I_{4686}/I_{5876}$ ) was of the order  $10^{-4}$ . According to Mewe (1967), for an electron density in the region  $2 \times 10^{16} \text{ cm}^{-3}$ , this puts the maximum electron

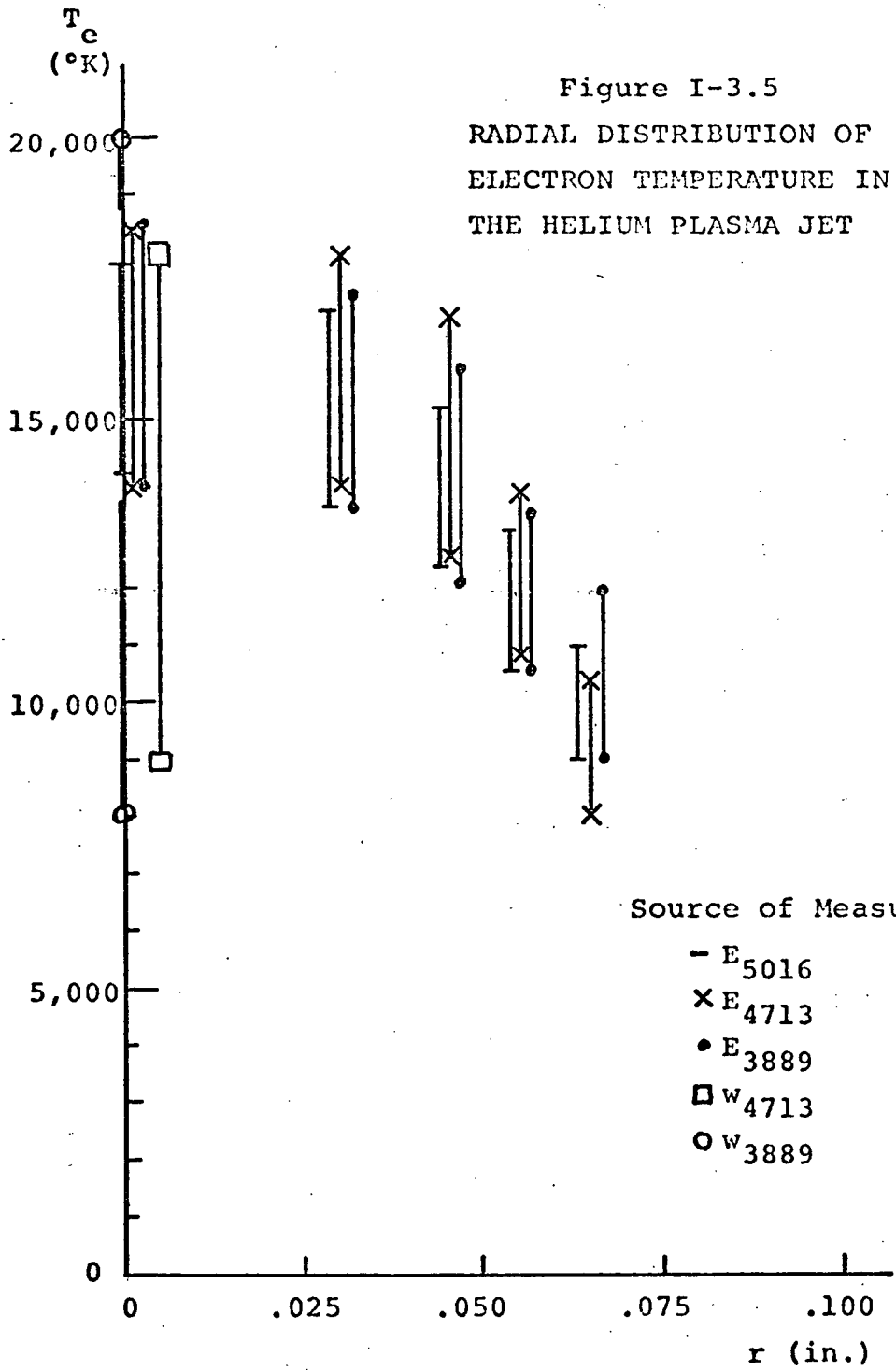
temperature at about  $20,000^{\circ}\text{K}$ . Thus, one can conclude that the absence of observable HeII radiation indicates the electron temperature is below  $20,000^{\circ}\text{K}$ .

Without the presence of continuum or HeII radiation, two possible spectroscopic techniques are left for determination of the radial distribution of  $T_e$ . They are: Stark width measurements at known electron density; and the absolute measurement of total emission coefficients of HeI lines.

The Stark widths of some neutral helium lines depend much more strongly on electron temperature than others. For the lines observed in this experiment, HeI 3889 and HeI 4713 were used for this purpose. The measured widths of these lines (see Appendix I, Figures AI-3 and AI-4) were translated into electron temperatures using Griem's calculations (loc.cit) and the measured radial distribution of electron density (Figure I-3.3).

As with the widths of HeI 5016, the near-axis temperatures derived from HeI 4713 can be considered reliable while the predominantly "program" broadened emission profiles for larger radii gave temperatures that were too high. Consequently, only values close to  $r=0$  are presented in Figure I-3.5.

The line HeI 3889, being much narrower than HeI 4713, is slightly broadened by the instrument function ( $0.2 \text{ \AA}$ ) even on-axis. This introduces a systematic error which tends to slightly over-estimate the on-axis temperature.



This is taken into account with the placing of the error bar for the on-axis value plotted in Figure I-3.5 as obtained from this line. Since the width of HeI 3889 becomes insensitive to  $T_e$  beyond 12,000°K, the upper limit of this error bar cannot really be established. Its termination at 20,000°K is allowed, however, by the absence of HeII lines as previously argued. The off-axis temperature determinations are not used from this line because of the increased effect of instrument broadening plus the addition of "program" broadening.

At this point, even though the determination of  $T_e$  is sketchy and certainly not spatially complete, it can be concluded that the maximum (on-axis) electron temperature falls in the region  $8,000^\circ\text{K} \leq T_e \leq 20,000^\circ\text{K}$ .

The other technique available for determination of  $T_e$  was the absolute measurement of total emission coefficient for a spectral line of known atomic parameters. The general procedure for this measurement is to:

1. Determine the system response,  $k_{\lambda_0}$  (as defined in Equations I-2.3 and I-2.4), using a source of known intensity;
2. Integrate the voltage emission profile to obtain:

$$S_{\lambda_0}(r) = \int_0^{\infty} u_{\lambda_0}(r, \lambda) d\lambda \quad \text{I-3.1}$$

3. Calculate the total emission coefficient  $E_{\lambda_0}(r)$  at radius  $r$  by:

$$E_{\lambda_0}(r) = k_{\lambda_0} S_{\lambda_0}(r) \quad \text{I-3.2}$$

4. If the emission coefficient for the line is a known function of electron temperature,  $E_{\lambda_0}(T_e)$ , then the radial distribution of electron temperature,  $T_e(r)$ , can be determined using the measured values  $E_{\lambda_0}(r)$ .

The dependence of the total emission coefficient on electron temperature as required in step 4, can in general be obtained by the following equation:

$$E_{\lambda_0}(T_e) = \frac{hc}{4\pi\lambda_0} A_{nm} n_m(T_e) \quad \text{I-3.3}$$

Where:  $n_m(T_e)$  is the population density of atoms in the upper state of the transition (with principal quantum number  $m$ );

$A_{nm}$  is the probability (per second) for electronic transitions from the upper state  $m$  to the lower state  $n$  resulting in radiation at wavelength  $\lambda_0$ .

Assuming one uses a line for which the transition probability is well established, the problem of calculating the emission coefficient reduces to the calculation of the population density of atoms in the upper state of the transition. In general, this is not a simple procedure and requires detailed knowledge of the rates and cross-sections for many types of plasma interactions.

To avoid the details of this calculation, one usually hopes the dominant plasma processes can be accurately approximated by one of the more tractable plasma models such as the LTE (Local Thermodynamic Equilibrium) model, the Corona model or the CR (Collisional-Radiative) model.

In high density arcs where collisional processes dominate radiative processes, the best choice of those available is the LTE model. If this one applies, the principle of detailed balance is invoked and the distribution of population densities among the energy levels is determined by the laws of statistical mechanics without requiring knowledge of atomic cross-sections. Instead, the distribution depends entirely on local values of temperature and pressure.

Under the conditions of complete LTE and known pressure, the upper state population density can be calculated by using the well known Saha-Boltzmann equation in conjunction with Dalton's Law of partial pressures. However, because of the large energy differences that characterize the helium level structure, it is unlikely, for the low temperatures of the jet, that such a state of complete LTE exists.

In particular, it is unlikely that the ratio of the population density of atoms in each excited state to the population density of atoms in the ground state can be characterized by a temperature in the Boltzmann factor which also characterizes the chemical equilibrium through the Saha equation plus the total pressure through the sums of partial pressures.

This expectation has been reinforced by two previous experiments (van der Kamp, 1968; Morris, 1968), both of which indicated that the helium jet could not be described by a complete LTE model.

It is possible, however, that a state of partial LTE will exist between the populations of the higher excited states of the neutral helium atoms and the population of the ground state helium ion -- the balance of which depends on the temperature of the electrons. This likelihood is due to the smaller energy differences involved which are roughly the same magnitude of the energy of the electrons. Since collisions with electrons is the dominant process for excitation and ionization it is the kinetic energy (or temperature) of the electrons which characterizes the state of equilibrium of the population densities dependent on these processes.

The Saha-Boltzmann equation (see Appendix IV) then gives the ratio between the product of the electron and ion populations and the excited state neutral population densities. Since the number of doubly ionized helium atoms is insignificant, the electron and ion densities must be identical to satisfy charge neutrality. Thus the excited state population density for a particular level can be determined in terms of the electron density and electron temperature.

Mewe (1967), using data on ionization cross sections from Drawin (1964), investigated the accuracy to which the

excited state population density can be predicted in this manner at various values if  $T_e$  and  $n_e$  for levels down to those with principal quantum number 3 in helium. Although his table terminates at an electron temperature of 2.75 eV, a reasonable extrapolation of his results predicts that estimation of the excited state population density using this technique should result in an error not exceeding about 25% for electron densities in the range  $10^{15} \text{ cm}^{-3}$  to  $10^{16} \text{ cm}^{-3}$  and down to levels with a principal quantum number of 3.

This estimate is in agreement with Griem's criterion for population densities within 10% of LTE which is satisfied at  $T_e = 1 \text{ eV}$  and  $n_e = 1.7 \times 10^{14} \text{ cm}^{-3}$  for all energy levels with principal quantum number 3 or greater.

It is also safe, at these low temperatures, to assume that the partition function for the ion can be approximated by the degeneracy of the ion ground state -- there being little chance of exciting the ion 41 eV to even its first excited state with 2 eV electrons.

Calculations of the excited state population, normalized by the degeneracy of the state,  $(n_m(T_e, n_e)/g_m)$  are presented in Appendix IV. These cover a range of electron densities from  $5 \times 10^{15} \text{ cm}^{-3}$  to  $3 \times 10^{16} \text{ cm}^{-3}$  and electron temperatures up to 20,000°K and for levels with principal quantum numbers 3 and 4.

In order to measure the radial distribution of upper state population densities in the plasma jet and thus obtain the radial distribution of electron temperature, the absolute response of the (optical and electrical) system was determined at the wavelengths of each of the neutral helium lines. This was done using a tungsten

ribbon lamp as a source of known intensity. The temperature of the lamp,  $T_W$ , was measured with an optical pyrometer and found to be  $(2.57 \pm .05) \times 10^3 \text{ }^\circ\text{K}$  at a lamp current of  $16.00 \pm .01$  amps.

The absolute response,  $k_{\lambda_0}$ , was then calculated from:

$$k_{\lambda_0} = \frac{1}{v_W(\lambda_0)} \epsilon_W(\lambda_0, T_W) I_B(\lambda_0, T_W) \quad \text{I-3.4}$$

where:  $\epsilon_W(\lambda, T)$  is the emissivity of tungsten (deVos, 1954)

$I_B(\lambda, T)$  is the black body function given by

$$I_B(\lambda, T) = \frac{2hc^2}{\lambda^5} \frac{1}{\exp\left\{\frac{hc}{\lambda kT}\right\} - 1} \quad \text{I-3.5}$$

$v_W(\lambda)$  is the system response (in volts) to the tungsten lamp at wavelength  $\lambda$ .

The voltage emission profiles for each of the experimental lines were integrated at various radii as described in Appendix III and multiplied by  $k_{\lambda_0}$  as in Equation I-2.4 to obtain the radial dependence of the emission coefficient,  $E_{\lambda_0}(r)$ . This was then used along with the appropriate transition probability (Wiese et. al. 1966),  $A_{nm}$ , upper level degeneracy,  $g_m$ , and physical constant values in Equation I-3.3 to obtain the radial dependence of the upper level population density,  $n_m(r)$ , and subsequently the ratio  $n_m(r)/g_m$ .

Since the radial distribution of electron density is known by previous measurements (Figure I-3.3), the radial distribution of electron temperature was easily obtained by using the graph of  $n_m(T_e)/g_m$  (in Appendix IV) corresponding to the principal quantum number,  $m$ , of the upper level of the specified spectral line.

The results of this procedure are displayed (along with the previous temperature findings) on Figure I-3.5 for the three lines HeI 3889, HeI 4713, and HeI 5016. The error bars arise from the absolute intensity calibration due to the uncertainty in the temperature of the tungsten lamp.

As was discussed in the previous section, the plasma was found to be optically thin for all of these spectral lines. Hence, there was no significant error introduced by self-absorption.

## CHAPTER I-4 STARK SHIFT MEASUREMENTS AND COMPARISONS

### A. SHIFT MEASUREMENTS

The radial distribution of the shift of the spectral lines was determined by using the wedge technique described in Part II of this thesis. Since the emission profiles already represented the profiles due to local (radial) conditions in the plasma, there was no necessity to apply the Abel transform to the wedge technique as described in Chapter II-5 of Part II. Also, since the detailed local emission profiles were held in computer storage, there was no need to use a real wedge mounted on the monochromator. Instead, an "ideal" wedge with transmission  $T(\lambda') = \lambda'$  was "manufactured" and applied to the emission profiles using the computer to calculate:

$$s_{\lambda_0}(r) = \int_0^W \lambda' u_{\lambda_0}(r, \lambda') d\lambda' \quad \text{I-4.1}$$

The shift ratio  $R_{\lambda_0}(r)$  for the line at nominal wavelength at various radii was calculated by:

$$R_{\lambda_0}(r) = \frac{s_{\lambda_0}(r)}{S_{\lambda_0}(r)} \quad \text{I-4.2}$$

Where:

$$S_{\lambda_0}(r) = \int_0^W u_{\lambda_0}(r, \lambda') d\lambda' \quad \text{I-4.3}$$

In order to determine the wavelength shift from the radial distribution of shift ratio, a helium Geissler tube was used to obtain the unshifted ratio  $R'_{\lambda_0}$  for the appropriate line. The radial distribution of shift,  $\Delta\bar{\lambda}_M(r)$  (in wavelength units), was then calculated by:

$$\Delta\bar{\lambda}_M(r) = C \Delta R_{\lambda_0}(r) \quad \text{I-4.4}$$

where:  $\Delta R_{\lambda_0}(r) = R_{\lambda_0}(r) - R'_{\lambda_0}$

and  $C = D_\lambda/b$   
 $D_\lambda$  is the dispersion of the system,  
 $b$  is the slope of the wedge ( $b = 1$  here).

The results of this procedure are presented in Figures I-4.1, I-4.2 and I-4.3 for each of the neutral helium lines examined.

The uncertainties shown on these graphs come from two major sources. The first of these involves the accuracies of the factors of Equation I-4.4. Taking the logarithm of this equation and then taking differentials gives:

$$\frac{d[\Delta\lambda_M(r)]}{\Delta\lambda_M(r)} = \frac{dC}{C} + \frac{d[\Delta R_{\lambda_0}(r)]}{\Delta R_{\lambda_0}(r)} \quad \text{I-4.5}$$

where:  $d[\Delta R_{\lambda_0}(r)] = dR_{\lambda_0}(r) + dR'_{\lambda_0}$

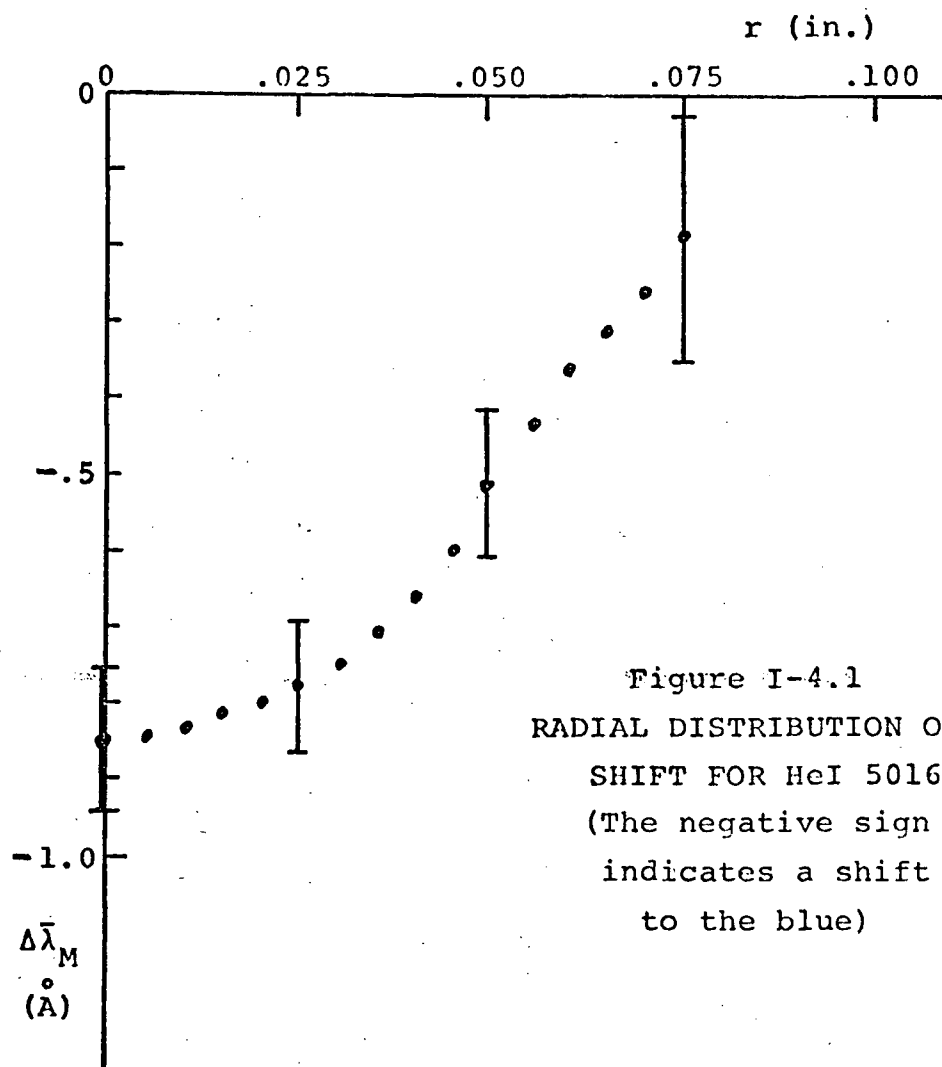


Figure I-4.1  
RADIAL DISTRIBUTION OF  
SHIFT FOR HeI 5016  
(The negative sign  
indicates a shift  
to the blue)

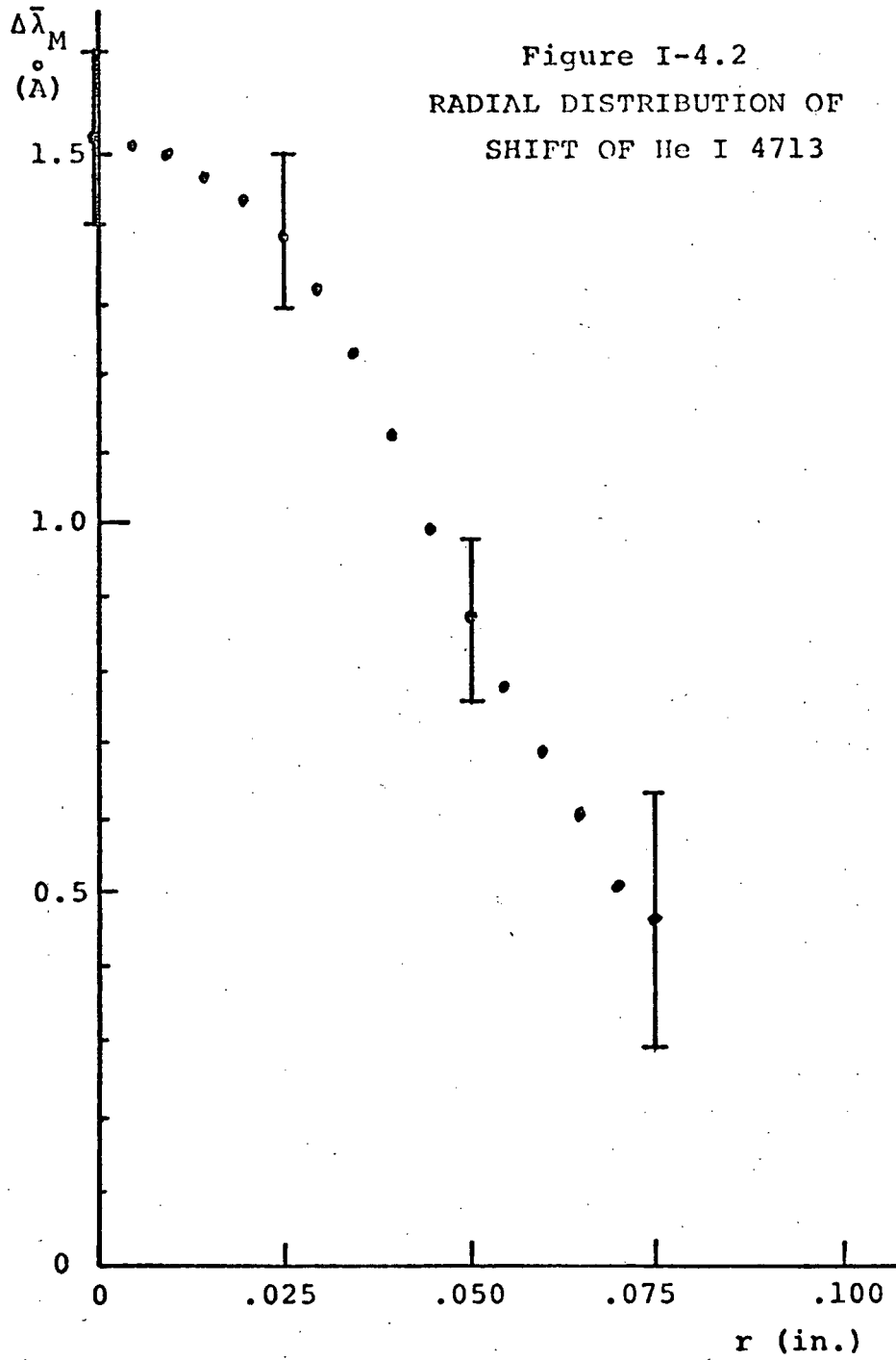
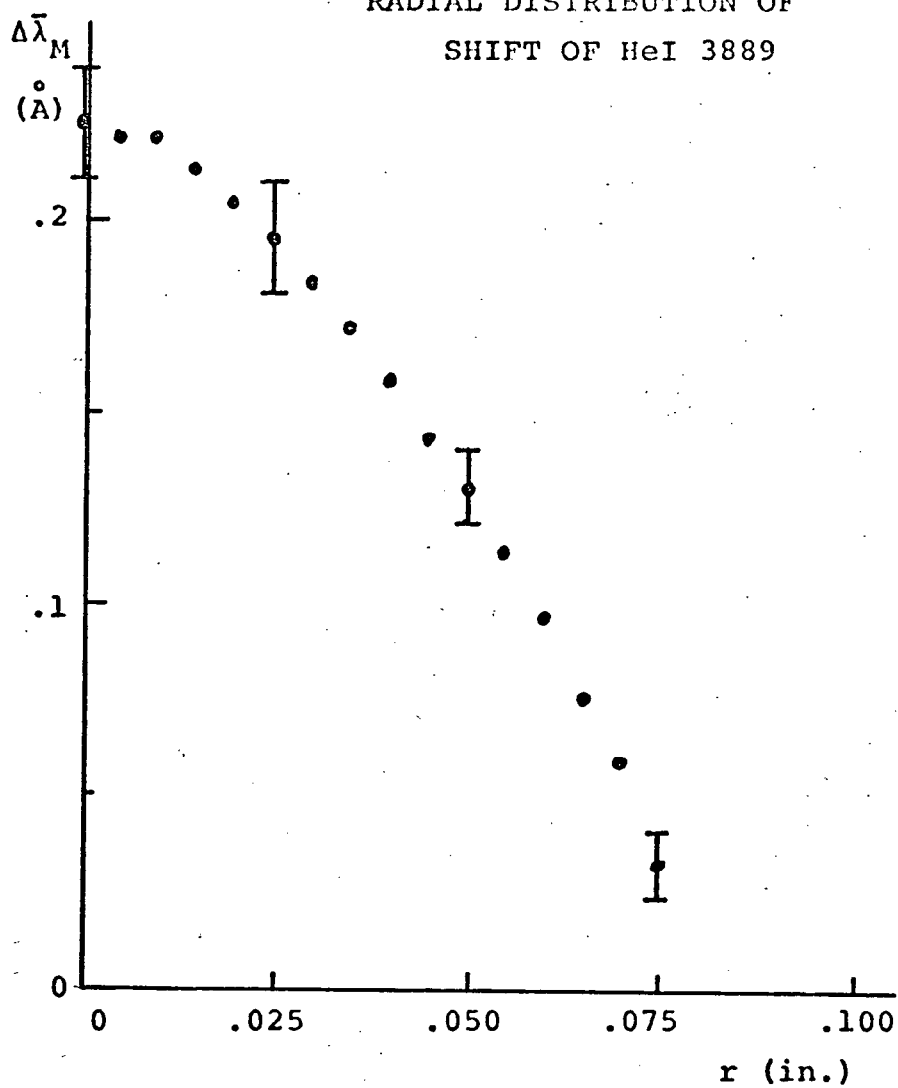


Figure I-4.3  
RADIAL DISTRIBUTION OF  
SHIFT OF HeI 3889



Since the slope of the wedge was perfectly known, the uncertainty in  $c$  was given entirely by the calibration of the wavelength scanning system. This was determined to an accuracy of 4% by scanning across well known spectral lines (such as the sodium D lines) that were conveniently separated in wavelength.

Fluctuations in the signals used to calculate  $R_{\lambda_0}(r)$  contributed negligible error. However, at large radii where the lines became weak, this ratio was sensitive to the background level due to stray light and photomultiplier dark current. On-axis, the ratio was negligibly sensitive to background as expected. The measurement of the Geissler ratio,  $R_{\lambda_0}$ , contributed less than 2% uncertainty to the measurements even at minimum values of  $\Delta R_{\lambda_0}(r)$ .

The other major source of uncertainty was introduced by the skewness of the lines. Whereas the measurement errors described above were relatively small on-axis (about 5%) and increased with radius, the error introduced by skewness was large on-axis (up to 5% of the (half) half-width) and decreased to being negligible at large radii. The estimation of this error is discussed in the following section.

Because the detailed emission profiles were required for the determination of the radial distribution of the electron temperature and density, it was possible to use these to determine the local shifts of the lines. Thus it was not necessary to use a "real" wedge to obtain these shifts. Also, since the profiles were already unfolded, it was not necessary to apply the Abel unfolding of shifts as described in the next part of the thesis. If line widths were not required, however, these techniques would have represented a considerable economy of effort.

## B. COMPARISON OF MEASURED AND CALCULATED SHIFTS

Griem has calculated and tabulated the Stark shifts of the helium lines examined in this work. He also gives a formula to correct these shifts for the inclusion of ion broadening. However, his values give the interval between the unperturbed wavelength and the position of the intensity peak of the profile. Since ion broadening introduces skewness into the line profile, these shifts are not equal to the shift in the mean of the profile. Hence, a comparison of Griem's tabulated shifts with those measured by the wedge technique (which is sensitive to the mean) would be incongruous. Instead, it was necessary to extract the mean wavelength from the reduced Stark profiles derived by GBKO so that a logical comparison could be made.

With the quasi-static approximation for the ions and the impact approximation for electrons, the reduced Stark profiles for allowed transitions is given by:

$$j(x) = \frac{1}{\pi} \int_0^{\infty} \frac{W_{rG}(\beta) d\beta}{1 + (x - \alpha^{1/3} \beta^2)^2} \quad \text{I-4.6}$$

where:  $x = \frac{\lambda - \lambda_0 - d}{w}$  is a wavelength variable given in terms of the electron impact width and shift,  $w$  and  $d$ , and the unperturbed wavelength,  $\lambda_0$ .

$\beta$  is the electric field strength produced by a perturbing ion in terms of the Holtzmark field strength.

$w_{r_G}(\beta)$  is the distribution of the ion field calculated at neutral emitters (see Hooper, 1968)

$r_G$  is the Debye-shielding parameter evaluated in Appendix II.

$\alpha$  is the quasi-static ion broadening parameter tabulated by Griem.

Since the reduced profile is normalized, the mean  $\bar{x}_G$ , can be obtained by

$$\int_{-\infty}^{\bar{x}_G} j(x) dx = 0.5 \quad \text{I-4.7}$$

This was done for  $r_G = 0, .4, .8$  and  $\alpha = 0, .1, .2, .3, .4$ . An empirical fit was applied to these results (in analogous fashion to Griem's evaluation of  $d_{\text{total}}$ ) to obtain:

$$\bar{x}_G \approx 4.1\alpha(1 - 0.5r_G) \quad \text{I-4.8}$$

which reproduces the integrated quantities to an accuracy of 5% over the ranges  $0 \leq \alpha \leq 0.4$  and  $0 \leq r_G \leq 0.8$ .

The shift of the mean can then be determined in terms of the electron impact shift,  $d$ , and width,  $w$ .

$$\begin{aligned} \Delta\bar{\lambda}_G &= \lambda - \lambda_0 \\ &\approx \left[ \frac{d}{w} \pm 4.1\alpha(1 - 0.5r_G) \right] w \quad \text{I-4.9} \end{aligned}$$

This relationship was used to calculate the theoretical shifts presented in Figure I-4.4. The values of  $d/w$ ,  $w$ , and  $\alpha$  were determined from Griem's tabulations under the plasma conditions at several convenient radii established from Figures I-3.3 and I-3.5 at which points the shift of the mean was also measured by the wedge technique. The uncertainties shown on  $\Delta\bar{\lambda}_G$  come from the ranges of  $d/w$ ,  $w$ , and  $\alpha$  which correspond to the uncertainties in the electron density and temperature.

As mentioned in the previous section, it was necessary to establish the uncertainty of the measured shifts,  $\Delta\bar{\lambda}_M$ , introduced by the asymmetry of the line profiles. Obviously, this error could be large if the wavelength pass band used to examine the line (ie. the width of the wedge) was not centered around the mean of the distribution and did not extend very far out into the asymmetric, Lorentz wings. To estimate the size of this effect, the wedge technique was applied to the reduced profiles simulating the pass band and line positions encountered in the experiment. This was done by evaluating the integral:

$$\bar{x}_M = \int_{x_1}^{x_2} xj(x) dx \quad \text{I-4.10}$$

for various values of  $x_1$  and  $x_2$ . The resulting values of  $\bar{x}_m$  were then compared with the mean,  $\bar{x}_G$ , as calculated from Equation I-4.8. The difference between these quantities was calculated to give the uncertainty in terms of the line width:

$$d(\Delta\bar{\lambda}_M) = (\bar{x}_M - \bar{x}_G)w \quad \text{I-4.11}$$

r (in.)	$n_e$ ( $\text{cm}^{-3}$ )	$T_e$ ( $^{\circ}\text{K}$ )	$r_G$	$\lambda_0$ ( $\text{\AA}$ )	d/w	$w$ ( $\text{\AA}$ )	$\alpha$	$\Delta\bar{\lambda}_G$ ( $\text{\AA}$ )	$\Delta\bar{\lambda}_M$ ( $\text{\AA}$ )
0	$(2.3 \pm .1) \times 10^{16}$	16,000 $\pm$ 2,000	.39 $\pm$ .03	5016	-.31 $\pm$ .03	.89 $\pm$ .06	.18	-.80 $\pm$ .08	-.85 $\pm$ .10
				4713	.90 $\pm$ .05	1.15 $\pm$ .08	.11	1.45 $\pm$ .16	1.52 $\pm$ .10
				3889	.42 $\pm$ .03	.29 $\pm$ .01	.08	.20 $\pm$ .02	.23 $\pm$ .014
.030	$(2.0 \pm .1) \times 10^{16}$	15,500 $\pm$ 2,000	.38 $\pm$ .03	5016	-.32 $\pm$ .03	.77 $\pm$ .06	.18	-.71 $\pm$ .08	-.75 $\pm$ .10
				4713	.91 $\pm$ .05	1.00 $\pm$ .08	.10	1.24 $\pm$ .15	1.30 $\pm$ .10
				3889	.43 $\pm$ .03	.25 $\pm$ .01	.08	.17 $\pm$ .014	.19 $\pm$ .012
.045	$(1.5 \pm .1) \times 10^{16}$	14,000 $\pm$ 2,000	.38 $\pm$ .03	5016	-.34 $\pm$ .03	.57 $\pm$ .06	.15	-.48 $\pm$ .07	-.60 $\pm$ .10
				4713	.94 $\pm$ .05	.73 $\pm$ .08	.09	.90 $\pm$ .13	1.00 $\pm$ .12
				3889	.45 $\pm$ .03	.19 $\pm$ .01	.07	.13 $\pm$ .013	.143 $\pm$ .01
.055	$(1.0 \pm .1) \times 10^{16}$	12,000 $\pm$ 1,500	.41 $\pm$ .03	5016	-.37 $\pm$ .03	.39 $\pm$ .05	.15	-.33 $\pm$ .05	-.44 $\pm$ .15
				4713	1.00 $\pm$ .06	.47 $\pm$ .07	.09	.61 $\pm$ .12	.77 $\pm$ .12
				3889	.47 $\pm$ .03	.13 $\pm$ .01	.06	.087 $\pm$ .01	.113 $\pm$ .009
.065	$(6.0 \pm 1.) \times 10^{15}$	10,000 $\pm$ 1,500	.38 $\pm$ .03	5016	-.41 $\pm$ .04	.25 $\pm$ .05	.12	-.20 $\pm$ .05	-.30 $\pm$ .15
				4713	1.08 $\pm$ .07	.27 $\pm$ .06	.08	.36 $\pm$ .10	.60 $\pm$ .15
				3889	.52 $\pm$ .04	.08 $\pm$ .01	.05	.055 $\pm$ .01	.075 $\pm$ .009

Figure I-4.4 - COMPARISON OF MEASURED AND CALCULATED SHIFTS

The remaining contributions to the measurement uncertainties quoted in Figure I-4.4 have been discussed in the previous section.

From a comparison of the results presented in Figure I-4.4, one observes that under all plasma conditions and for each plasma line considered, the measured shifts,  $\Delta\bar{\lambda}_M$ , and the corresponding theoretical shifts,  $\Delta\bar{\lambda}_G$ , agree within the uncertainties of the measurements. While all of the measured shifts are slightly larger than theory predicts, the size of this discrepancy is not significant in this experiment. Confirmation of its existence would require slightly better accuracy in the measurements than is presented here.

These results lead one to the conclusion that the GBKO theory is generally reliable in predicting the shifts of the means of the isolated neutral helium lines. Or, more specifically, Equation I-4.9 can be used to calculate the wavelength separation between the unperturbed line and the mean wavelength at least within the accuracies attained here. This discovery allows one to replace Equation I-4.9 for Griem's equation for the total shift of the maximum:

$$d_{\text{total}} \approx \left[ \frac{d}{w} \pm 2.0\alpha(1 - 0.75r_G) \right] w \quad \text{I-4.12}$$

It is expected that Equation I-4.9 will prove to be more useful than Equation I-4.12 in view of the fact that the mean of a line profile can usually be measured more accurately than the position of the intensity peak -- especially when the shift and width are comparable in size.

PART II - DESIGN CRITERIA FOR APPLICATION OF THE WEDGE  
TECHNIQUE TO THE MEASUREMENT OF LINE SHIFTS

CHAPTER II-1 INTRODUCTION

The first Part of this thesis demonstrated how measurement of the shift of the mean of a Stark broadened spectral line could be a valuable plasma diagnostic tool. The wedge technique was used to perform these measurements. However, the application of this method is not restricted to Stark shifts, but applies to any situation where the shift in the mean of a reasonably isolated spectra line is of significance.

Because of this general applicability of the technique, it is presented here as a separate Part of the thesis. In this way, more relevant design criteria can be presented in detail (which would otherwise be superfluous) as an aid to those who desire to use the technique.

Initially, Ahlborn and Barnard (1966) proposed a shift measuring technique which used a pair of identical linear spatial filters or "wedges" mounted in the exit plane of a monochromator. The proposal was later investigated experimentally by Potter (1967).

During the course of this work, the technique was significantly improved so that only one wedge is required -- a feature which eliminates the need for an extended source. In addition, the technique has been extended to incorporate the measurement of local shifts in an inhomogeneous, cylindrically symmetric plasma (Ahlborn and Morris, 1969).

Thus, in the following pages, the general technique is described in detail along with the application to the cylindrical plasma as mentioned. To complete the discussion, the important design criteria are presented. These include the response of the technique to several different types of line profile, the resolution, the sensitivity, and the linearity of the technique.

## CHAPTER II-2: THE WEDGE TECHNIQUE (DESCRIPTION)

In a completely general fashion, the mean of an arbitrary spectral intensity distribution,  $i_1(\lambda)$ , may be defined by:

$$\bar{\lambda}_1 = \frac{\int_0^{\infty} \lambda i_1(\lambda) d\lambda}{\int_0^{\infty} i_1(\lambda) d\lambda} \quad \text{II-2.1}$$

If, for any reason, this distribution is altered to  $i_2(\lambda)$ , its new mean can be calculated in the same manner and the shift in the mean,  $\Delta\bar{\lambda}$ , determined by:

$$\Delta\bar{\lambda} = \bar{\lambda}_1 - \bar{\lambda}_2 \quad \text{II-2.2}$$

The following discussion will demonstrate that if the intensity distributions involved ( $i_1$  and  $i_2$ ) are restricted to isolated spectral lines, then the limits of integration in Equation II-2.1 can be altered in such a way that it is possible, in practice, to use this definition for measuring line shifts.

Consider a monochromator which has a plane half-silvered mirror mounted between the camera mirror and exit slit. (see Figure II-2.1). The mirror is situated such that it allows a fraction  $f_T$  of the light to reach the exit slit while reflecting the remaining fraction  $f_R$  90° up to an additional exit slit mounted so as to be optically

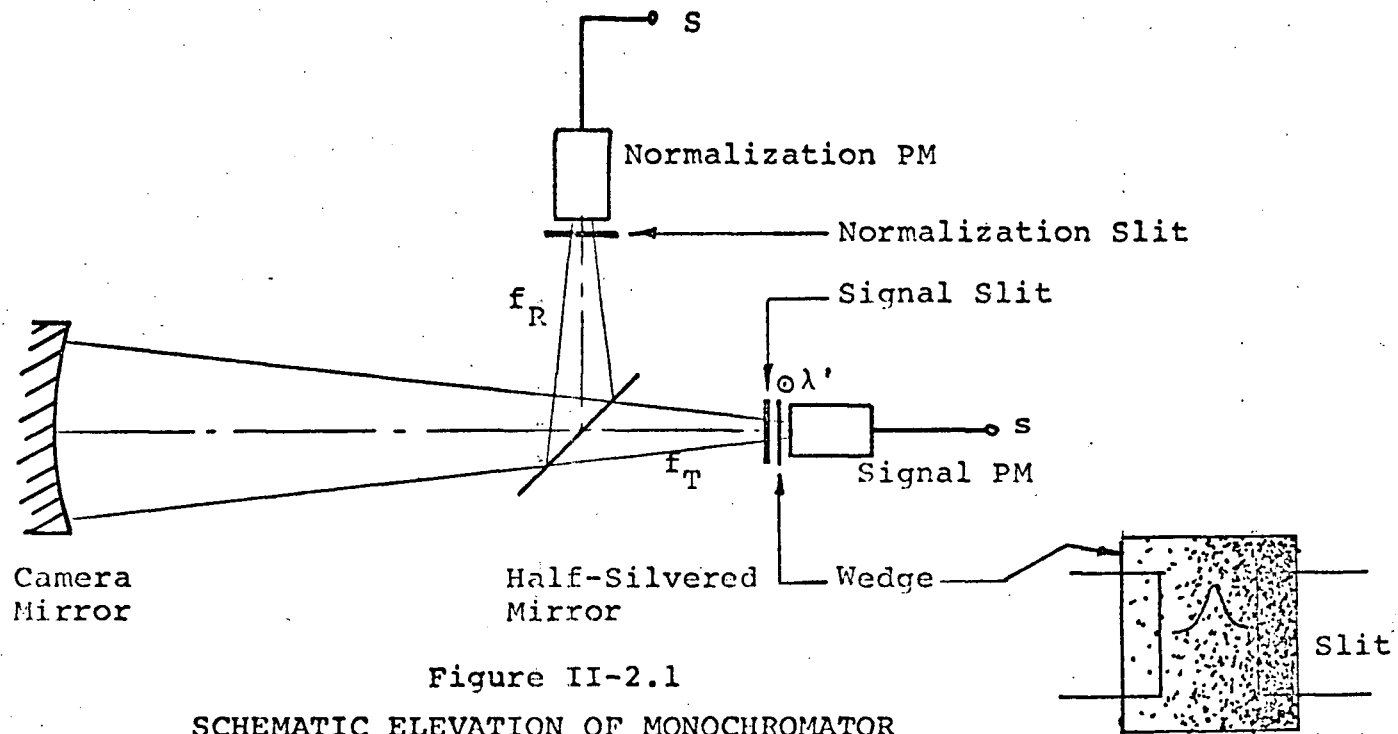


Figure II-2.1  
 SCHEMATIC ELEVATION OF MONOCHROMATOR

coincident with the first (usual) exit slit. Both of the exit slits are extremely wide. For the sake of convenience the new or upper exit slit will be referred to as the "normalization" slit while the lower or usual exit slit will be termed the "signal" slit. (The reasons for these choices of terminology will become clear in the ensuing discussion.)

Since both exit slits are optically coincident, they have identical wavelength coordinate systems which will be designated by  $\lambda'$ . Over the extent of these exit slits, this variable is related to the true wavelength,  $\lambda$ , by the linear transformation:

$$\lambda = D_{\lambda} \lambda' + C_{\lambda} \quad \text{II-2.3}$$

where:  $D_{\lambda}$  is the dispersion of the monochromator and  $C_{\lambda}$  is the constant that defines the zero of the  $\lambda'$  coordinate system.

The variable  $\lambda'$ , of course, is a spatial coordinate running perpendicular to each slit.

A spectral line whose unobstructed intensity distribution in the lab frame could be specified by  $\psi(\lambda')$  will now have a distribution  $f_R \psi(\lambda')$  in the normalization slit and  $f_T \psi(\lambda')$  in the signal slit.

If a photomultiplier tube is placed above the normalization slit, its output signal to the above spectral line will be:

$$S = K f_R \int_0^w \psi(\lambda') d\lambda' \quad \text{II-2.4}$$

where:  $K$  is the response of the normalization photomultiplier tube. The limits of integration in Equation II-2.4,  $0$  and  $W$ , are given by the edges of the normalization slit.

Over the signal slit, suppose there is a neutral density filter whose transmission across the slit width is described by  $T(\lambda')$ . A photomultiplier with response,  $k$ , located behind the slit and observing the spectral line through this filter would produce a signal:

$$s = kf_T \int_0^W T(\lambda') \psi(\lambda') d\lambda' \quad \text{II-2.5}$$

Assume, further, that the filter between the signal slit and signal photomultiplier has a linear spatial dependence of transmission. In particular (see Figure II-2.2):

$$\begin{aligned} T(\lambda') &= b\lambda' & 0 \leq \lambda' \leq W & \quad \text{II-2.6} \\ &= 0 & W \leq \lambda' \leq 0 & \end{aligned}$$

where:  $b$  is the slope of the wedge.

In practice, this distribution of transmission is approximated by a wedge manufactured from a photographic plate which has been exposed and developed so as to give a transmission as indicated by the dotted curve in Figure II-2.2. Since the wedge overlies the exit slit, the resulting transmission falls to zero at and beyond the edges of the slit.

It can be seen that this transmission defines the zero of the  $\lambda'$  coordinate system at the slit edge where the ideal wedge has zero transmission.

Also, the slope of the wedge,  $b$ , is given by the width of the exit slit,  $W$ , and the maximum transmission of the wedge,  $T_{\max}$  by the equation:

$$b = \frac{T_{\max}}{W} \quad \text{II-2.7}$$

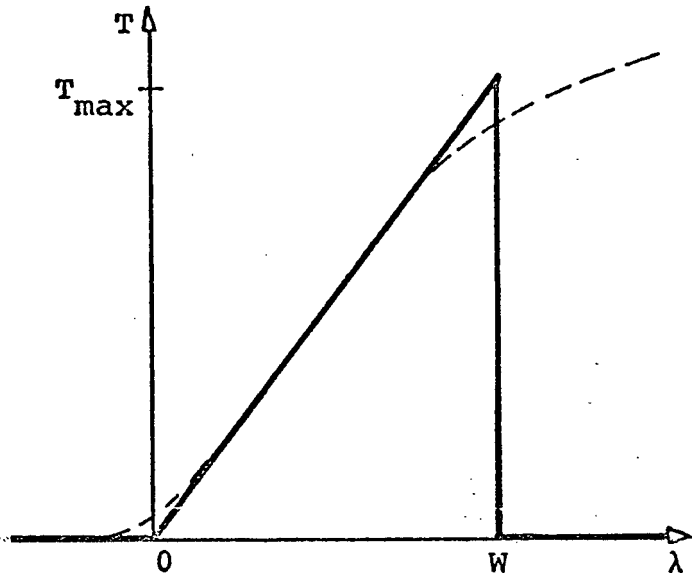


Figure II-2.2

WEDGE TRANSMISSION

From Equations II-2.4 and II-2.5, the ratio of the photo-multiplier signals is given by:

$$\frac{S}{R} = \frac{k f_T b \int_0^W \lambda' \psi(\lambda') d\lambda'}{K f_R \int_0^W \psi(\lambda') d\lambda''} \quad \text{II-2.8}$$

If the intensity distribution is non-zero over the range  $0 \leq \lambda' \leq W$  and vanishes for all wavelengths outside this range, then the true mean of the distribution in the laboratory coordinates,  $\bar{\lambda}'$ , is exactly equal to the ratio of the limited integrals as appear in Equation II-2.8.

Therefore:

$$\bar{\lambda}' = \frac{\int_0^{\infty} \lambda' \psi(\lambda') d\lambda'}{\int_0^{\infty} \psi(\lambda') d\lambda'} = \frac{\int_0^W \lambda' \psi(\lambda') d\lambda'}{\int_0^W \psi(\lambda') d\lambda'} \quad \text{II-2.9}$$

Thus, by substituting  $\bar{\lambda}'$  for the ratio of the integrals on the right hand side of Equation II-2.8, one finds that the ratio of the photomultiplier signals can be related to the mean of the intensity distribution by:

$$\frac{s}{S} = \frac{Kf_T b}{Kf_R} \bar{\lambda}' \quad \text{II-2.10}$$

Or, equivalently, the mean is measured by:

$$\bar{\lambda}' = \frac{Kf_R}{Kf_T} \frac{1}{b} \frac{S}{s} \quad \text{II-2.11}$$

From the coordinate transformation expressed in Equation II-2.3, the mean of the intensity distribution in true wavelength units is then:

$$\bar{\lambda} = D_{\lambda} \bar{\lambda}' + C_{\lambda} \quad \text{II-2.12}$$

Since  $C_\lambda$  is the wavelength at which the wedge has zero transmission, its value will depend on the position of the wedge with respect to the exit slit and on the wavelength setting of the monochromator. In practice, it is usually not convenient to measure this constant precisely. However, if one measures differences of means while keeping  $C_\lambda$  constant, then there is no need to determine it. An arbitrary shift under this circumstance will be given by:

$$\Delta\bar{\lambda} = D_\lambda \Delta\bar{\lambda}' \quad \text{II-2.13}$$

Or, in terms of measured quantities:

$$\Delta\bar{\lambda} = D_\lambda \frac{Kf_R}{kf_T} \frac{1}{b} \left( \frac{s_1}{S_2} - \frac{s_1}{S_2} \right) \quad \text{II-2.14}$$

where it has been assumed that the shift in the mean was caused by the intensity distribution shifting from  $\psi_1(\lambda')$  to  $\psi_2(\lambda')$  both of which are zero for  $W \leq \lambda' \leq 0$ .

## CHAPTER II-3 LINEARITY

One of the principal advantages of this technique for measuring line shifts is its independence of fluctuations in the shape, or width, of the intensity distribution. Ideally, however, this condition holds only when the intensity distribution lies completely within the wavelength range  $0 \leq \lambda' \leq W$  and when the wedge transmission is strictly linear over the same region. As with all experimental techniques whose ideal conditions do not strictly hold in reality, these two conditions are rarely, if ever, completely met. Therefore, it is valuable to consider the response of the system under a variety of non-ideal circumstances to gain an estimate of the error introduced by the failure of these conditions.

### A. EDGE EFFECTS

The first of the two categories of non-linearities can be termed "edge effects" because the response of the system is affected by the position of the integration limits with respect to the mean position and shape of the intensity distribution. Since these effects involve the integrals only, it is convenient to ignore the constants (such as the wedge slope and the system responses) considering only the ratio,  $R$ , defined as:

$$R = \frac{\int_0^W \lambda' \psi(\lambda') d\lambda'}{\int_0^W \psi(\lambda') d\lambda'} \quad \text{II-3.1}$$

measured in wavelength units.

As a simplest example, consider an intensity distribution which is rectangular with height  $A'$  and total width  $2\beta'$  around its mean wavelength  $\lambda_0'$ . In other words (see Figure II-3.1):

$$\begin{aligned} \psi(\lambda') &= A' & \lambda_0' - \beta' \leq \lambda' \leq \lambda_0' + \beta' & \quad \text{II-3.2} \\ &= 0 & \text{elsewhere} & \end{aligned}$$

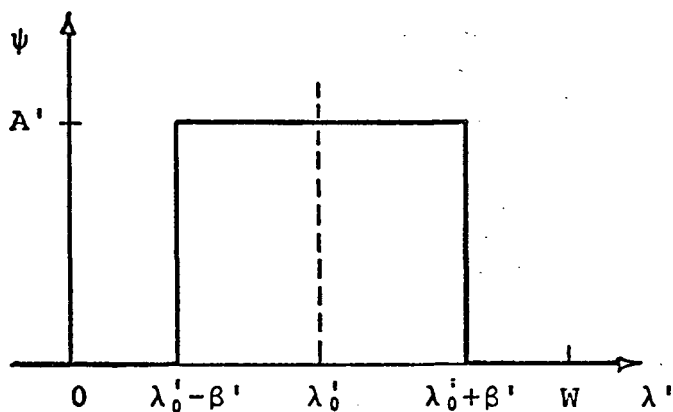


Figure II-3.1

A RECTANGULAR INTENSITY PROFILE

Substituting this intensity distribution into Equation II-3.1 and calculating the integrals gives:

$$R = \lambda_0 \quad \beta' \leq \lambda_0' \leq W - \beta' \quad \text{II-3.3a}$$

$$= \frac{1}{2}(\lambda_0' + \beta') \quad 0 \leq \lambda_0' \leq \beta' \quad \text{II-3.3b}$$

$$= \frac{1}{2}(W + \lambda_0' - \beta') \quad W - \beta' \leq \lambda_0' \leq W \quad \text{II-3.3c}$$

From this result, it can be seen that when the mean of the distribution is too close to the edges of the slit as is the case in Equations II-3.3b and II-3.3c, the ratio shows a dependence on the width of the distribution.

It should be noted here that for this rectangular distribution and as well as for the following distributions, it is always assumed that the full width of the intensity distribution never exceeds the width of the wedge.

Symbolically that is:

$$2\beta' \leq W \quad \text{II-3.4}$$

In order to eliminate the explicit dependence of the ratio on the wedge width,  $W$ , it is convenient to define the nondimensional ratio:

$$R_W = \frac{R}{W} \quad \text{II-3.5}$$

This variable indicates the relative position of the mean of the distribution compared to the position of the wedge. A value of  $R_W = 0$  indicates the mean of the distribution lies at  $\lambda' = 0$  while a value of  $R_W = 1$  indicates the mean lies at  $\lambda' = W$ . Therefore,  $R_W = 0.5$  indicates that the mean of the distribution lies at the exact midpoint of the wedge  $\lambda' = W/2$ .

It will also be convenient to define two more dimensionless variables:

- The dimensionless mean;

$$x_0 = \frac{\lambda_0'}{W} \quad \text{where} \quad 0 \leq x_0 \leq 1 \quad \text{II-3.6}$$

- The dimensionless width;

$$x_\beta = \frac{W}{\beta'} \quad \text{where} \quad 1 \leq x_\beta \leq \infty \quad \text{II-3.7}$$

The first of these, the dimensionless mean, is just a change of the wavelength coordinate system to a system which is independent of the actual width of the wedge. Thus, if the dimensionless ratio,  $R_W$ , has a value of 0.5, then the dimensionless mean also has a value of 0.5 since the mean of the distribution lies exactly at the midpoint of the wedge.

The dimensionless width variable gives an indication of the width of the spectral distribution with respect to the width of the wedge. Actually, it should be called the dimensionless inverse width since it is inversely proportional to the actual width of the distribution. Thus, as  $x_\beta$  gets large, the spectral distribution becomes very narrow in comparison with the width of the wedge. In the limit when  $x_\beta$  tends to infinity, the distribution approaches something like an impulse (or delta) function. Low values of  $x_\beta$  indicate spectra distributions which are comparable in width to the width of the wedge. Since, in this discussion, it is always assumed that the (full)

width of the spectral distribution never exceeds the width of the wedge, the lower limit of  $x_\beta = 1$  is imposed. The width of the distribution,  $\beta'$ , which appears here is not a well defined quantity; rather, it is some convenient scale width of the distribution which will vary with each distribution. Most commonly, however, this will indicate the (half) half-intensity width of the spectral profile.

Using the above definitions, the ratios specified earlier for the rectangular distribution become:

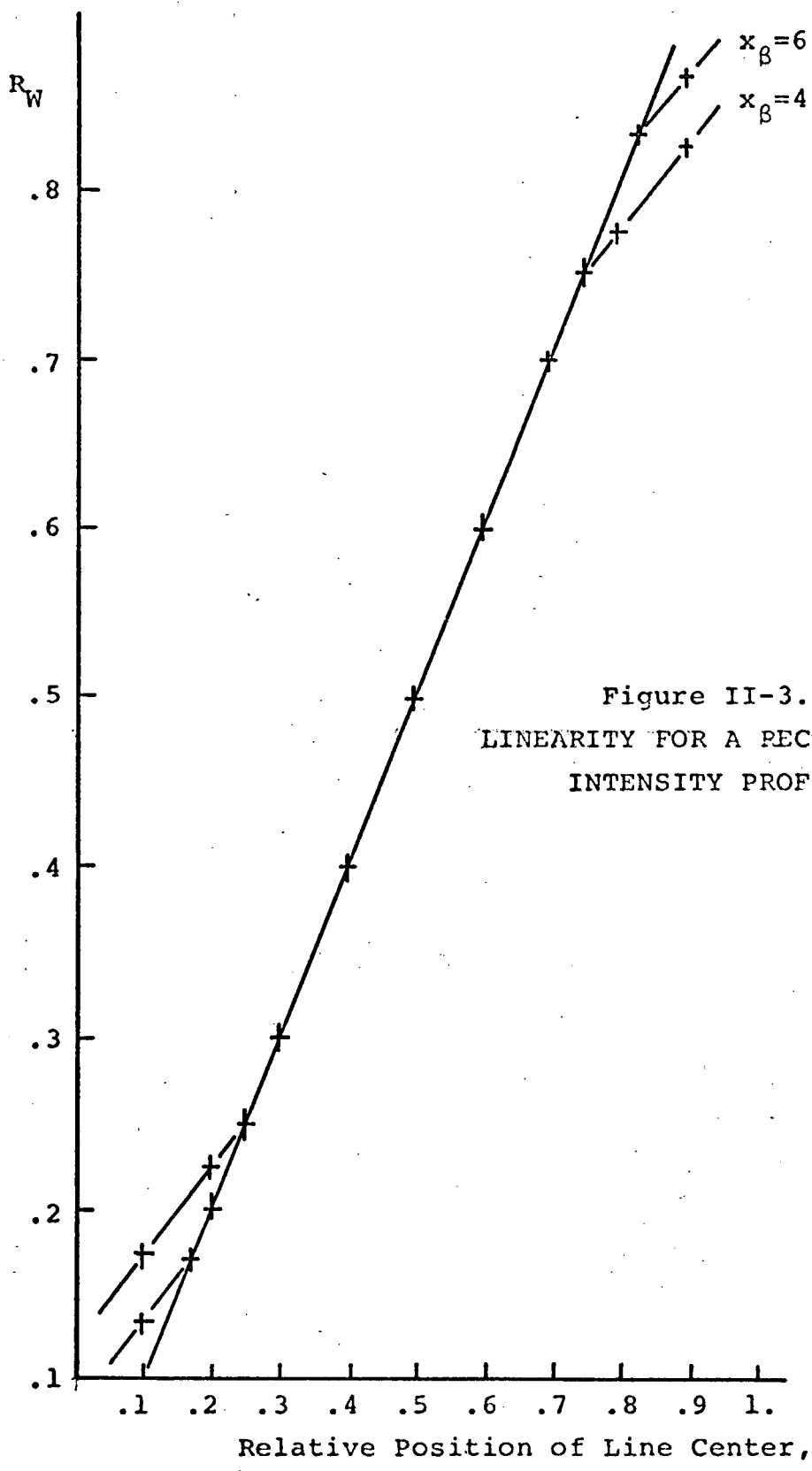
$$R_W = x_0 \quad \frac{1}{x} \leq x_0 < 1 - \frac{1}{x_\beta} \quad \text{II-3.8a}$$

$$= \frac{1}{2} \left( x_0 + \frac{1}{x_\beta} \right) \quad 0 \leq x_0 < \frac{1}{x_\beta} \quad \text{II-3.8b}$$

$$= \frac{1}{2} \left( 1 + x_0 - \frac{1}{x_\beta} \right) \quad \frac{1}{x_\beta} \leq x_0 \leq 1 \quad \text{II-3.8c}$$

The results of this calculation are plotted in parametric form in Figure II-3.2 with  $R_W$  given as a function of  $x_0$  for several values of  $x_\beta$ .

This graph indicates the usefulness of the non-dimensional treatment of the variables. If one were designing an experiment where the shift of a rectangular distribution were to be measured, Figure II-3.2 shows the range of mean position and width which will give reliable results. For instance, if the distribution has a (half) width which is one quarter of the width of the wedge (or conversely), one is using a wedge which has a width four times the (half) width of the distribution then the ratio  $R_W$ , and thus the experimental measurement, will give linear and reliable results when the mean of the profile lies in the middle region of the wedge as indicated by the curve  $x_\beta = 4$  in Figure II-3.2.



It can also be noted from Figure II-3.2 that if the mean of the rectangular profile is located on the wedge such that  $x_0$  lies in the region 0.25 to 0.75., the distribution can reduce its width without affecting the ratio. However, if the mean were located at  $x_0 = 0.2$  and the width reduced, changing  $x_\beta$  from 4 to 6, then the ratio (and thus the measurement) would change spuriously with no change in the mean of the intensity distribution.

Thus, a graph such as that shown in Figure II-3.2 provides an indication of the useful range of the wedge technique for any set of experimental circumstances. To be useful in experimental design procedure, one needs to know the range of shift expected and the range of width fluctuation expected. It will then be possible, using these calibration graphs, to choose the narrowest (and thus the steepest) wedge to assure the most sensitivity while not endangering the required linearity of the response.

Another profile of interest is the Gaussian distribution:

$$\psi(\lambda') = A' \exp \left[ - \frac{1}{2} \frac{(\lambda' - \lambda'_0)^2}{\beta'^2} \right] \quad \text{II-3.9}$$

If this distribution is inserted into the integrals of Equation II-3.1 and  $R_W$  calculated in terms of  $x_0$  and  $x_\beta$  as was done with the rectangular distribution, the result is:

$$R_W = \frac{1}{x_\beta} \frac{\exp\{-\frac{u_1^2}{2}\} - \exp\{-\frac{u_2^2}{2}\}}{\int_{u_2}^{u_1} \exp\{-\frac{u^2}{2}\} du} + x_0 \quad \text{II-3.10}$$

$$\text{where: } u_1 = \frac{W - \lambda'_0}{\beta'} = x_\beta (1 - x_0)$$

$$u_2 = -\frac{\lambda'_0}{\beta'} = -x_\beta x_0$$

The demonimator of this equation has been evaluated using integral tables for a standard normal distribution for three values of  $x_\beta$ . The results are plotted in parametric form in Figure II-3.3.

It can be seen from these results that, unlike the situation with the rectangular distribution, there is no region of  $x_0$  where the ratio is independent of  $x_\beta$ . Instead, as  $x_\beta$  becomes larger (or the line width smaller) its effect on the ratio decreases. This situation will be discussed more fully later.

A similar, but more pronounced, effect is observed if the intensity distribution reaching the wedge is Lorentzian:

$$\psi(\lambda') = \frac{A'}{1 + \left\{ \frac{\lambda' - \lambda'_0}{\beta'} \right\}^2} \quad \text{II-3.11}$$

In this case the dimensionless ratio as calculated by Equations II-3.1 and II-3.5 is:

$$R_W = \frac{1}{x_\beta} \frac{\{\log[1+(x_\beta - x_\beta x_0)^2] - \log[1+(-x_\beta x_0)^2]\}}{\{\tan^{-1}[x_\beta - x_\beta x_0] - \tan^{-1}[-x_\beta x_0]\}} + x_0 \quad \text{II-3.12}$$

This ratio has been evaluated for several values of  $x_\beta$  and the results plotted in Figure II-3.4.

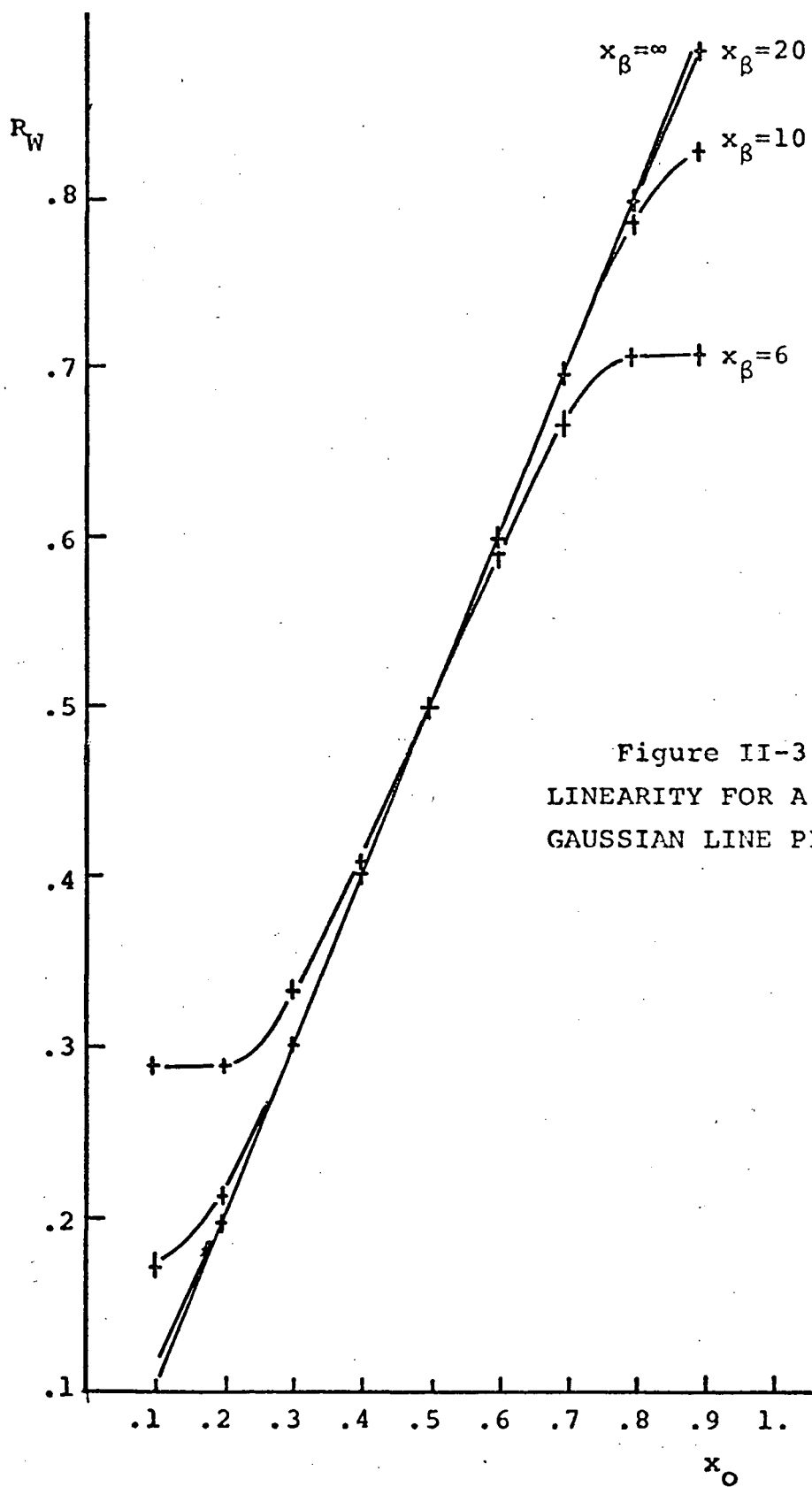


Figure II-3.3  
LINEARITY FOR A PURE  
GAUSSIAN LINE PROFILE

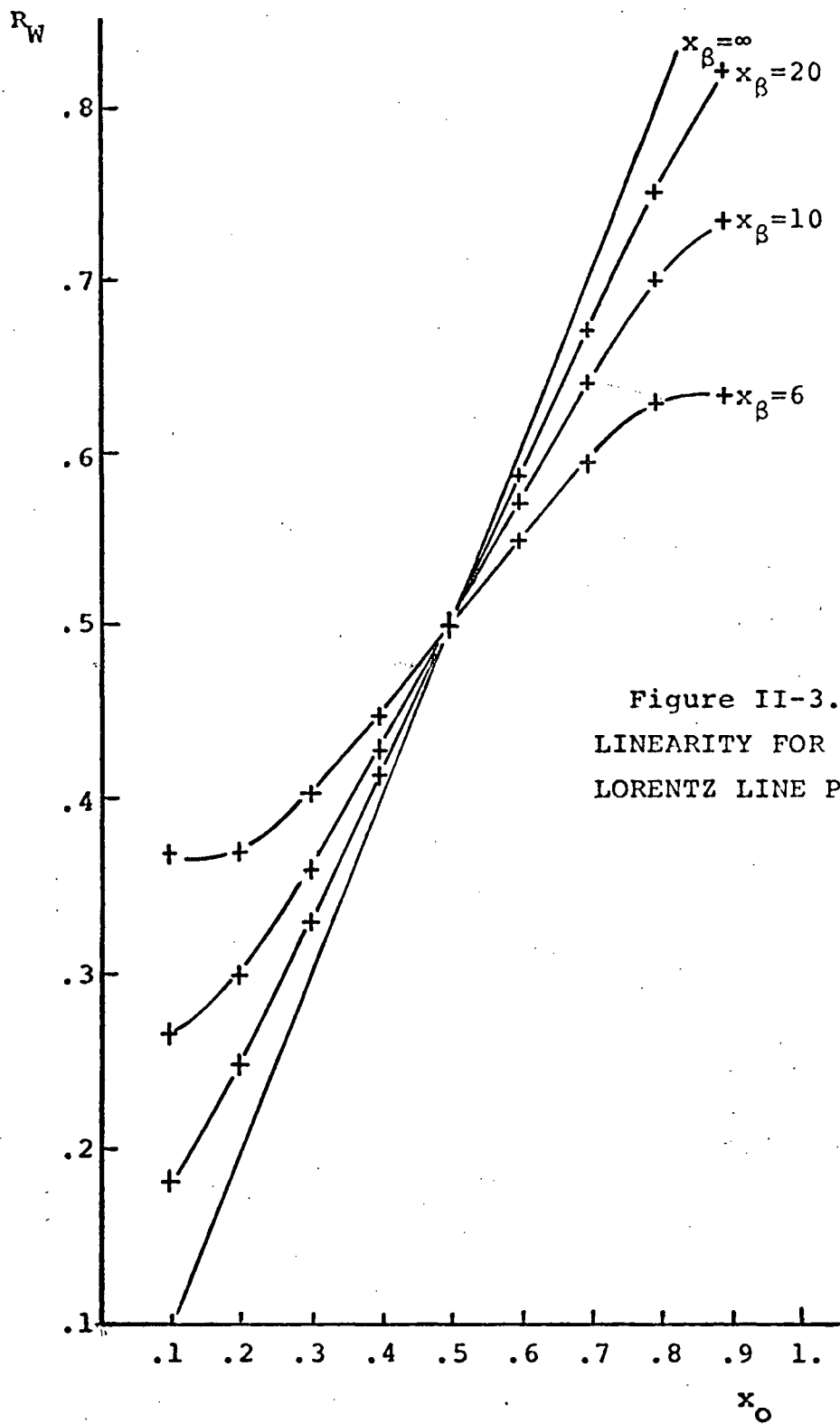


Figure II-3.4  
LINEARITY FOR A  
LORENTZ LINE PROFILE

It can be seen from Figures II-3.3 and II-3.4 that although the ratio depends on line width, the ratio is very close to being a linear function of the mean position in the region  $0.2 \leq x_0 \leq 0.8$  with a slope that depends on  $x_\beta$ . Thus, instead of dealing with the clumsy expressions shown in Equations II-3.10 and II-3.12, it is possible to write the ratio as:

$$R_W = m(x_\beta) [x_0 - 0.5] + 0.5 \quad \text{II-3.13}$$

Then the slope,  $m$ , can be written as an approximate function of  $x_\beta$  for the two important line profiles treated above. For Gaussian and Lorentzian profiles respectively:

$$m_G(x_\beta) = 1 - \frac{120}{x_\beta^4} \quad \text{II-3.14a}$$

$$m_L(x_\beta) = 1 - \frac{2.8}{x_\beta} \quad \text{II-3.14b}$$

These relationships can now be easily used for design criteria given some prior knowledge of the type of profile, the changes in both width and mean, and the accuracy required.

Another situation which is common to experimental circumstances and also results in the violation of the assumption of vanishing intensity at the edges of the wedge, occurs when the line profile being studied overlies continuum. This is similar to the cases of the Gaussian and Lorentzian line profiles in that the line has high "wings" that cause the slope of  $R_W(X_0)$  to differ from unity. This situation can be represented by an intensity distribution of the form:

$$\psi(\lambda') = A'\psi_0(\lambda') + B' \quad \text{II-3.15}$$

where the arbitrary line profile is normalized:

$$\int_0^W \psi_0(\lambda') d\lambda' = 1$$

with mean:

$$\int_0^W \lambda' \psi_0(\lambda') d\lambda' = \lambda'_0$$

and sits on a background of continuum radiation of height  $B'$ . In this case,  $A'$  represents the total intensity of the line.

By substituting Equation II-3.15 into Equation II-3.1 and calculating the dimensionless ratio, it is found that:

$$R_W = \frac{1}{1 + \alpha W} x_0 + \frac{1}{2} \frac{\alpha W}{1 + \alpha W} \quad \text{II-3.16}$$

where the new variable:

$$\alpha = \frac{B'}{A'} \quad \text{II-3.17}$$

is the ratio of the background level to the total intensity of the line.

Thus, the ratio with background present can be written as Equation II-3.13 with the slope criterion

$$m_B = \frac{1}{1 + \alpha W} \quad \text{II-3.18}$$

It is worth noting that the effect of continuum depends not only on the relative background level,  $\alpha$ , but also on the absolute width of the wedge,  $W$ . This is, of course, intuitively obvious since a wider wedge will pass a greater amount of continuum radiation and thus have a greater effect on the measurement.

Although the presence of continuum can be very disruptive of shift measurements, its effects can be completely offset. Theoretically this is accomplished by defining and using the new ratio,  $R_B$ , in place of the integral ratio  $R$ , where:

$$R_B = \frac{\int_0^W \lambda' \psi(\lambda') d\lambda' - \int_{-W}^0 \lambda' \psi(\lambda') d\lambda'}{\int_0^W \psi(\lambda') d\lambda' - \int_{-W}^0 \psi(\lambda') d\lambda'} \quad \text{II-3.19}$$

Provided  $\psi_0(\lambda')$  is zero in the region  $-W \leq \lambda' \leq 0$ , by virtue of Equation II-3.15 and the independence of the continuum level on wavelength, this ratio becomes:

$$R_B = \frac{\int_0^W \lambda' \psi_0(\lambda') d\lambda'}{\int_0^W \psi_0(\lambda') d\lambda'} \quad \text{II-3.20}$$

which is exactly the ratio for the line profile alone without the influence of continuum.

In practice, this method of eliminating the effects of background means that one more set of readings must be taken with the grating screw of the monochromator set so the line is moved out of the region of the wedge. While the range of integration in Equation II-3.19 of this second measurement are shown as  $-W$  to  $0$ , they could just as easily have been  $-2W$  to  $W$  or  $W$  to  $2W$  or any other set of values outside the line profile range (but not so far that the continuum might have changed). If the line profile involved is Lorentzian, it is wise to be well away from the line to avoid subtracting the remainder of the Lorentz wing.

## B. WEDGE NON-LINEARITIES

The second of the two categories of non-linearities results from possible non-linearities of the wedge transmission. More precisely, if the wedge transmission cannot be accurately described by equation 2.6, the ratio and thus the mean measurement will not be independent of fluctuations in the width of the line profile.

Since wedges are normally manufactured using a photographic process, this situation could arise through two mechanisms: small scale film granularity or large scale non-linearity caused by the generally logarithmic response of photographic emulsions.

In order to eliminate the first of these two problems, one usually uses a low grain, high contrast emulsion. This effectively reduces the granularity to zero, however, it also tends to accentuate the second of the two. (For a description of the manufacture of wedges and the importance of emulsion contrast, see Potter, 1967).

Whereas it is difficult to anticipate accurately in a general way what these large scale non-linearities might be, it is possible to make a reasonable assumption about a possible real transmission curve and examine the resulting effect of width fluctuations on the measurement ratio.

In this regard, assume that instead of Equation II-2.6, the transmission of the wedge can be described by:

$$T(\lambda') = b\lambda' - c\lambda'^2; \quad 0 \leq \lambda' \leq W, \quad c > 0 \quad \text{II-3.21}$$

$$= 0 \quad \text{elsewhere}$$

so that the signal ratio defined in Equation II-2.8 becomes:

$$\frac{S}{S} = \frac{kf_T}{Kf_R} b[R - c'R'] \quad \text{II-3.22}$$

where: R is given by Equation II-3.1;

$$R' = \frac{\int_0^W \lambda'^2 \psi(\lambda') d\lambda'}{\int_0^W \psi(\lambda') d\lambda'} \quad \text{II-3.23}$$

with:

$$c' = \frac{c}{b} \quad \text{II-3.24}$$

The variable  $c'$  (with units of  $\lambda'^{-1}$ ) can be considered as a measure of the wedge non-linearity since the transmission is completely linear for  $c' = 0$  and becomes increasingly non-linear for larger values of  $c'$  as demonstrated in Figure II-3.5.

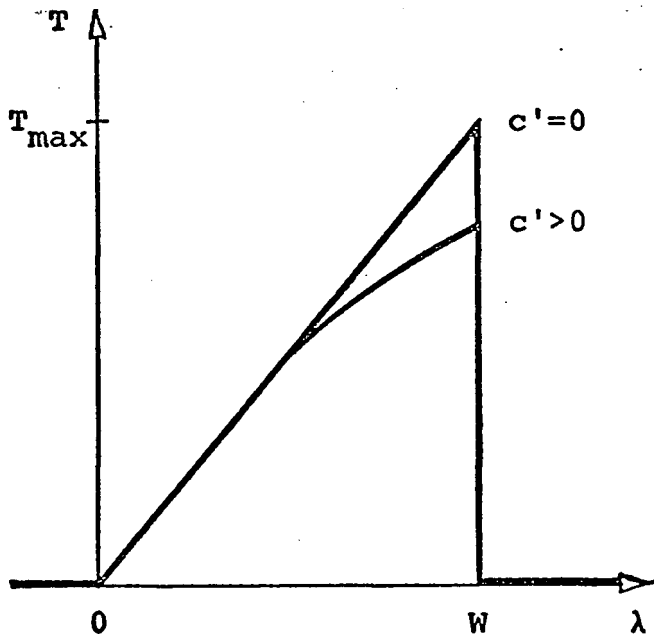


Figure II-3.5  
WEDGE NON-LINEARITIES

As an example, suppose that  $c'$  is such that the transmission of a non-linear wedge is 90% of the corresponding linear value at its maximum. In other words:

$$T(W) = 0.9T_{\max}$$

Using this value with Equation II-3.24 in Equation II-3.21, it can be seen that:

$$c' = \frac{0.1}{W}$$

One could thus speak of this wedge as being 10% non-linear.

If the normalized non-linear ratio,  $R'_W$ , is defined in analogy to Equation II-3.5:

$$R'_W = \frac{R'}{W} \quad \text{II-3.25}$$

and the ratio calculated for the above wedge and a rectangular profile, the result is:

$$c'R'_W = 0.1 \left[ x_0^2 + \frac{1}{3} \frac{1}{x_\beta} r \right] \quad \text{II-3.26}$$

An extremely wide profile with  $x_\beta = 2$  located in the middle of the wedge,  $x_0 = 0.5$ , which would produce a linear ratio of  $R_W = 0.5$  results, here, in a non-linear ratio term which is a maximum for variations due to width changes alone.

For this case:

$$c'R'_W = 0.0333$$

which is 6.7% of the linear value of  $R_w = 0.5$ . Thus, as a rule of thumb, for a worst-case design criterion, the maximum ratio changes due to width fluctuations on a non-linear wedge will be two thirds of the linearity figure given by  $C = C'W$ . For Gaussian or Lorentzian profiles this source of non-linearity will be considerably reduced.

The other extreme in non-linear response due to a non-linear wedge occurs when the intensity distribution is very narrow ( $x_\beta = \infty$ ) with no fluctuation in width but maximum fluctuation in shift (up to  $x_0 = 1$ ). In this case, the full non-linearity of the wedge is in effect as can be seen from substitution of these values of  $x_0$  and  $x_\beta$  into Equation II.3.26.

## CHAPTER II-4 - ACCURACY AND RESOLUTION

While the ratio of the integrals discussed in the previous chapter typify the linearity of the measurement, the sensitivity of the measurement is dependent on the constants which are determined by the experimental apparatus. For convenience, these can be grouped into one constant of proportionality,  $G$ , defined by:

$$G = \frac{Kf_R}{kf_T} \frac{1}{b} \quad \text{II-4.1}$$

so that Equation II-2.11 can be written as:

$$\bar{\lambda}' = G \frac{s}{\beta} \quad \text{II-4.2}$$

Taking the differential of this equation gives the uncertainty in measuring the line mean,  $d(\lambda')$ , with respect to the calibration and measurement uncertainties  $dG$ ,  $ds$  and  $d\beta$ :

$$d(\bar{\lambda}') = \frac{s}{\beta} \left\{ dG + G \frac{ds}{s} + G \frac{d\beta}{\beta} \right\} \quad \text{II-4.3}$$

If a measurement of shift is imagined wherein the signals  $s$  and  $\beta$  do not change appreciably (this represents the small shift of a line which does not change its total intensity during the shift), then  $d(\lambda')$  as expressed by this equation can be taken as the resolution of the technique.

For a shift measurement where  $s$  and  $S$  do change appreciably (a line which varies from bright to faint), the accuracy in measuring a shift of  $\Delta\bar{\lambda}'$  must be determined from:

$$d[\Delta\lambda'] = d(\bar{\lambda}'_1) + d(\bar{\lambda}'_2) \quad \text{II-4.4}$$

where it is assumed that  $\bar{\lambda}'_1$  arises from  $s_1$  and  $S_1$  and similarly  $\bar{\lambda}'_2$  arises from  $s_2$  and  $S_2$ .

The uncertainties  $ds$  and  $dS$  must be determined by the noise conditions that are present in the experiment. As an example, suppose the major noise process is due to the random (Poisson) arrival of current pulses in the photomultiplier tubes. The line profile can be written as

$$\psi(\lambda') = \bar{\nu}L(\lambda')$$

where  $\bar{\nu}$  is the mean Poisson rate and  $L(\lambda')$  is a normalized line profile completely contained within  $0 \leq \lambda' \leq W$ , with mean  $\lambda'_0$  and (half) half-width  $\beta'$ .

The wedge signal for this line (assuming a perfect wedge) will be:

$$s = kf_T b \bar{\nu} \int_0^W \lambda' L(\lambda') d\lambda' = kf_T b \bar{\nu} \lambda'_0$$

with uncertainty given by the Poisson standard deviation:

$$ds = kf_T b \left\{ \frac{\bar{\nu}}{\tau} \right\}^{\frac{1}{2}} \lambda'_0$$

where  $\tau$  is the time taken for a measurement.

Similarly, the signal from the normalization photomultiplier will be:

$$S = Kf_R \bar{\nu} \int_0^W L(\lambda') d\lambda' = Kf_R \bar{\nu}$$

with uncertainty:

$$dS = Kf_R \left\{ \frac{\bar{\nu}}{\tau} \right\}^{\frac{1}{2}}$$

Consider that there is negligible uncertainty in the measurement of the calibration constants involved in G. Then the uncertainty in  $\bar{\lambda}'$  as calculated from Equation I-4.3 is:

$$d(\bar{\lambda}') = \frac{2\lambda'_0}{\{\bar{\nu}\tau\}^{\frac{1}{2}}}$$

If this is made nondimensional with respect to the line width,  $\beta'$ , as follows:

$$\frac{d(\bar{\lambda}')}{\beta'} = 2 \frac{\lambda'_0}{\beta'} \frac{1}{\{\bar{\nu}\tau\}^{\frac{1}{2}}}$$

and the nondimensional variables  $x_0$  and  $x_\beta$  introduced, then the limiting shift to width ratio (expressed in non dimensional form by the product  $x_\beta dx_0$ ) is determined by this equation for a Poisson process sampled for a time  $\tau$  by:

$$x_\beta dx_0 = 2 \frac{x_\beta x_0}{\{\bar{\nu}\tau\}^{\frac{1}{2}}}$$

For good linearity it is necessary to have  $x_\beta$  quite large (say 20). Then, assuming the line is centered on the wedge ( $x_0 = 0.5$ ), exhibits a mean Poisson rate of  $10^6 \text{ sec}^{-1}$  and is observed (integrated) for a period of 1 sec., the limiting shift to width ratio is:

$$x_\beta dx_0 = 0.02$$

Thus, under these conditions one would expect to be able to just resolve a shift which was 0.02 times the (half) half-width of the line profile. This result does not take into account the pulse height noise nor the dark current noise of the photomultiplier.

## CHAPTER II-5 EXPERIMENTAL EXAMPLE USING A REAL WEDGE

An experimental investigation of a real wedge under several conditions was made to examine the real accuracy and practicality of the technique.

A wedge whose transmission varied linearly from about 5% to about 70% over a distance of about 3.5 mm was used against a slit of the same width.

Initially, a helium Geissler line (HeI 3889) whose profile was determined by the instrument function of the monochromator was used (see Figure II-5.1). A shift of this line was simulated by scanning it across the wedge with the aid of a rotating scan plate (see Part I, Chapter I-2B) mounted inside the monochromator between the camera mirror and the exit slits.

The signals from the signal photomultiplier,  $s$ , and from the normalization photomultiplier,  $S$ , were recorded separately by an XY plotter and used to calculate the signal ratio,  $s/S$ . This ratio was then plotted against the nondimensional mean of the line,  $x_0$ . This variable defined in Equation II-3.6, expresses the position of the mean with respect to the zero of the lab coordinate system,  $\lambda'$ , in units of the width of the wedge,  $W$ .

This same procedure was repeated with the same Geissler line except with the entrance slit very wide so as to produce an almost rectangular profile (see Figure II.5.2).

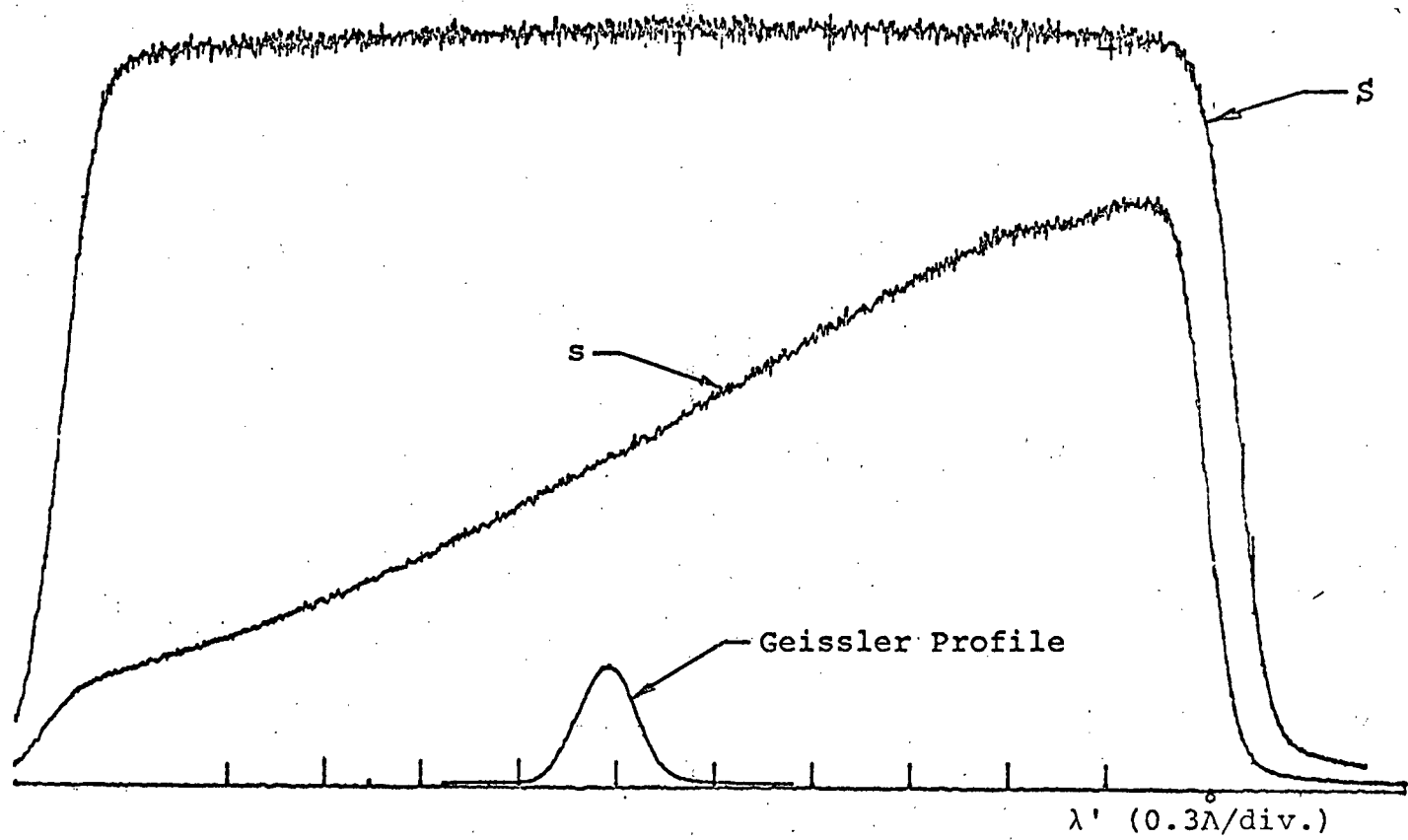


Figure II-5.1 - WEDGE OUTPUT SIGNALS FOR A NARROW GEISSLER LINE

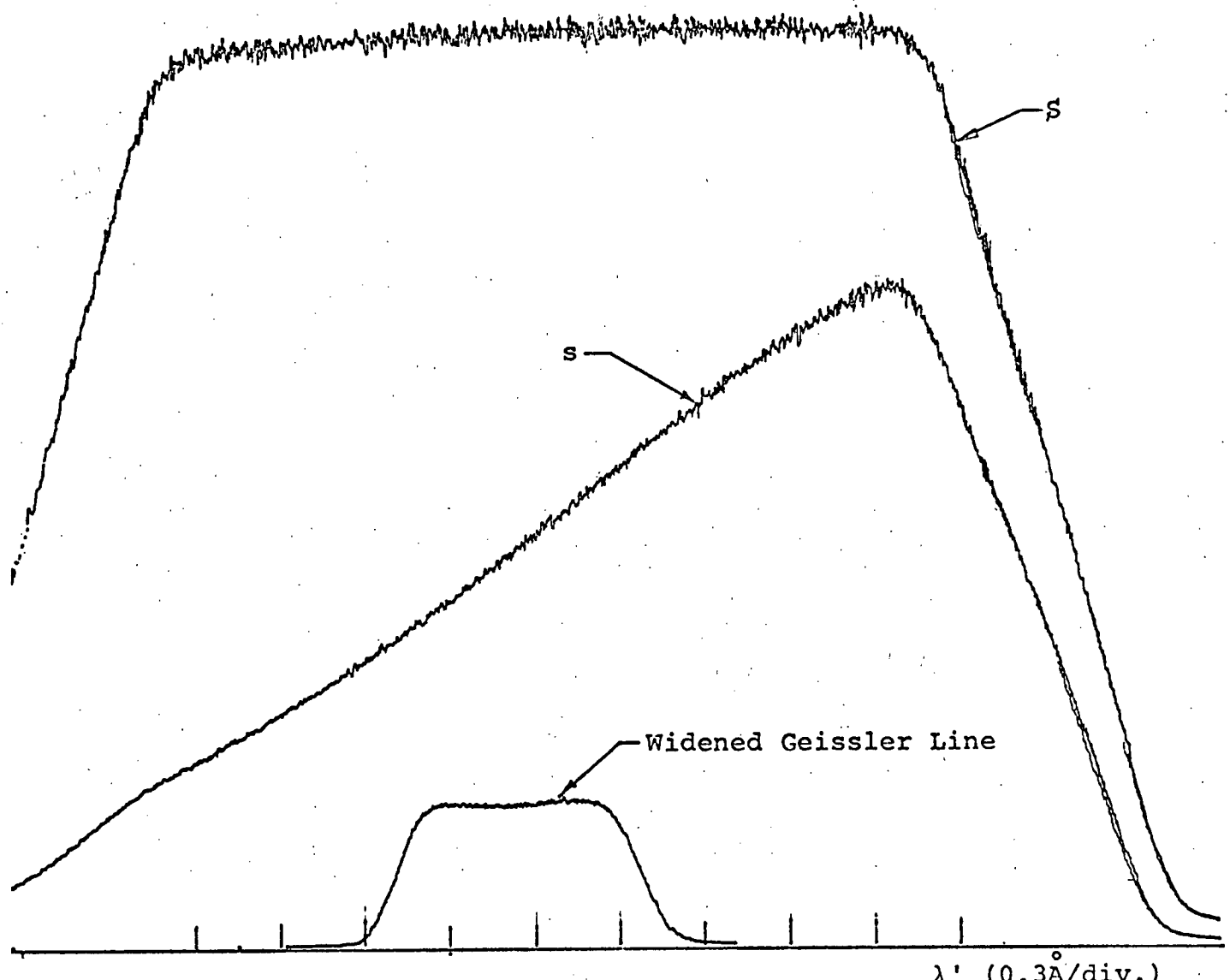


Figure II-5.2 - WEDGE OUTPUT FOR A WIDENED GEISSLER LINE

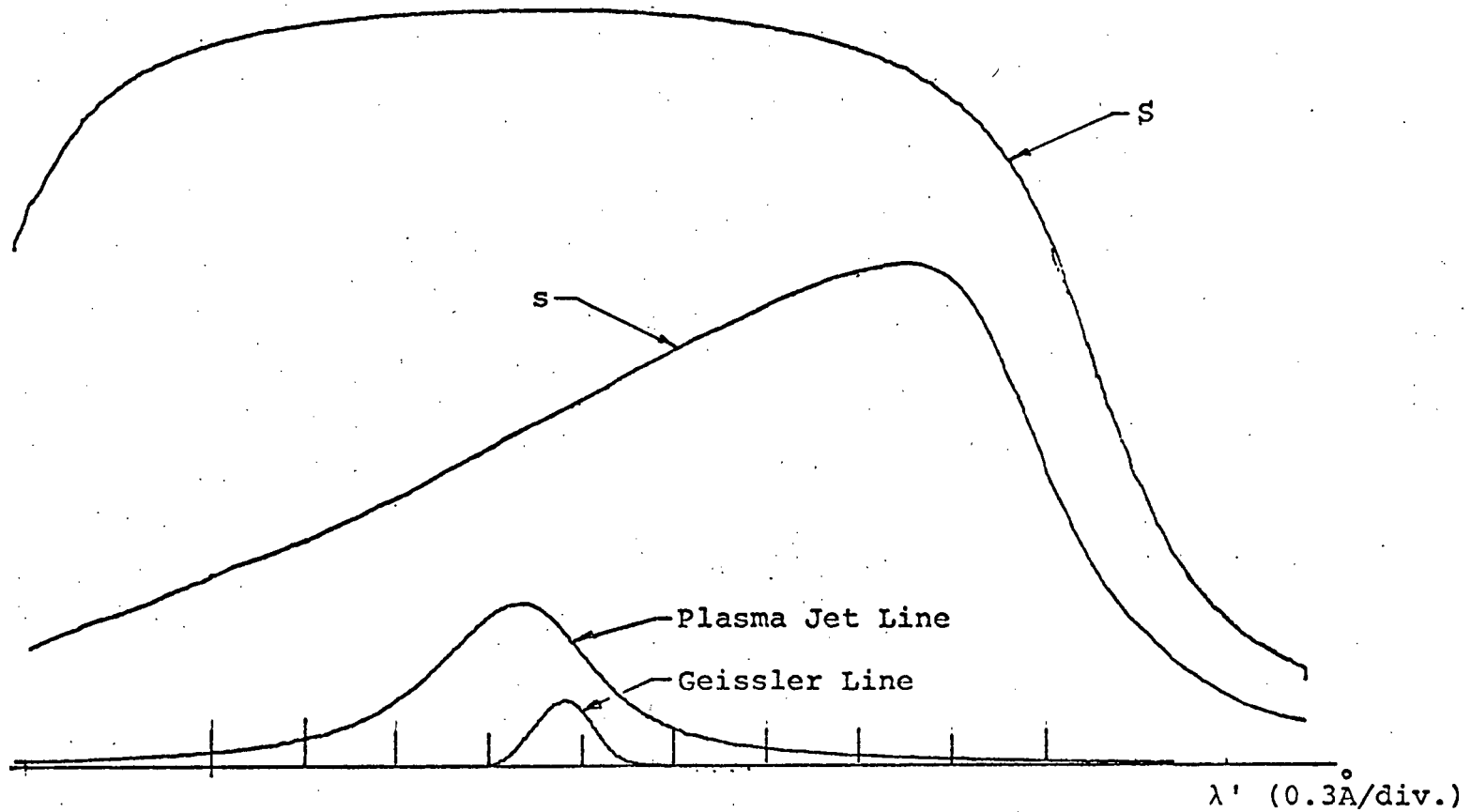
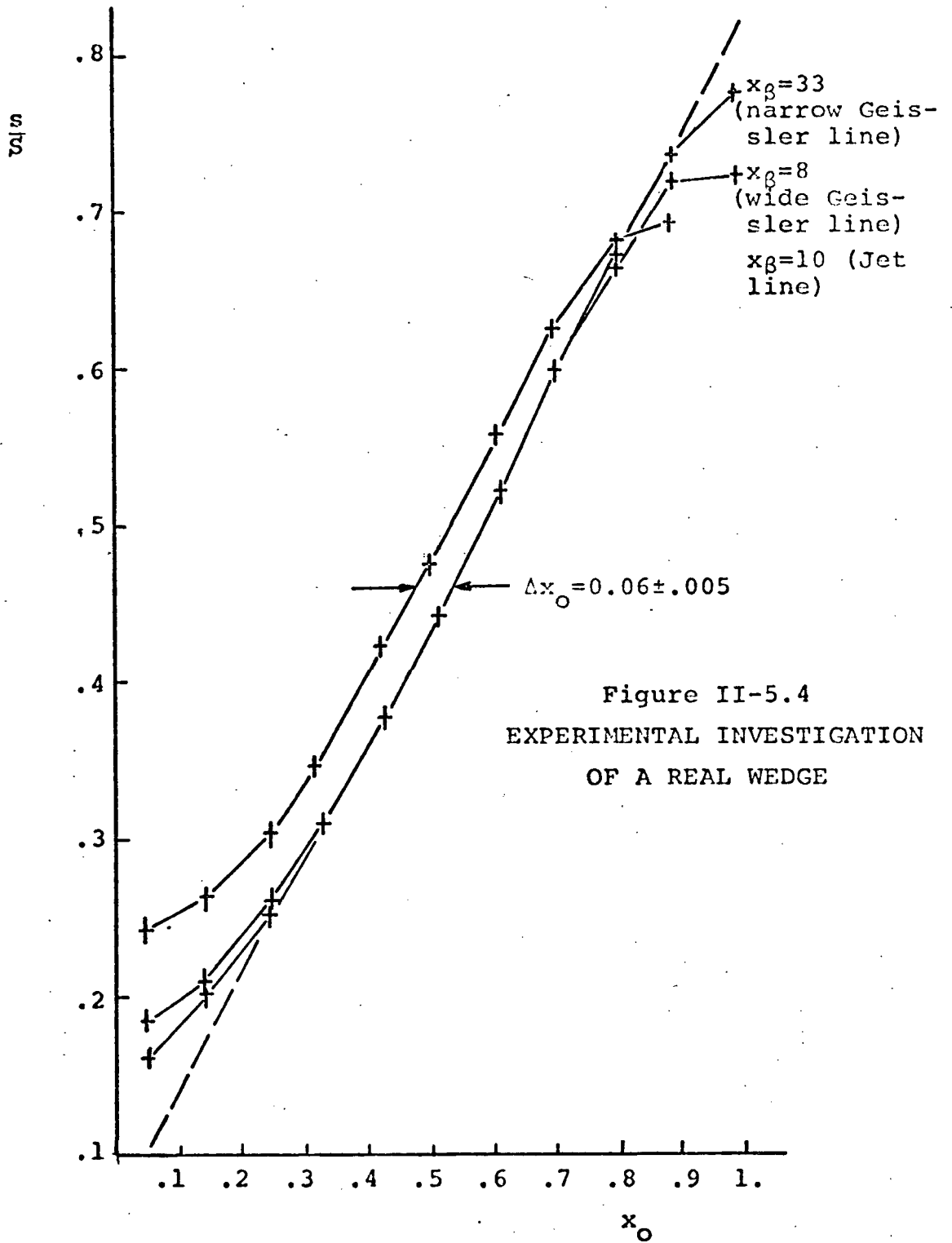


Figure II-5.3 - WEDGE OUTPUT FOR A BROADENED LINE



Finally, without any changes in the optical or electronic systems, the procedure was repeated using the same line from a helium plasma jet. This line is broadened into roughly a Lorentz profile and shifted by the Stark effect as can be seen in Figure II-5.3 by its relationship to the cool Geissler line.

The resulting signal ratios are plotted against  $x_0$  in Figure II-5.4 to demonstrate the response of the system. One can see that, since the two Geissler outputs overlap one another, the entrance slit opened symmetrically. Had this not been the case, the line would have been shifted parallel in a manner similar to the output of the jet line.

Besides demonstrating the linearity of the system, this technique of artificially shifting the line is the most satisfactory way of calibrating the system response. Determination of the slope of the line due to the narrow Geissler line determine the factor  $G$  defined in Equation II-4.1 (involving  $b, k, K, f_R, f_T$ ). This calibration can be carried out easily every time the system is used and aids as well in making sure the observed line lies in a favourable region of the wedge prior to running the experiment.

In this example, the slope of the Geissler response gives a nondimensional sensitivity of

$$G_0 = \frac{\Delta x_0}{\Delta \left(\frac{S}{S}\right)} = 1.33$$

or a dimensional sensitivity of

$$G = WG_0 = 4.67 \text{ \AA}$$

since: 
$$\Delta x_0 = \frac{\Delta \lambda'}{W}$$

where:  $W$ , the width of the wedge, is  $3.5 \text{ \AA}$ .

In other words:

$$\begin{aligned} \Delta \bar{\lambda}' &= G \Delta \left( \frac{S}{S} \right) \\ &= 4.67 \left\{ \frac{S}{S} - \left( \frac{S}{S} \right)_{\text{Geissler}} \right\} \end{aligned}$$

Applying this result to the shift of the jet line one finds, at any  $x_0$  in the region of linear response, a shift of  $0.21 \pm 0.04 \text{ \AA}$ . The amount of shift is slightly larger than that observed in Figure II-5.3 between the Geissler peak and the peak of the plasma jet line. This is to be expected since the jet line is slightly asymmetric, causing the mean of the line to lie some small distance from its peak.

CHAPTER II-6 APPLICATION OF THE WEDGE TECHNIQUE TO SHIFT  
MEASUREMENTS IN AN INHOMOGENEOUS (CYLINDRI-  
CALLY SYMMETRIC) PLASMA

As has been previously discussed (Part I), spectroscopic observations of inhomogeneous plasmas do not result in emission profiles which characterize conditions in small, local regions of the plasma. Instead, the observations result in line profiles which are composites of the local profiles because of the unavoidable integration along the line of sight through the inhomogeneities in the plasma. Consequently, the line shifts, widths and total intensities which are indicative of local plasma conditions cannot be observed directly.

However, if something is known about the distribution of inhomogeneity, it is sometimes possible to operate on the observed profiles to unfold the component, local ones. The most common situation where this is done occurs when the observed plasma, while inhomogeneous, is cylindrically symmetric.

This exact process is described in detail in part I of this thesis. That discussion demonstrates that while possible to accomplish, the procedure is very complicated and unwieldy. If one is not interested in the widths of the local profiles, but just shifts and total intensities, then the procedure can be considerably simplified.

The following chapter describes this simplification. Firstly, the method of unfolding shifts is discussed as a general problem. And secondly, these results are mixed with the wedge technique for measuring line shifts. The acquisition of the unfolded total intensities comes as a necessary part of the unfolding of shifts and so is not discussed as a separate procedure.

## A. ABEL UNFOLDING OF SHIFTS

Consider a cylindrically shaped plasma whose properties are all separable functions of the cylindrical coordinates  $r$  and  $z$  only -- independent of the angular coordinate  $\theta$ . At constant values of  $z$ , all properties of such a plasma (such as temperatures and densities) can be represented by the functional form  $f_z(r)$ .

Written in this form, the local emission profile (power per unit wavelength per unit volume per unit solid angle) is  $\epsilon_z(r, \lambda)$ . The intensity profile (power per unit wavelength per unit area per unit solid angle),  $i_z(y, \lambda)$ , observed from along a path  $p$  as a function of the side-on position  $y$  (see Figure II-6.1) is given by: (see Griem)

$$i_z(y, \lambda) = 2 \int_y^{r_0} \frac{\epsilon_z(r, \lambda) r dr}{[r^2 - y^2]^{\frac{1}{2}}} \quad \text{II-6.1}$$

where  $\epsilon_z(r_0, \lambda) = 0$  and  $r_0 = r_0(z)$

Since the function  $\epsilon_z(r, \lambda)$  refers to the emission at a point on a particular spectral line, an integration of Equation II-6.1 over wavelength relates the observed total line intensity,  $I_z(y)$ , to the local emission coefficient,  $E_z(r)$ :

$$I_z(y) = 2 \int_y^{r_0} \frac{E_z(r) r dr}{[r^2 - y^2]^{\frac{1}{2}}} \quad \text{II-6.2}$$

where the emission coefficient was defined as:

$$E_z(r) = \int_0^{\infty} \epsilon_z(r, \lambda) d\lambda \quad \text{II-6.3}$$

and the observed total intensity as:

$$I_z(y) = \int_0^{\infty} i_z(y, \lambda) d\lambda \quad \text{II-6.4}$$

The mean of the observed line can be defined (as previously stated) completely generally as:

$$\bar{\lambda}_z(y) = \frac{\int_0^{\infty} \lambda i_z(y, \lambda) d\lambda}{\int_0^{\infty} i_z(y, \lambda) d\lambda} \quad \text{II-6.5}$$

which becomes by virtue of Equations II-6.1 and II-6.4 plus a change in the order of integration:

$$\bar{\lambda}_z(y) = \frac{2}{I_z(y)} \int_y^{r_0} \frac{r}{[r^2 - y^2]^2} \left[ \int_0^{\infty} \lambda \epsilon_z(r, \lambda) d\lambda \right] dr \quad \text{II-6.6}$$

The mean of the local emission profile which one seeks to measure, can be similarly defined as:

$$\bar{\lambda}_z(r) = \frac{\int_0^{\infty} \lambda \epsilon_z(r, \lambda) d\lambda}{\int_0^{\infty} \epsilon_z(r, \lambda) d\lambda} \quad \text{II-6.7}$$

which can be construed (using Equation II-6.3) to be:

$$E_z(r) \tilde{\lambda}_z(r) = \int_0^{\infty} \lambda \epsilon_z(r, \lambda) d\lambda \quad \text{II-6.8}$$

The tildas (~) in Equations II-6.7 and II-6.8 are used to denote the different functional form of the local mean as a function of  $r$  as compared with the observed mean noted by a bar (-) in Equations II-6.5 and II-6.6 which is a function of  $y$ .

Equation II-6.8 now substitutes directly into Equation II-6.6 to give:

$$\bar{\lambda}_z(y) I_z(y) = 2 \int_y^{r_0} \frac{r}{[r^2 - y^2]^{\frac{1}{2}}} \lambda_z(r) E_z(r) dr \quad \text{II-6.9}$$

This is an integral equation which can be solved for the kernel by applying the Abel transformation:

$$\lambda_z(r) E_z(r) = -\frac{1}{\pi} \int_r^{r_0} \frac{1}{[y^2 - r^2]^{\frac{1}{2}}} \frac{d}{dy} [\bar{\lambda}_z(y) I_z(y)] dy \quad \text{II-6.10}$$

from which, for brevity, the Abel Transform, A.T., is defined:

$$\lambda_z(r) E_z(r) = \text{A.T.} \{ \bar{\lambda}_z(y) I_z(y) \} \quad \text{II-6.11}$$

Since Equation II-6.2 can also be solved by the Abel transform:

$$E_z(r) = \text{A.T.} \{ I_z(y) \} \quad \text{II-6.12}$$

Substitution of Equation II-6.12 into Equation II-6.11 gives the final result:

$$\lambda_z(r) = \frac{\text{A.T.}\{\bar{\lambda}_z(y) I_z(y)\}}{\text{A.T.}\{I_z(y)\}} \quad \text{II-6.13}$$

which expresses the mean of the local emission profile in terms of the observed mean and the observed total intensity.

#### B. RELATING THE WEDGE TECHNIQUE TO UNFOLDING SHIFTS

Early in Chapter II-2 the real wavelength coordinate,  $\lambda$ , and the lab frame coordinate,  $\lambda'$ , were related by a linear transformation (Equation II-2.3) which depended on the conditions of the monochromator. The spectral line was specified by the function  $\psi(\lambda')$  which arose from this linear transformation of the intensity distribution  $i(\lambda)$ . Later in the chapter, constraints were made on the distribution  $\psi(\lambda')$  such that it was non-zero only in the region  $0 \leq \lambda' \leq w$ . By implication,  $i(\lambda)$  must also have limits specified by the transformation making integrations over the entire range  $0 \leq \lambda < \infty$  unnecessary.

Applying the same conditions to the observed intensities  $i_z(y, \lambda)$  and  $\psi_z(y, \lambda')$  and noting from Equation II-2.3 that:

$$d\lambda = D_\lambda d\lambda' ,$$

the following integral relations are easily derived:

$$I_z(y) = \int_0^{\infty} i_z(y, \lambda) d\lambda = D_\lambda \int_0^W \psi_z(y, \lambda') d\lambda' \quad \text{II-6.14}$$

$$\begin{aligned} \bar{\lambda}_z(y) I_z(y) &= \int_0^{\infty} i_z(y, \lambda) d\lambda \\ &= D_\lambda^2 \int_0^W \lambda' \psi_z(y, \lambda') d\lambda' + D_\lambda C_\lambda \int_0^W \psi_z(y, \lambda') d\lambda' \quad \text{II-6.15} \end{aligned}$$

If the wedge apparatus is used, with the normalization signal given by (as in Equations II-2.4 and II-2.5):

$$S_z(y) = Kf_R \int_0^W \psi_z(y, \lambda') d\lambda' \quad \text{II-6.16}$$

and the wedge signal by:

$$s_z(y) = kf_T b \int_0^W \lambda' \psi_z(y, \lambda') d\lambda' \quad \text{II-6.17}$$

then the local mean can be related to the Abel transforms of the observed signals  $s_z(y)$  and  $S_z(y)$  by substituting Equations II-6.14 and II-6.15 into Equation II-6.13 and replacing the integrals by the signal values obtained from Equations II-6.16 and II-6.17. The result is:

$$\bar{\lambda}_z(r) = \frac{\text{A.T.} \left\{ D_\lambda^2 \frac{1}{Kf_T} \frac{1}{b} s_z(y) + D_\lambda C_\lambda \frac{1}{Kf_R} S_z(y) \right\}}{\text{A.T.} \left\{ D_\lambda \frac{1}{Kf_R} S_z(y) \right\}} \quad \text{II-6.18}$$

For any functions  $f$  and  $g$  and constant  $c$ , the following rules for Abel transforms can be derived:

$$A.T.\{f + g\} = A.T.\{f\} + A.T.\{g\}$$

$$A.T.\{cf\} = c A.T.\{f\}$$

provided both  $f$  and  $g$  approach zero at and beyond some value of the independent variable.

These rules, applied to Equation II-6.18 give the result:

$$\tilde{\lambda}_z(r) = D_\lambda \frac{Kf_R}{kf_T} \frac{1}{b} \frac{A.T.\{s_z(y)\}}{A.T.\{S_z(y)\}} + C_\lambda \quad \text{II-6.19}$$

which relates the mean of the local emission profile to the Abel transform of the wedge signals within an unknown additive constant.

If, as was suggested in a previous chapter, differences of means are measured under identical experimental circumstances, the constant  $C_\lambda$  is eliminated. This can be done, for example, by using a Geissler line with mean given by:

$$\tilde{\lambda}_g = D_\lambda \frac{Kf_R}{kf_T} \frac{1}{b} \frac{s_g}{S_g} + C_\lambda$$

and calculating:

$$\Delta_1 \tilde{\lambda}_z(r) = \tilde{\lambda}_z(r) - \tilde{\lambda}_g$$

Or, the constant can be eliminated by calculating either of the differences:

$$\Delta_2 \tilde{\lambda}_z(r) = \tilde{\lambda}_z(r) - \tilde{\lambda}_z(0)$$

or

$$\Delta_3 \tilde{\lambda}_z(r) = \tilde{\lambda}_z(r) - \tilde{\lambda}_z(r_0)$$

where, of course, one should observe:

$$\Delta_2 \tilde{\lambda}_z(r) = -\Delta_3 \tilde{\lambda}_z(r)$$

If the edge of the plasma is sufficiently cool and has a low electron density then probably:

$$\tilde{\lambda}_g = \tilde{\lambda}_z(r_0)$$

so that the same results are obtained by using either a Geissler tube or the outer part of the flame as the zero of shift:

$$\Delta_1 \tilde{\lambda}_z(r) = \Delta_2 \tilde{\lambda}_z(r)$$

The mean which is chosen to specify the zero shift should be that which is most accurately determined.

### PART III - CONCLUSIONS

Before discussing the more general or universal aspects of this work, it might be appropriate at this time to collate the definitive accomplishments reported throughout the thesis. They can be summarized in four points as follows:

1. The previously proposed "double wedge" technique of Ahlborn and Barnard (1966) has been refined to the point where only one wedge is required to perform the measurement (see Chapters I-1 and I-2). This improvement has the important effect that an extended source is not required to make use of the technique. In addition, the wedge technique has been investigated (see Chapters II-3 and II-4) for its resolution, linearity and sensitivity under a variety of conditions which are routinely encountered in experiments. The effects of wedge non-linearity, line shape (including line wing effects) and underlying continuum have been investigated and a convenient set of design criteria have been prepared for interested users as well as a description on how to use these data (see Appendix V);
2. For the first time, it has been shown that the local shift of the mean of a spectral line for a cylindrically symmetric plasma can be unfolded from side-on shift measurements which do not require detailed knowledge of (nor any assumptions about) the line profile (see Equation II-6.13). This finding yields a considerable reduction in the effort one would otherwise expend obtaining the position of the local mean wavelengths. In addition, this result has been combined with the wedge technique to allow very convenient determination of local shifts of a cylindrical plasma.

3. An approximate relationship has been obtained (Equation I-4.9) that determines the position of the mean of a Stark broadened plasma line. This relationship was derived from the GBKO theory and is analogous to Griem's equation giving the total shift of the maximum intensity of a line when ion broadening cannot be neglected (see Equation I-4.12). The equation presented in this work determines the shift of the mean of a line to an accuracy of 5% of the electron impact width over the range  $0 \leq \alpha \leq 0.4$  and  $0 \leq r \leq 0.8$ ;
4. The shift in the mean of three neutral helium lines were examined under known plasma conditions and compared with the shifts as predicted by the GBKO theory (see Figure I-4.4). Previous experiments compared the shift of the maximum of the line to a lesser degree of accuracy. Consequently, it was not possible to generate much confidence that the shifts as predicted by the theory were reliable. In this work, it was found that the theory always predicted the position of the mean correctly within experimental accuracy (nominally within about 15% of the measured shift).

The implications of these results are much wider ranging than this simple summary would suggest and are worth greater consideration. First, let us consider the measuring technique itself.

The wedge technique for measuring shifts is restricted neither to the measurement of Stark shifts as used here, nor to the steady state type of plasma which was used in the work. The technique may be applied to either steady (d.c.) plasmas or pulsed plasmas just by changing the method of recording the photomultiplier output signals. For example, if a dual beam oscilloscope were used, both signals would be recorded for a pulsed plasma and the ratio

of the signals would be a temporal representation of the position of the mean of the observed line. Under steady state conditions, any number of recording devices (such as chart recorders, DVM's or pulse counting systems) would suffice. The technique can even be applied to microdensitometer traces of a spectrographic plate by incorporating the response of the plate into the shape of a "mathematical" wedge used to analyze the traces.

As well as being useful in a variety of experimental conditions, the wedge technique may prove useful in a variety of scientific problems in which the shift of the mean of a plasma line is the interesting feature. In this work, Stark shifts were of interest. In other experiments, the technique may be used to observe Doppler shifts, van der Waals shifts or Zeemann shifts. The scientific adaptability of the technique is left to the imaginations and the problems of other physicists.

Looking beyond the development of the measuring technique, the most exciting aspect of this work is the revival of interest in the use of Stark shifts as a diagnostic tool of plasma physics. The reason for this revival lies in the several important features that Stark shifts present which are actual pitfalls of the more widely recognized use of Stark widths as a diagnostic technique.

Firstly, in many cases the shift of the mean of a line is much easier to measure than the width. For example, one can imagine the amount of extra effort required to obtain the temporal behavior of the width of a plasma line as opposed to following the temporal behavior of the position of the mean as suggested above using the wedge technique. Another example appears when the shift is unfolded for a cylindrical plasma. The amount of effort required to unfold the shifts is

insignificant as compared with that needed to unfold the detailed profiles to obtain the local widths of the lines.

It is not possible to generalize about the comparable accuracy of measuring shifts as opposed to widths since the conditions of the particular experiment will have a significant contribution to make to this comparison. However, whereas it was previously assumed that widths were always more accurately determined, now this is not the case. Shift measurements can usually be made to comparable and often better accuracy than can measurements of line width. So, although this is not a feature which favours the use of Stark shifts, it is an important reversal in attitude that previously was a serious bias against their use.

A second favourable feature of using Stark shifts in plasma diagnostics is the sensitivity to electron temperature that many plasma lines display. The temperature dependence of the width, by comparison, is usually small. This makes Stark shift measurements extremely useful for measuring electron temperature -- especially when other techniques are not available to the experimenter.

As a third feature, Stark shift measurements are not affected by some of the mechanisms that limit the usefulness of width measurements in plasma diagnostics. Most notably, shift measurements are not strongly affected by the instrument function of a monochromator. This becomes very important at low electron densities and temperatures where the line width is comparable with the instrument width. Also, Stark shift measurements are not significantly affected by self-absorption, resonance broadening or Doppler broadening. These broadening mechanisms must always be considered when using width measurements to determine plasma conditions.

The last feature that supports the use of Stark shifts has been one of the most compelling incentives behind the use of width measurements as a diagnostic technique. That incentive has come from the success with which broadening theory has been able to predict the widths of many plasma lines under a variety of conditions. In this experiment, using increased accuracy, the GBKO theory proved capable of determining the shift of the mean. Thus, although this feature is not yet complete, as further data is obtained and agreement with theory is further substantiated, a wealth of calibration data will be available for reference in the same way as calculated widths are presently used.

Thus, as a general conclusion, it is felt that this work will provide new incentive in plasma spectroscopy to pursue the use of Stark shifts. The definite advantages of their use as a diagnostic technique make the subject too enticing to leave in abeyance.

In more specific terms, the further work can take the following course:

- a) It is possible to devise a scheme whereby scientists can obtain both electron density and electron temperature. This scheme should be delineated;
- b) Specific pairs of lines must be investigated to determine their sensitivity to electron density and temperature in various regions of plasma conditions. These results would provide a basis for deciding when the measurement of Stark shifts offered the most favourable diagnostic technique available under the circumstances of a particular experiment;
- c) Other plasma lines must be investigated experimentally to further ascertain the accuracy with which theory

predicts the shifts of the means of plasma lines. Specifically, investigation of helium ion lines as well as the neutral and ion lines of heavier atomic species should be investigated.

Should this further work continue to bear out the facts uncovered here, the results will undoubtedly be met with much enthusiasm by all plasma physicists.

## APPENDIX I

## RADIAL DISTRIBUTION OF LINE WIDTHS

The (full) half-widths of the lines  $H_{\beta}$  (4861A) and the three neutral helium lines used in the experiment (HeI 3889, HeI 4713 and HeI 5016) were measured from computer (CALCOMP) plots of the unfolded local emission profiles as described in Part I, Chapter 2.

The error bars represent the absolute limits of uncertainty and are due to the uncertainty of measuring both the background and peak intensity levels as well as the uncertainty in the actual width measurement.

The values plotted are the total measured (full) half-widths. No attempt has been made to eliminate broadening due to the instrument function or the unfolding program.

Figure AI-1  
RADIAL DISTRIBUTION OF  
(FULL) HALF WIDTHS OF  $H_{\beta}$

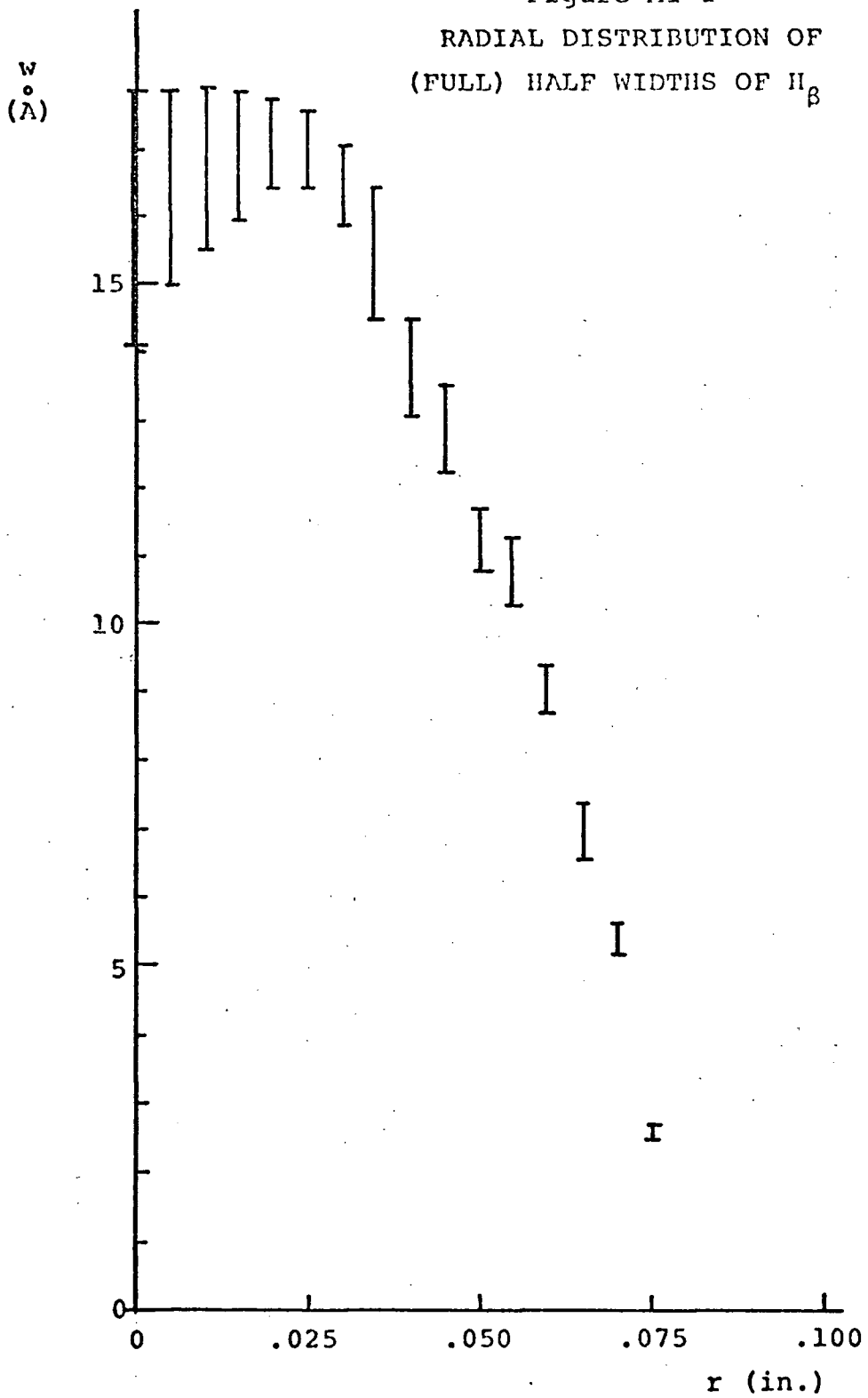


Figure AI-2  
RADIAL DISTRIBUTION OF  
(FULL) HALF WIDTHS OF  
HeI 5016

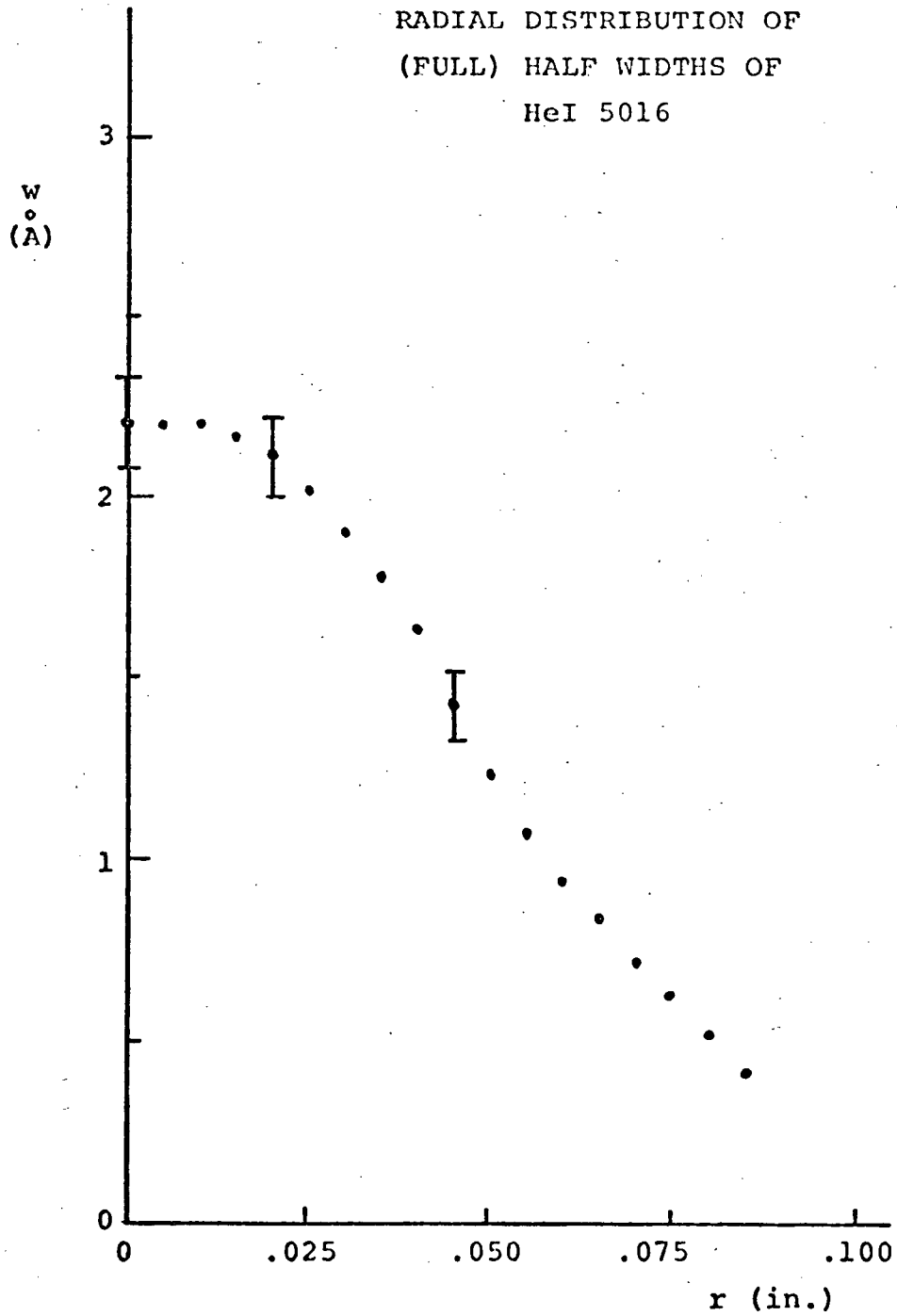


Figure AI-3  
RADIAL DISTRIBUTION OF  
(FULL) HALF WIDTHS OF  
HeI 4713

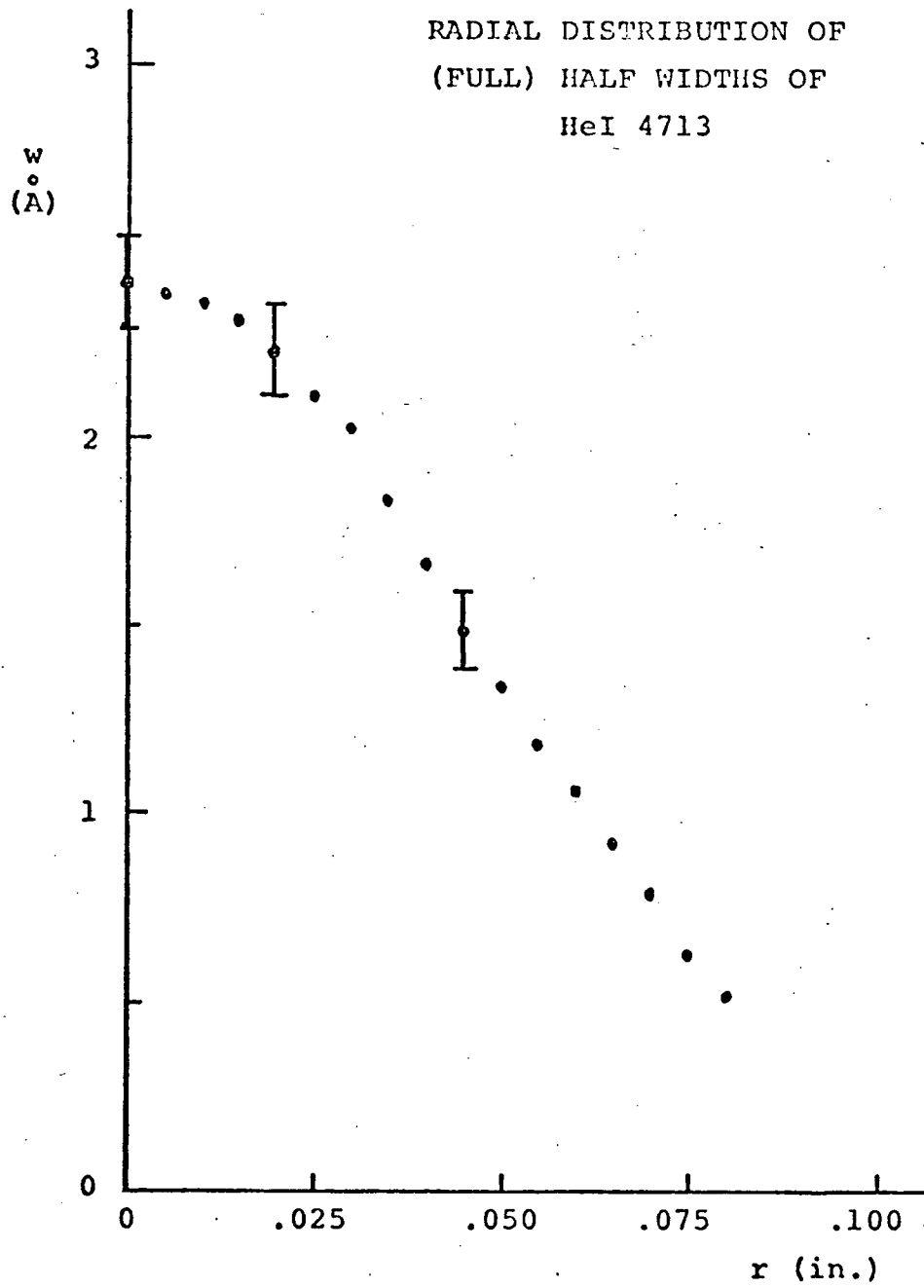
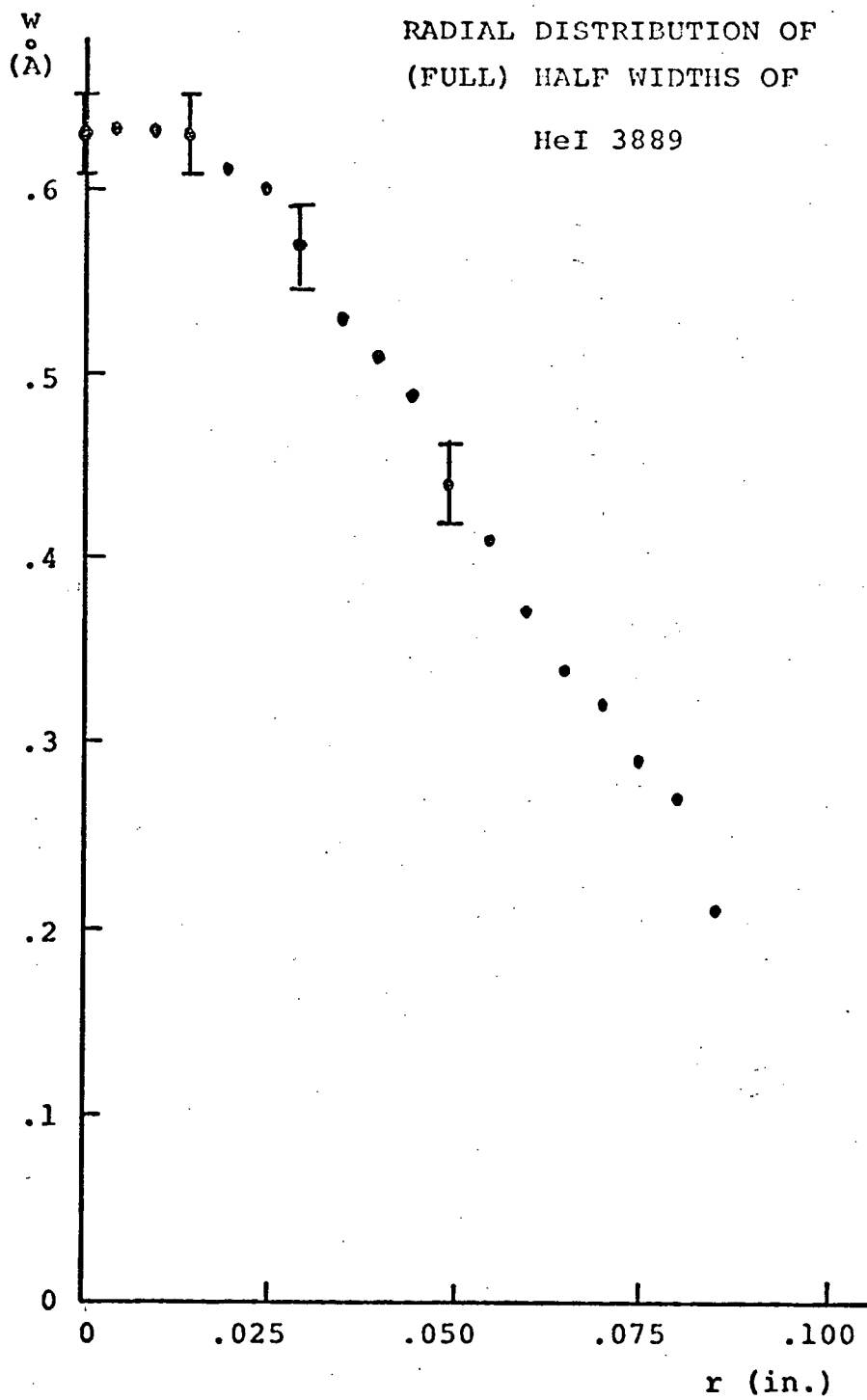


Figure AI-4  
RADIAL DISTRIBUTION OF  
(FULL) HALF WIDTHS OF  
HeI 3889



## APPENDIX II - THEORETICAL WIDTHS AND SHIFTS

The following line widths for the neutral helium lines HeI 5016, HeI 4713 and HeI 3889 are the results of applying Griem's (1964,P) formula

$$w_{\text{total}} = [1 + 1.75\alpha(1 - 0.75r_G)]w$$

under conditions of known temperature and density. The electron (half) half-widths,  $w$ , as well as the quasi-static ion-broadening parameter,  $\alpha$ , are obtained from Griem's tabulations for the appropriate line. The Debye-shielding parameter,  $r_G$  is determined by:

$$r_G = 6^{\frac{1}{3}} \pi^{\frac{1}{6}} \left( \frac{e^2}{4\pi\epsilon_0 kT} \right)^{\frac{1}{2}} N^{\frac{1}{6}}$$

where  $N$  is the ion population density and all other symbols have their conventional meaning. A tabulation of  $r_G$  for various electron densities and temperatures is also presented.

The graph showing the (full) half-width of  $H\beta$  as a function of electron density is a copy of that presented by Wiese (1965) who extracted the widths from Griem's calculations of the detailed profile for various values of electron temperature as well as electron density.

Figure AII-1

(FULL) HALF WIDTH OF  $H_{\beta}$  AS A FUNCTION  
OF  $n_e$  FOR  $5,000^{\circ}\text{K} \leq T_e \leq 40,000^{\circ}\text{K}$

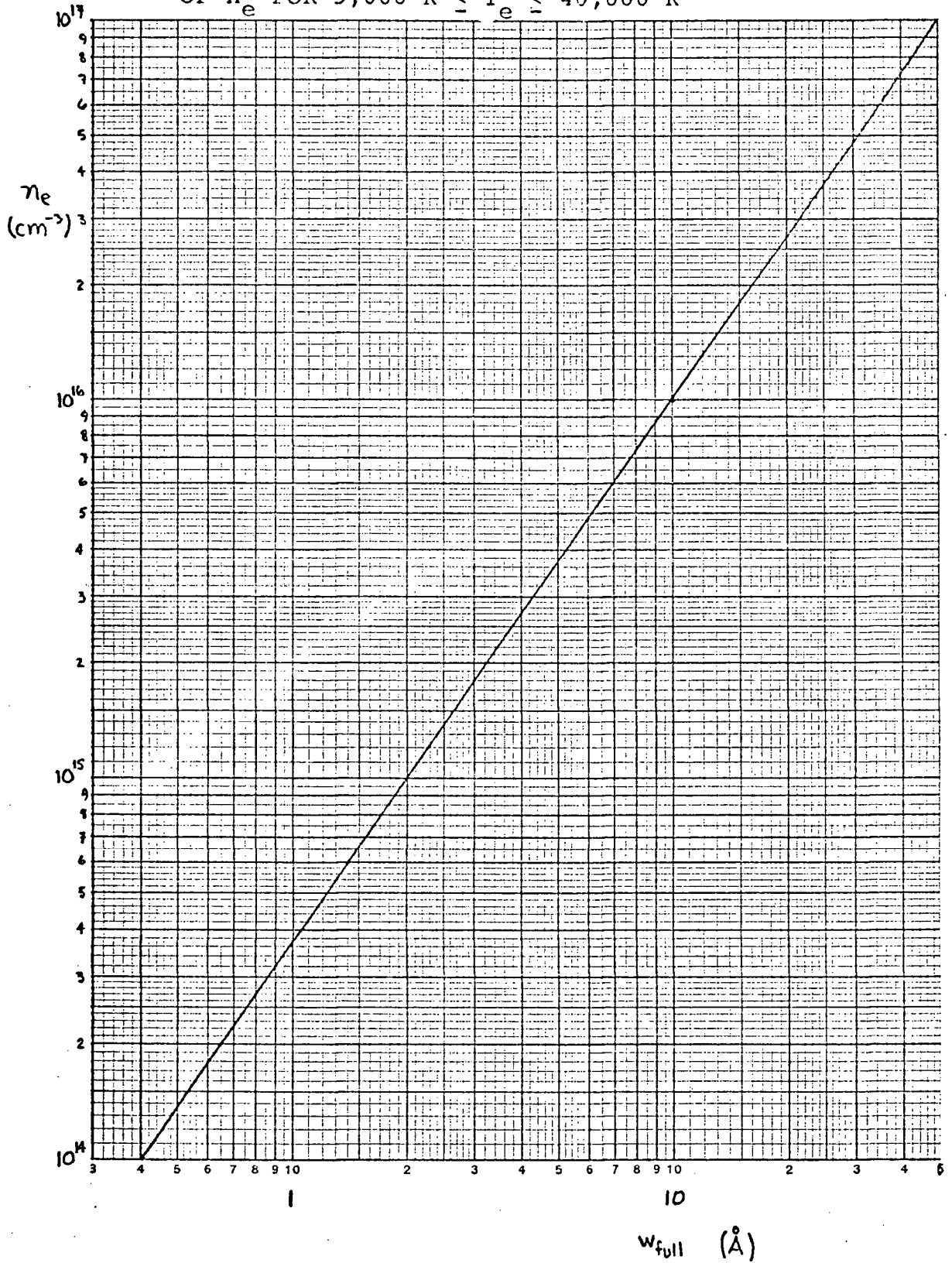
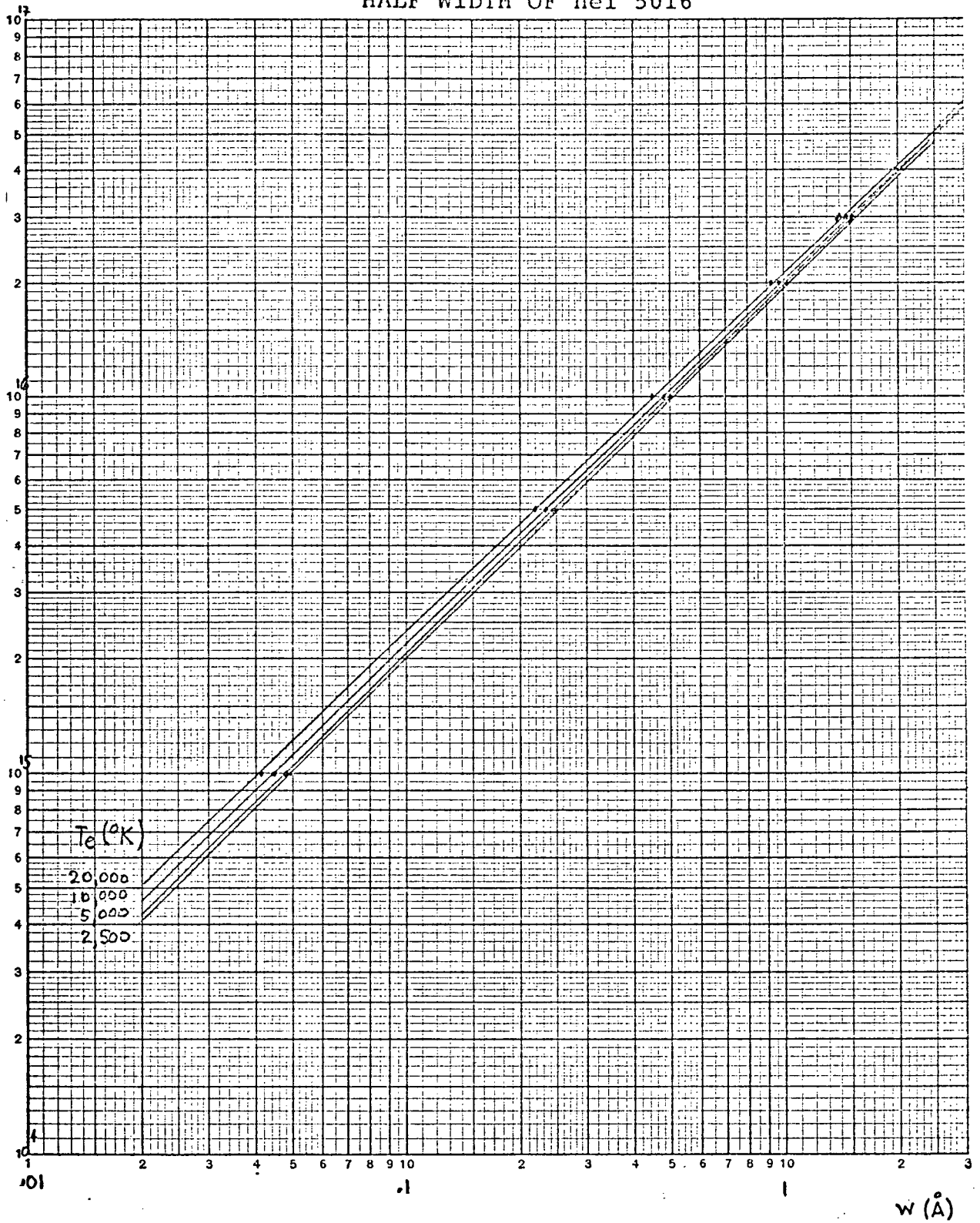


Figure AII-2

ELECTRON DENSITY vs. (HALF)  
HALF WIDTH OF HeI 5016

$n_e$   
( $\text{cm}^{-3}$ )



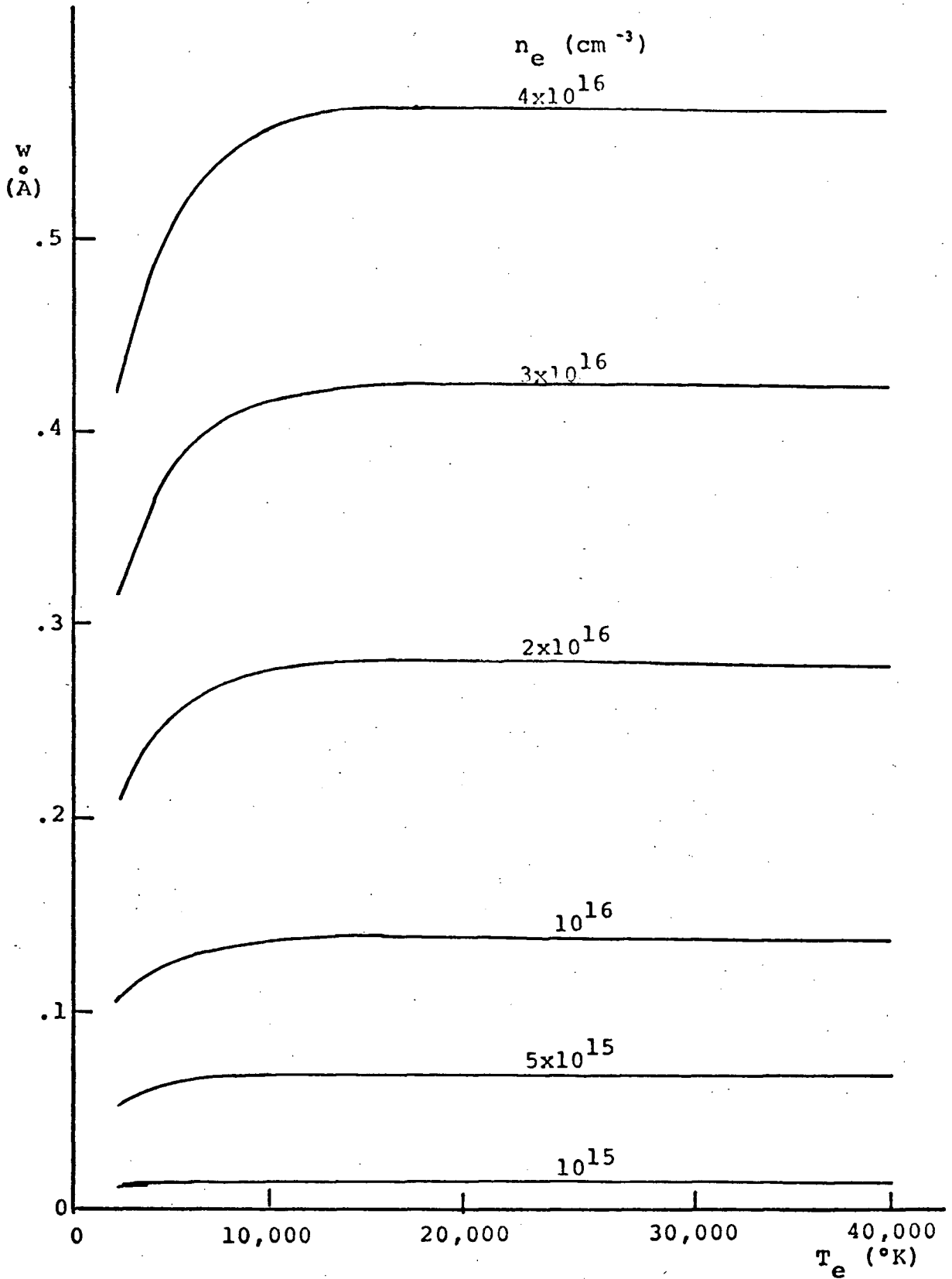


Figure AII-3  
(HALF) HALF WIDTHS OF HeI 3889

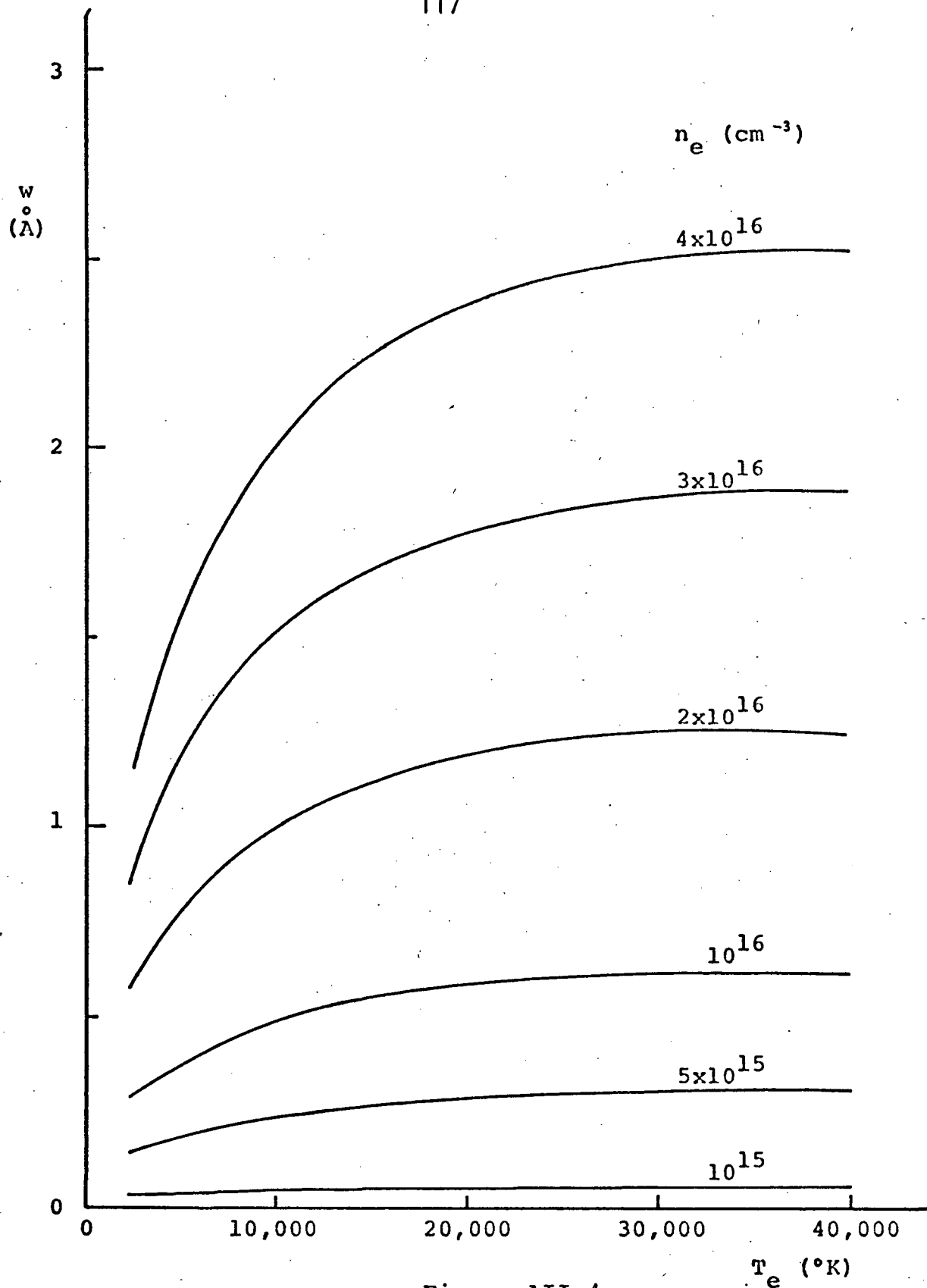


Figure AII-4  
(HALF) HALF WIDTHS OF He I 4713

$N_i$ ( $\text{cm}^{-3}$ ) \backslash T ( $^{\circ}\text{K}$ )	2500	5000	10000	20000	40000
$10^{15}$	.568	.402	.284	.201	.142
$5 \times 10^{15}$	.743	.526	.372	.263	.186
$10^{16}$	.834	.590	.417	.295	.209
$2 \times 10^{16}$	.937	.662	.468	.331	.234
$3 \times 10^{16}$	1.00	.709	.501	.354	.251
$4 \times 10^{16}$	1.05	.743	.526	.372	.263
$5 \times 10^{16}$	1.09	.772	.546	.386	.273

Figure AII-5

DEBYE SHIELDING PARAMETER,  $r_G$

APPENDIX III - AREA CORRECTION FOR INTEGRATION OF A LORENTZ  
PROFILE TO FINITE LIMITS

When the total intensity of an experimental line profile is determined by numerical integration to finite limits, significant error may be introduced by overlooking the fraction of total area contained in the line wings. This is particularly true if the line profile is Lorentzian -- as is often the case with plasma lines. However, it is possible to estimate and to correct for the bulk of this error if the type of profile, the experimental half-width of the profile and the experimental integration limits are known.

For a Lorentz profile with peak intensity  $A$ , mean zero and (half) half-width  $\beta$ , the intensity distribution is given by:

$$i(x) = \frac{A}{1 + \left(\frac{x}{\beta}\right)^2}$$

If, under experimental conditions, an integration is carried out symmetrically to the finite limits,  $\pm x_0$ , then the area in both wings from  $x_0$  to  $\infty$  will have been ignored. The area measured will be given by:

$$I_{\text{meas.}} = 2 \int_0^{x_0} i(x) dx = 2\beta A \tan^{-1} \left(\frac{x}{\beta}\right) \Big|_0^{x_0}$$

while the amount of area ignored will be given by:

$$I_{\text{wings}} = 2 \int_{x_0}^{\infty} i(x) dx = 2\beta A \tan^{-1} \left(\frac{x}{\beta}\right) \Big|_{x_0}^{\infty}$$

The ratio,  $r_L$ , of ignored area to measured area is, therefore:

$$r_L = \frac{I_{wings}}{I_{meas.}} = \frac{\tan^{-1} \left( \frac{x}{\beta} \right) \Big|_{x_0}^{\infty}}{\tan^{-1} \left( \frac{x}{\beta} \right) \Big|_0^{x_0}}$$

If  $I_{total}$  is the correct area given by integration to infinite limits, then obviously:

$$\begin{aligned} I_{total} &= I_{meas.} + I_{wing} \\ &= I_{meas.} [1 + r_L] \end{aligned}$$

Hence, by calculating  $r_L$ , the correct area can be determined from the measured area.

For convenience, it is useful to define

$$x' = \frac{x}{\beta} \quad (\text{and } x'_0 = \frac{x_0}{\beta})$$

which is the nondimensional variable given by the ratio of the integration (half) limit and the line (half) half-width. Using these new variables, the correction ratio can be determined by:

$$r_L(x'_0) = \frac{\tan^{-1} x' \Big|_{x'_0}^{\infty}}{\tan^{-1} x' \Big|_0^{x'_0}} \quad \text{AIII-1}$$

This ratio has been calculated for a useful range of  $x'_0$  and the results are presented in Figure III-1.

Under experimental conditions, when the observed line is approximated by a Lorentz profile and the numerical integration is roughly symmetric about the mean, the nondimensional integration limit,  $x'_0$ , can be calculated by taking the ratio of the (full) integration range to the (full) half-width of the profile. The wing correction ratio,  $r_L$ , can then be obtained from Figure III-1 and applied to the measured area using equation III-1.

The following procedure was followed to obtain the integrated experimental emission profiles used to calculate the upper level population densities and hence the radial distribution of electron temperature as described in Part I, Chapter I-3c.

The integral,  $S_{\lambda_0}(r)$ , of the unfolded profiles is defined by:

$$S_{\lambda_0}(r) = \int_{\lambda_1}^{\lambda_2} u_{\lambda_0}(r, \lambda) d\lambda$$

where:  $\lambda_1$  and  $\lambda_2$  determine the spectral limits of observation around the line;

$u_{\lambda_0}(r, \lambda)$  is the voltage emission profile at the radius,  $r$ , as described in Part I, Chapter 2.

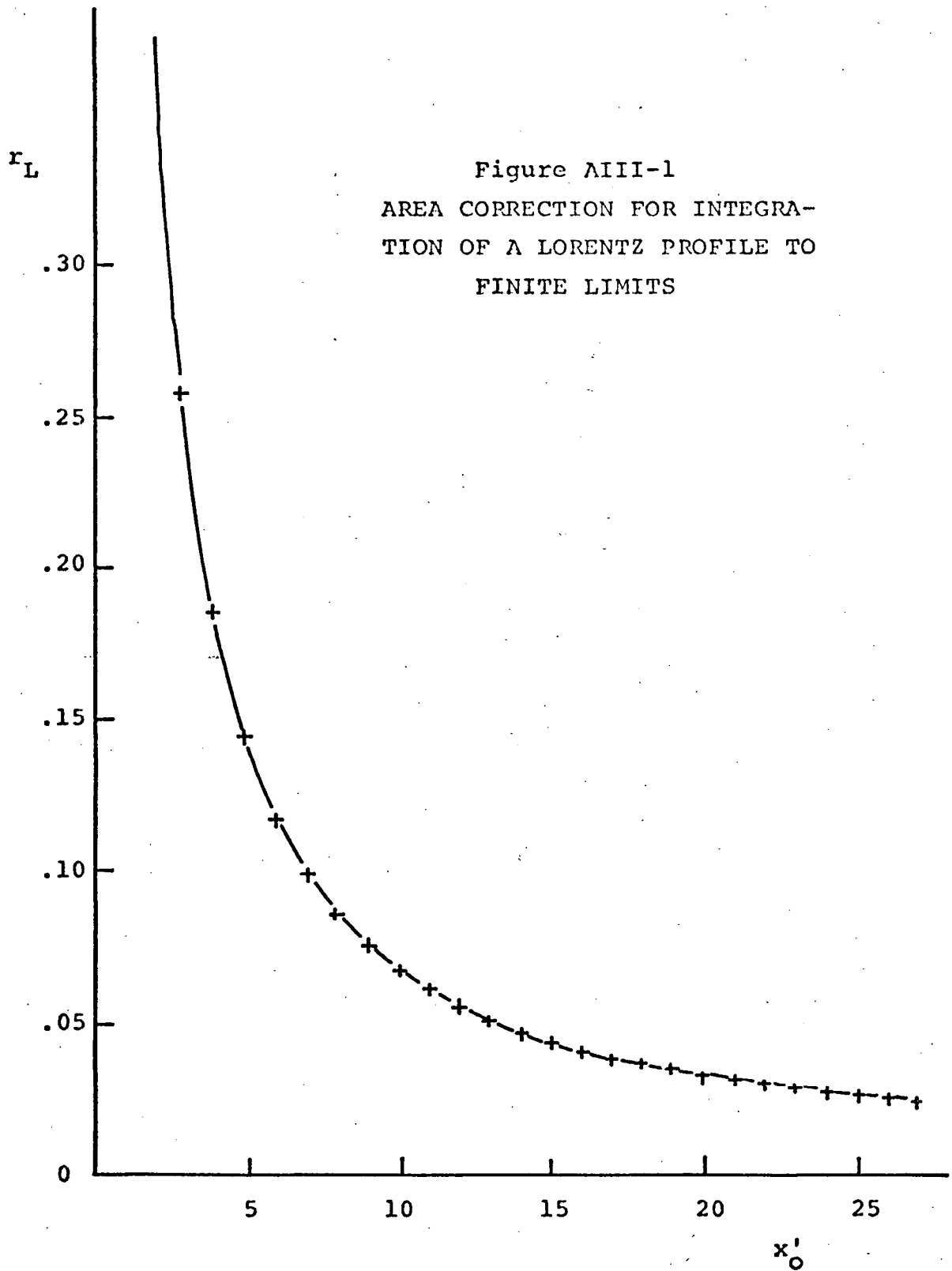
This integral was evaluated by applying a trapezoidal integration program to the 150 experimental points of each profile held in computer storage.

No continuum was subtracted from these curves. However, a background level (independent of radius), determined by the average level in the far wings of the profiles from the edge of the flame, was determined and subtracted from the profiles before integration. Subtraction of this

background had negligible effect on the near-axis integrals, but significantly reduced the values of the extreme outer integrals. This was understandable since the low background, when integrated over a wide range, could contribute a signal comparable to the integral over the same region of a spectral line, which was very narrow in the cool regions of the flame.

The variable,  $x'_0$ , (the nondimensional integration limit) was determined from the measured line widths and used to apply the wing correction ratio,  $r_L$ , assuming a Lorentzian line profile to the measured integral as described above.

The corrected value subsequently was used in the temperature calculations.



#### APPENDIX IV - EXCITED STATE POPULATION DENSITIES

If a state of Local Thermodynamic Equilibrium exists in a plasma, the population densities of the excited states of the neutral atoms can be calculated by the Saha-Boltzmann equation: (see Mewe, 1967):

$$\frac{n_m}{g_m} = \left( \frac{h^2}{2\pi m k T_e} \right)^{\frac{3}{2}} \frac{n_e^2}{2g_i} \exp\left( \frac{E_{mc}}{k T_e} \right)$$

where:  $n_m$  is the number density in the excited state with principal quantum number  $m$ ;  
 $g_m$  is the degeneracy of the excited state;  
 $g_i$  is the degeneracy of the ion ground state;  
 $E_{mc}$  is the difference between the ionization energy and the excitation energy;  
 $n_e$  is the electron density and all other symbols have their conventional meaning.

It has been assumed in this equation, that second ionization of helium is negligible at the temperatures considered and hence that the electron number density and the ion number density are equivalent. Also, the partition function for the helium ion has been approximated by the degeneracy of the ion ground state.

The temperature which appears in the equation is interpreted as the electron temperature as argued in the text (Part I, Chapter 3 C).

This equation was evaluated for electron densities in the range  $5 \times 10^{15} \text{ cm}^{-3} \leq n_e \leq 3 \times 10^{16} \text{ cm}^{-3}$  and for electron temperatures up to  $20,000^\circ\text{K}$ . The results of these calculations are plotted for  $m=3$  and  $m=4$  in Figure IV-1 and Figure IV-2 respectively.

10<sup>14</sup> Figure AIV-1 - EXCITED STATE POPULATION DENSITIES FOR n=3

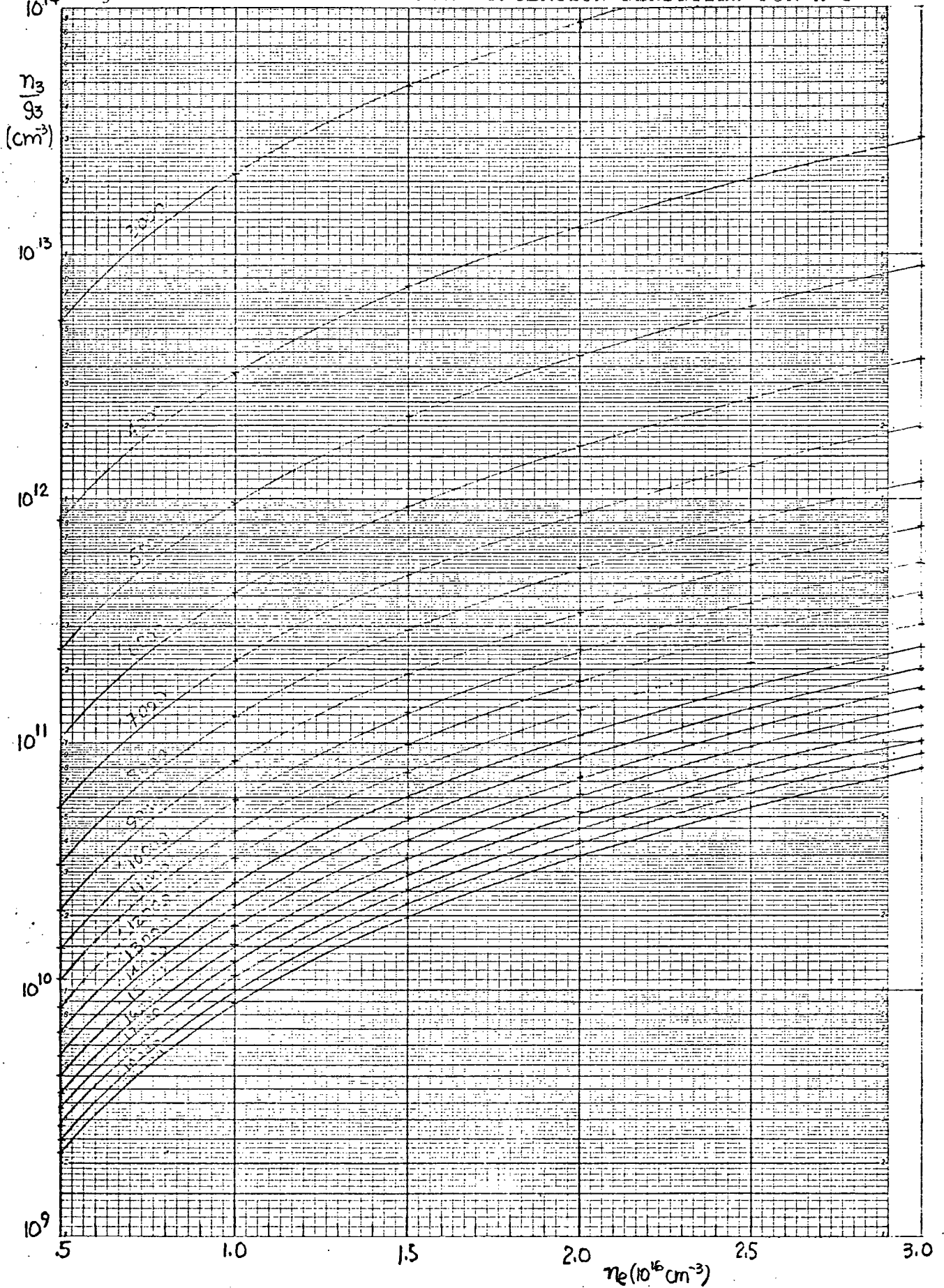
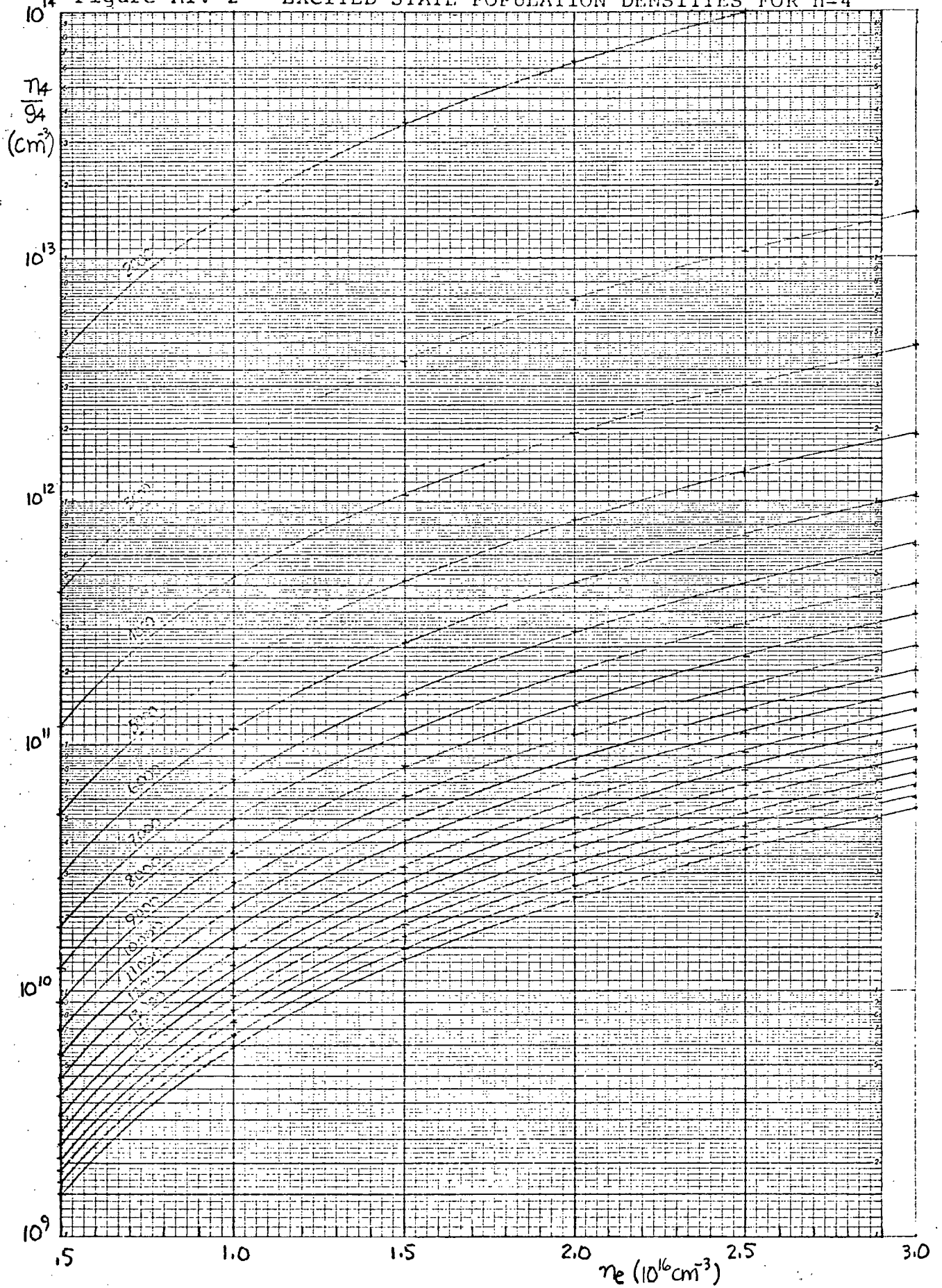


Figure AIV-2 - EXCITED STATE POPULATION DENSITIES FOR n=4



## APPENDIX V - WEDGE TECHNIQUE DESIGN PROCEDURE

To summarize the details and facilitate the use of the wedge technique for measuring shifts in the mean of spectral lines, the following is a complete set of instructions that explain how to apply the design criteria derived in Part II to a particular experimental situation.

1. The following information about the experiment is necessary for both the unshifted (subscripted 1 below) and the shifted line (subscripted 2):
  - the types of line profiles (roughly, whether rectangular, triangular, Gaussian or Lorentzian);
  - the approximate total line intensities,  $A_1'$  and  $A_2'$ ;
  - the expected (half) half-widths,  $\beta_1'$ , and  $\beta_2'$ ;
  - the expected shift of the mean from one profile to the other,  $\Delta\bar{\lambda}$  ;
  - the dispersion of the monochromator;  $D_\lambda$ ;
  - the continuum levels underlying the lines,  $B_1'$  and  $B_2'$ ;
  - the accuracy required;
  - the approximate normalization signal levels expected,  $S_1$  and  $S_2$ .
  - some estimate of the noise processes that will cause uncertainties in the measured signals:  $ds_1$ ,  $ds_2$ ,  $dS_1$  and  $dS_2$ .

2. Assume a width,  $W$ , for the wedge which adequately covers the widest line plus the expected shift;
3. Calculate the nondimensional widths of the two lines  $x_{\beta_1}$  and  $x_{\beta_2}$  using the assumed wedge width ( $x_{\beta} = W/\beta'$ ) and the approximate line widths;
4. Assume the mean of the broadest line lies at the center of the wedge ( $x_{O_1} = 0.5$ ) and the shift is to  $x_{O_2} = 0.5 + \Delta\bar{\lambda}'/W$ , where  $\Delta\bar{\lambda}' = \Delta\bar{\lambda}/D_{\lambda}$ ;
5. Determine the ideal ratio change,  $R_W$  (linear), from  $R_{W1} = 0.5$  to  $R_{W2}$  as determined from  $X_{O_2}$  and the appropriate nondimensional calibration graph (such as Figures II-3.2, II-3.3, or II-3.4) assuming a completely linear response (i.e.  $x_{\beta} = \infty$ );
6. Determine the non-linear ratio change,  $R_W$  (non-lin.), from  $R_{W1} = 0.5$  to  $R_{W2}$  along the curve specified by  $x_{\beta_2}$  instead of along the linear response curve as in step 5 above;
7. Calculate the error introduced by non-linear response:

$$\frac{\Delta R_W(\text{linear}) - \Delta R_W(\text{non-lin.})}{\Delta R_W(\text{linear})}$$

8. Compare this error with the required accuracy. If the accuracy is insufficient, increase the assumed width of the wedge,  $W$ , and repeat the above procedure;
9. Using the narrowest (shifted) line, calculate the relative background level:

$$\alpha = \frac{B_2'}{A_2'}$$

10. Using Equation II-3.18 in Part II, Chapter II-3, calculate the background slope criterion;

$$M_B = \frac{1}{1 + \alpha W} .$$

11. Substitute  $m_B$  and  $x_{O_2}$  into Equation II-3.13 to find the ratio change due to shift plus background,  $\Delta R_W$  (bkgd.);
12. Calculate the error in the ratio due to the presence of background:

$$\frac{\Delta R_W(\text{linear}) - \Delta R_W(\text{backg'd})}{\Delta R_W(\text{linear})}$$

If this, plus the previous error, exceeds the required limits, then extra measurements must be taken to eliminate the effects of background as described in Part II, Chapter II-3B.

13. Make a rough estimate of the effects of wedge non-linearity based on the type of film used and the width of the wedge as indicated in Part II, Chapter II-3C. (Generally speaking, narrow wedges with  $W \approx 0.02$  mm are easier to make linear than wide wedges with  $W \approx 0.5$  mm. However, in the middle of the range stated here a linearity of 5% is easily attained making the maximum non-linearity of the output due to width fluctuations about 3%, with more realistic figures around 1%. In any case, the true transmission of the wedge can be measured with a scanning microdensitometer to more accurately assess the linearity of the wedge.)

If errors due to wedge non-linearity plus errors due to edge effects as estimated by step 7 of this procedure are too large, then again, the width of the wedge must be increased;

14. Given the width of the wedge,  $W$ , which will allow sufficient accuracy and then  $T_{m \max}$ , the maximum transmission range attainable for the photographic plate used to make the wedge, the slope of the wedge,  $b$ , can be calculated. (For design purposes it is safe to assume that  $T_{\max} \approx 0.6$  is possible.)

$$b = \frac{T_{\max}}{W}$$

15. Assume that the photomultiplier responses are identical ( $k = K$  in Equation II-2.10) and that the monochromator is a perfect beam splitter ( $f_R = f_T = 0.5$ ). Calculate the anticipated change in the signal ratio given the expected shift and dispersion of the monochromator,  $D_\lambda$ , using Equation II-2.10:

$$\left(\frac{s}{S}\right) = b\Delta\lambda' = \frac{1}{D_\lambda} b\Delta\bar{\lambda}$$

16. On the basis of the anticipated signals  $S_1$  and  $S_2$  (assuming  $s \approx 0.5S$ ) and the expected uncertainties  $ds$ ,  $ds$ ,  $dS$ , and  $dS$ , calculate the uncertainty in measuring the signal ratio difference:

$$d\left(\frac{s_1}{S_1} - \frac{s_2}{S_2}\right)$$

17. Compare this accuracy with the expected ratio change as calculated in step 15 to determine if the noise processes will allow the measurement to be made within the necessary accuracy.

## BIBLIOGRAPHY

- Ahlborn, B. and Barnard, A.J., 1966, AIAA J., , 1136.
- Ahlborn, B. and Morris, R.N., 1969, J. Quant. Spectrosc. Radiative Transfer, 9, 1519.
- Ahlborn, B. and Potter, M.U., 1968, AIAA Journal, 6, 2227.
- Baldis, H., 1971, Ph.D. Thesis, University of B.C.
- Barr, W.L., 1962, J. Opt. Soc. Am., 52, 885.
- Berg, H.F., Ali, A.W, and Griem, H.R., 1962, Phys. Rev., 125, 199.
- Bracewell, R.N., 1956, Australian J. Phys., 9, 198.
- Cooper, J., 1966, Rep. Prog. Phys., 29, 35.
- De Vos, J.C., 1954, Physica, 20, 690.
- Drawin, H.W., 1964, Z. Naturf., 19a, 1451.
- Greig, J.R., Griem, H.R. and Nicolas, K.R., 1968, Am. Phys. Soc. B., 13, 1511.
- Greig, J.R. and Jones, L.A., 1970, Phys. Rev. A, 1, 1261.
- Griem, H.R., Baranger, M., Kolb, A.C. and Oertel, G., 1962, Phys. Rev., 125, 177.
- Griem, H.R., 1964, "Plasma Spectroscopy", McGraw-Hill.
- Hooper, C.F., 1968, Phys. Rev., 165, 215.
- Mewe, R., 1967, Brit. J. Appl. Phys., 18, 107.
- Morris, R.N., 1968, M.Sc. Thesis, University of B.C.
- Morris, R.N. and Knopf, T., 1972, Lab Report #22, Plasma Physics Group, University of B.C.
- Potter, M.U., 1967, M.Sc. Thesis, University of B.C.
- Stansfield, B.L., Ph.D. Thesis, University of B.C.
- Wiese, W.L., 1965, "Plasma Diagnostic Techniques"  
Ed. by R.H. Huddleston and S.L. Leonard, Academic Press.
- Wiese, W.L., Smith, M.W. and Glennon, B.M., 1966, "Atomic Transition Probabilities", Vol. I NBS 4 Dept. of Commerce, Washington D.C.
- Wulff, H., 1958, Z. Physik, 150, 614